ANL/RERTR/TM-12-37 Rev. 1

Technical Basis in Support of the Conversion of the University of Missouri Research Reactor (MURR) Core from Highly-Enriched to Low-Enriched Uranium – Steady-State Thermal-Hydraulic Analysis

Nuclear Engineering Division

About Argonne National Laboratory
Argonne is a U.S. Department of Energy laboratory managed by UChicago Argonne, LLC under contract DE-AC02-06CH11357. The Laboratory's main facility is outside Chicago, at 9700 South Cass Avenue, Argonne, Illinois 60439. For information about Argonne and its pioneering science and technology programs, see www.anl.gov.

DOCUMENT AVAILABILITY

Online Access: U.S. Department of Energy (DOE) reports produced after 1991 and a growing number of pre-1991 documents are available free via DOE's SciTech Connect (http://www.osti.gov/scitech/)

Reports not in digital format may be purchased by the public from the National Technical Information Service (NTIS):
U.S. Department of Commerce
National Technical Information Service
5301 Shawnee Rd
Alexandria, VA 22312
www.ntis.gov
Phone: (800) 553-NTIS (6847) or (703) 605-6000
Fax: (703) 605-6900
Email: **orders@ntis.gov**

Reports not in digital format are available to DOE and DOE contractors from the Office of Scientific and Technical Information (OSTI):
U.S. Department of Energy
Office of Scientific and Technical Information
P.O. Box 62
Oak Ridge, TN 37831-0062
www.osti.gov
Phone: (865) 576-8401
Fax: (865) 576-5728
Email: **reports@osti.gov**

Disclaimer
This report was prepared as an account of work sponsored by an agency of the United States Government. Neither the United States Government nor any agency thereof, nor UChicago Argonne, LLC, nor any of their employees or officers, makes any warranty, express or implied, or assumes any legal liability or responsibility for the accuracy, completeness, or usefulness of any information, apparatus, product, or process disclosed, or represents that its use would not infringe privately owned rights. Reference herein to any specific commercial product, process, or service by trade name, trademark, manufacturer, or otherwise, does not necessarily constitute or imply its endorsement, recommendation, or favoring by the United States Government or any agency thereof. The views and opinions of document authors expressed herein do not necessarily state or reflect those of the United States Government or any agency thereof, Argonne National Laboratory, or UChicago Argonne, LLC.

ANL/RERTR/TM-12-37 Rev.1

Technical Basis in Support of the Conversion of the University of Missouri Research Reactor (MURR) Core from Highly-Enriched to Low-Enriched Uranium – Steady-State Thermal-Hydraulic Analysis

---

prepared by

E. E. Feldman[1], coordinating author

and

B. Dionne[1], L. P. Foyto[2], M. Kalimullah[1], K. Kutikkad[2], J. C. McKibben[2], A. P. Olson[1], N. J. Peters[2], J. G. Stevens[1], and J.A. Stillman[1]

[1]Nuclear Engineering Division, Argonne National Laboratory
GTRI Reactor Conversion Program
9700 S. Cass Avenue
Argonne, Illinois 60439

[2]University of Missouri-Columbia Research Reactor
1513 Research Park Drive
Columbia, Missouri 65211

January, 2013

This work is sponsored by the U.S. Department of Energy,
National Nuclear Security Administration Office of Global Threat Reduction (NA-21)

Executive Summary

The thermal performance of the proposed low-enriched uranium (LEU) core for the University of Missouri Research Reactor (MURR) during steady-state operation is predicted. This conceptual design core, core CD35, is to replace the existing MURR Highly-Enriched Uranium (HEU) core. An earlier proposed LEU core design, the Feasibility Study Design (FSD) core, which was subsequently superseded due to issues of fuel plate manufacture, is also analyzed. Acceptable margins to both flow instability and critical heat flux (CHF) are demonstrated for both LEU cores.

The designs of the HEU core and the two LEU cores are similar in that each has eight geometrically-identical wedge-shaped fuel elements that are arranged in a circle to form an annulus. Each element has 23 or 24 parallel curved fuel plates depending on the element design, which are separated by thin curved rectangular coolant channels. There is an additional coolant channel outside the first fuel plate of each element and another one outside the last fuel plate. Downward flow through these coolant channels removes the power deposited in the core. Geometric tolerances and the clearances needed for insertion and removal of the elements from the reactor vessel are considered in the analysis.

For each of the three cores, the core neutron physics analysis, which is provided in a separate report, considered 24 cases that together bound the most-limiting thermal-hydraulic state for each core. All 24 cases for each core were individually modeled in the thermal-hydraulic analysis. In each case all eight elements were modeled simultaneously.

An acceptable LEU core must have sufficient margins to both flow instability and critical heat flux (CHF) events. Flow instability can occur in a reactor core that has parallel coolant channels. Added hydraulic resistance due to boiling in one channel can divert flow to another channel and cause the boiling channel to have a flow reduction excursion, or instability. When CHF occurs due to a flow excursion, the event is classified as a flow instability event rather than a CHF event. The CHF event is defined as one that is not caused by a flow reduction excursion. The operational safety margin to each event is predicted for all 24 cases of each of the three cores.

The steady-state thermal-hydraulic analysis performed for the existing Safety Analysis Report (SAR) for the HEU core is well understood and can be easily duplicated. In 2011 some of the authors of the current report reviewed, replicated, and revised that analysis.

For the current analysis, a form of the Whittle and Forgan flow stability criterion that is based on channel coolant temperature rise is used in assessing the margin to flow instability. An extended form of the Groeneveld 2006 CHF Table is used in assessing the margin to CHF. The selection of this CHF correlation is a result of considerable literature research and analysis, which are described in the current report. These two metrics – margin to flow instability and margin to CHF – were applied in all 24 cases for each of the three cores. For the most limiting flow instability case of each core, the limiting channel

was further analyzed with two other flow instability criteria. One of them assumes that flow instability occurs at the onset of significant voids, as predicted by Saha and Zuber[10]. The other assumes that flow instability occurs when the minimum CHF ratio, based on the Bernath CHF correlation[6], is 2.0.

For the most limiting CHF case of each core, as predicted by the extended form of the Groeneveld 2006 CHF Table, the limiting channel was further analyzed with the Bernath CHF correlation. The Bernath CHF correlation was used in the original HEU SAR to predict both flow instability and CHF. For the most limiting of the 24 LEU CD35 CHF cases as predicted by the extended form of the Groeneveld 2006 CHF Table, the full eight-element model analysis was repeated with the Sudo and Kaminaga CHF correlation.

The correlation used in the analysis to predict the Nusselt number is an improved form of the Dittus-Boelter correlation that has an added factor to account for differences between the coolant viscosity at the bulk coolant temperature and at the fuel plate surface temperature.

Hot channel factors were used in the thermal-hydraulic analyses in order to take into account the potential adverse effects of manufacturing tolerances and uncertainties in modeling on the quantities being predicted in the safety analysis. The five random contributors to hot channel factors that were considered in the analysis are the tolerances for 1) the combined local effects of fuel meat thickness and ^{235}U homogeneity, 2) the ^{235}U fuel plate loading, 3) the power density, 4) the channel thickness, and 5) the flow distribution. The random hot channel factor components were combined multiplicatively, rather than statistically. In the analysis channel-dependent local hot channel factors were applied to each coolant channel, fuel plate, and fuel plate surface separately.

A global, or systematic, hot channel factor of 1.20 was applied to the Nusselt number correlation. Limiting safety system settings (LSSS) values of reactor power, flow rate, inlet coolant temperature, and pressurizer pressure were used in the predictions of margins to flow instability and CHF. In the operation of the MURR, the reactor trip setting values take measurement uncertainties into account. Therefore, global hot channel factors are not needed to account for measurement errors in reactor power, flow rate, inlet coolant temperature, or pressurizer pressure.

In the operation of the MURR, the pressure at the pressurizer is carefully controlled. There is a significant pressure drop from the pressurizer to the core inlet. Because the pressure at the core inlet is needed for the analysis, this pressure drop is predicted for each combination of pressurizer pressure, pressurizer level, coolant inlet temperature, and core flow rate used in the analysis. A pressure-drop model that is based on analysis and past measurement is fully described and used to predict these values of pressure drop.

The HEU fuel plate when manufactured has three layers – a fuel meat layer and an aluminum clad layer on either side. The LEU fuel plate has a similar design, but it has a layer of zirconium on each side of the fuel meat that forms a barrier between the fuel meat and the aluminum clad. While the fuel is being irradiated, a thin layer of oxide gradually forms on the heated exterior surfaces of the clad and thickens over time with operation. Therefore, the HEU fuel plate is modeled as a five-layer solid consisting of a

fuel meat layer, two aluminum layers, and two oxide layers. The LEU fuel plate is modeled as a seven-layer solid consisting of a fuel meat layer, two zirconium layers, two aluminum layers, and two oxide layers. The fuel, zirconium, and aluminum layer thicknesses are explicitly modeled. The oxide layers are represented as thermal resistances that consequently have no explicit thickness.

The thermal resistance due to the buildup of oxide on the clad surfaces can influence the margins to flow instability and CHF because heat is transferred from one coolant channel to the next through the intervening fuel plate. This is a second-order effect that typically is most pronounced when the limiting channel is an end channel or is next to an end channel because this is a location where the temperature difference between two adjacent coolant channels could be relatively large. For a 2-mil oxide layer on each heated fuel plate surface, the flow instability power for the LEU CD35 core was predicted to be about 0.7% lower than when there were no oxide layers. A maximum oxide thickness of about 1 mil at discharge burnup is expected for all three cores. In the analysis of flow instability and CHF for all except a few sensitivity cases, the thermal resistance of the oxide layer was taken to be 0.

The reduction in channel thickness due to fuel plate swelling and oxide buildup reduces the flow through the channel. This adversely affects the bulk coolant temperature rise and the film temperature rise at the surface of the fuel plate. For the HEU core the maximum reduction in channel thickness due to fuel plate swelling and oxide buildup for channels bounded by two fuel plates is assumed to be 10 mils. For the two LEU cores this value was reduced to 8 mils to reflect expected fuel swelling and oxide growth. In the past, the actual channel thickness as burnup proceeds in the HEU core has been monitored. A similar monitoring approach will be used for the LEU CD35 core. For all three cores the reduction in the coolant channel thickness on the outside of the first and last fuel plate of each element is taken to be half of the internal channel values, i.e., 5 mils for the HEU and 4 mils for each of the two LEU cores. For the fresh fuel the channel thickness reduction is assumed to be zero. The channel thickness reduction is assumed to be linearly proportional to burnup.

The PLTEMP/ANL code is the primary thermal-hydraulic computational tool that was used in evaluating the margins to flow instability and critical heat flux during steady-state operation. It is capable of modeling all of the MURR fuel elements at one time and considering all of the fuel plates and coolant channels of each element simultaneously. In the PLTEMP/ANL code the only coupling between parallel fuel elements is hydraulic (by imposing a uniform pressure drop across the core). The axial power distribution of each fuel plate is explicitly represented.

The code divides the axial length of the core into a series of parallel horizontal layers and predicts the temperatures and heat fluxes of each layer. The heated region of the fuel meat was subdivided into 24 equal axial layers. Starting at the first layer next to the inlet, the code solves simultaneously the entire system of plates and channels in a particular fuel element. Then the process repeats for each layer downstream. The thermal boundary conditions in the channel on each side of a fuel plate determine the fraction of the power emanating from each face of the fuel plate. This simultaneous solution can be particularly important when the channel on one side of a fuel plate is much cooler than the channel on the other side, such as in the end channels of the element.

In the PLTEMP/ANL models of the MURR cores, the curved arc length of each coolant channel was subdivided into three subchannels. The middle subchannel was adjacent to the fuel meat. The two edge subchannels on either side were unheated. In the analysis it was assumed that all of the power deposited in the core went into the middle subchannels and the coolant of all of the edge subchannels remained at the coolant inlet temperature.

In the core neutron physics analysis, the azimuthal arc length of the fuel meat region of each fuel plate was subdivided into nine vertical strips. For each of the nine strips the ratio of the average heat flux for the strip to the average heat flux for the entire heated region of the fuel plate was estimated. The largest of the nine ratios for each fuel plate was used in the analysis to account for the power variation along the curved span of the fuel meat.

Moody friction factors, which are a function of both relative roughness and Reynolds number, were used in the hydraulic analysis.

For the HEU core, the minimum flow instability power was found to be 14.61 MW, which is 2.11 MW above the LSSS power of 12.5 MW for the HEU core. For this core the minimum power at which CHF was predicted to occur was at 29.88 MW. For the LEU cores the LSSS power is 15.0 MW. The minimum flow instability powers for these two cores are 2.12 and 2.10 MW above this LSSS value for the FSD and CD35 cores, respectively. The minimum CHF powers for the LEU FSD and CD35 cores are 30.55 and 31.26 MW, respectively.

For the limiting flow instability case for the CD35 core, which is the one that yielded 17.10 MW, a parametric study is performed with the full eight-element PLTEMP/ANL model. In this study pressurizer pressures of 60, 75, and 85 psia are considered. For each of these pressures six reactor inlet temperatures ranging between 120 and 200° F are considered. For each of these 18 combinations of pressure and inlet temperature, 11 values of reactor flow rate ranging from 400 to 4000 gpm are considered. For each of these 198 combinations of pressure, temperature, and flow rate, the allowed flow instability power is determined. For the limiting CHF case for the CD35, which is the one that yielded 31.26 MW, the analogous 198 point parametric study is performed.

Every PLTEMP/ANL solution that provided a value of flow instability power for this report also provided the corresponding value of minimum CHF ratio, based on the extended Groeneveld 2006 CHF Table. In every case this CHF ratio is greater than 2.0.

To independently verify the results of the PLTEMP/ANL code calculations, a separate thermal model of a single channel was developed and implemented on a computer spreadsheet as a checker program. For a few selected PLTEMP/ANL cases the channel that is identified as limiting is analyzed with this specially-developed checker program. These cases include the limiting flow instability case and the limiting CHF power case for each of the three cores.

The checker program calculated the axial distribution of channel bulk coolant temperature. For each heated surface it also calculated the axial distributions of surface temperature, film coefficient, heat flux, critical heat flux based on both the extended Groeneveld 2006 CHF Table correlation and the Bernath CHF correlation, and CHF ratio for each correlation. The program also determined the margin to flow instability based on the Whittle and Forgan correlation, the Saha-Zuber onset of significant voids relationship, and the Bernath-CHF-ratio-of-2.0 criterion.

For the HEU and LEU CD35 cores, analyses were performed with aid of the PLTEMP/ANL code in which three of the four reactor parameters, pressurizer pressure, inlet temperature, inlet flow rate, and reactor power, were constrained at their LSSS values and the value of the fourth at which the onset of flow instability occurs was obtained. The corresponding results from the analysis of the MURR Hazards Summary Report for the HEU core were also tabulated. For each of these three sets of results, the margins to flow instability relative to LSSS values for pressurizer pressure, inlet temperature, inlet flow rate, and reactor power were obtained. Differences in margins to flow instability among the three sets of results were tabulated and compared.

Appendix A is an independent section of this report that was added in Revision 1 to provide a detailed analysis of the load on the grid plate, or “spider”, that supports the eight core elements. This analysis shows that for a normal core operating flow rate of 3750 gpm, the load on the spider is 220 pounds less for the CD35 core than it is for the HEU core that it replaces.

In conclusion, very detailed steady-state thermal-hydraulic analyses were performed of the existing HEU and of two LEU cores. The results demonstrate acceptable margins to flow instability and CHF for all three cores. For each core all 24 cases identified by the neutron physics analysis was considered. For each case all eight fuel elements were explicitly represented in the analytical model. Each model included plate-by-plate and channel-by-channel hot channel factors to account for manufacturing tolerances, assembly clearances, and modeling uncertainties. The components of these factors were combined multiplicatively, which assumes that the worst combination of conditions occur at the most limiting location in the core. The axial power distribution of each fuel plate was explicitly represented. The variation in heat flux along the curved span of each fuel meat was taken into account. No credit was taken for coolant mixing along the curved span of each coolant channel. For these safety analyses, the pressurizer pressure, the reactor inlet temperature, and the reactor flow rate were simultaneously set at the extreme of their LSSS values, which is an extremely unlikely combination of conditions. The proposed LEU CD35 core design has acceptable flow instability and CHF safety margins, as does the LEU FSD core design. For both of the LEU cores, the predicted margin to flow instability is 2.12 (FSD) or 2.10 (CD35) MW above the LSSS power, which is essentially the same as the 2.11 MW margin for the HEU core. All three cores have CHF powers that are substantially greater than their flow instability powers and all values of CHF ratio evaluated at the values of flow instability power are greater than 2.0. Under normal operating conditions, the load on the core support spider is 220 pounds less for the LEU CD35 core than for the HEU core that it replaces.

Table of Contents

Executive Summary iii

Table of Contents ix

List of Figures xi

List of Tables xii

1. Geometry of the Fuel Elements 1

2. Core Configurations and Operating Conditions 5

3. Thermal Criteria to Be Met 5

4. Replication of the Existing HEU Steady-State Thermal Analysis 9

5. Correlations for Predicting Flow Instability Power 9

6. Correlations for Predicting Critical Heat Flux 11

6a. Extended Groeneveld 2006 11

6b. Bernath CHF Correlation 15

6c. Sudo and Kaminaga CHF Correlation 15

7. Nusselt Number Correlation for Predicting Film Coefficient 16

8. Hot Channel Factors 16

8a. Local Hot Channel Factor Contributors 17

8b. Evaluating and Combining Local Hot Channel Factor Components 20

8c. Global Hot Channel Factors 27

9. Pressure Drop from the Pressurizer to the Inlets of the Coolant Channels 28

10. Fuel Plate Thermal Model 31

11. Channel Thickness Reduction Due to Fuel Plate Swelling and Oxide Buildup 34

12. The PLTEMP/ANL Code[38] 35

13. Application of the PLTEMP/ANL Code to the MURR Cores 37

14. Results 40

15. Verification of the PLTEMP/ANL Results 55

16. Discussion 57

16a Comparison of PLTEMP/ANL Flow Instability Predictions with the Checker Program Results for Three Flow Instability Correlations 57

16b. Beneficial Effect of Reduced Channel Thickness on the Margin to Flow Instability 58

16c. Effect of Mixing Along the Width of the Coolant Channel 59

16d. Comparison of PLTEMP/ANL CHF Predictions with the Checker Program Results for Two CHF Correlations 60

16e. Critical Heat Flux Ratio and Critical Heat Flux Power 61

16f. The Combined Effect of the Hot Channel Factor for Velocity and the Beneficial Effect of the Reduced Channel Thickness on the Margin to CHF 62

16g. Predictions Made with the Sudo and Kaminaga CHF Correlation[15,31] 64

16h. Flow Instability Power Envelope for the LEU CD35 Core 64

16i. Margin to Flow Instability Relative to LSSS Values 65

17. Summary and Conclusions 67

References: 69

Appendix A. Load on the Grid Plate (Spider) A.1

List of Figures

FIGURE 1. MURR CORE LAYOUT WITH CONTROL BLADES IDENTIFIED 1
FIGURE 2. THICKNESSES OF OUTER CHANNELS 3
FIGURE 3. COMPARISON OF CHFS BY HALL_MUDAWAR ICC AND GROENEVELD 2006 TABLE (DH = 0.008 M) 13
FIGURE 4. COMPARISON OF THE SARMA, THE CAIRA, THE LOMBARDI, AND THE HALL-MUDAWAR ICC 14
FIGURE 5. SCHEMATIC REPRESENTATION OF THE REACTOR CORE INLET PIPING 28
FIGURE 6. THERMAL CONDUCTIVITY OF ZIRCONIUM 33
FIGURE 7. LEU CORE CD35 FLOW INSTABILITY POWER FOR PRESSURIZER PRESSURE AT 60 PSIA 47
FIGURE 8. LEU CORE CD35 FLOW INSTABILITY POWER FOR PRESSURIZER PRESSURE AT 75 PSIA 48
FIGURE 9. LEU CORE CD35 FLOW INSTABILITY POWER FOR PRESSURIZER PRESSURE AT 85 PSIA 49
FIGURE 10. LEU CORE CD35 CRITICAL HEAT FLUX POWER FOR PRESSURIZER PRESSURE AT 60 PSIA 52
FIGURE 11. LEU CORE CD35 CRITICAL HEAT FLUX POWER FOR PRESSURIZER PRESSURE AT 75 PSIA 53
FIGURE 12. LEU CORE CD35 CRITICAL HEAT FLUX POWER FOR PRESSURIZER PRESSURE AT 85 PSIA 54

FIGURE A - 1. SPIDER LOAD MODEL A.1

List of Tables

TABLE 1. NOMINAL COOLANT CHANNEL THICKNESSES (CHANNEL 1 IS AT THE INNER WALL OF THE VESSEL.) 2
TABLE 2. END CHANNEL DIMENSIONS.....4
TABLE 3. SUMMARY OF POWER DISTRIBUTION EVALUATIONS – HEU CORE.....6
TABLE 4. SUMMARY OF POWER DISTRIBUTION EVALUATIONS – FSD CORE (LEU) 7
TABLE 5. SUMMARY OF POWER DISTRIBUTION EVALUATIONS – CD35 CORE (LEU).....8
TABLE 6. REACTOR OPERATING CONDITIONS 9
TABLE 7. LEU FSD PLATE OVERLOAD TOLERANCE FRACTIONS, % 18
TABLE 8. LEU CD35 PLATE OVERLOAD TOLERANCE FRACTIONS, %.....18
TABLE 9. SAMPLE HOT CHANNEL FACTOR CALCULATION FOR CHANNEL 23 AND PLATE 23 OF THE LEU CD35 CORE 21
TABLE 10. HOT CHANNEL FACTORS FOR THE HEU CORE (NO FUEL PLATE SWELLING OR OXIDE GROWTH) 24
TABLE 11. HOT CHANNEL FACTORS FOR THE LEU FSD CORE (NO FUEL PLATE SWELLING OR OXIDE GROWTH) 25
TABLE 12. HOT CHANNEL FACTORS FOR THE LEU CD35 CORE (NO FUEL PLATE SWELLING OR OXIDE GROWTH).....26
TABLE 13. REFERENCE HYDRAULIC CONDITIONS USED IN CONJUNCTION WITH EQUATIONS 12 AND 13 TO DETERMINE ΔP_{HR}.....30
TABLE 14. THERMAL CONDUCTIVITIES OF HEU AND LEU FUEL PLATE MATERIALS, W/M-K 31
TABLE 15. ELEMENT BURNUP* 32
TABLE 16. REACTOR FLOW INSTABILITY AND CRITICAL HEAT FLUX RATIOS AND POWERS (MW) FOR THE HEU CORE 43
TABLE 17. REACTOR FLOW INSTABILITY AND CRITICAL HEAT FLUX RATIOS AND POWERS (MW) FOR THE LEU FSD CORE 44
TABLE 18. REACTOR FLOW INSTABILITY AND CRITICAL HEAT FLUX RATIOS AND POWERS (MW) FOR THE LEU CD35 CORE 45
TABLE 19. LEU CORE CD35 FLOW INSTABILITY POWER, MW, WITH THE PRESSURIZER PRESSURE AT 60 PSIA 46
TABLE 20. LEU CORE CD35 FLOW INSTABILITY POWER, MW, WITH THE PRESSURIZER PRESSURE AT 75 PSIA 46
TABLE 21. LEU CORE CD35 FLOW INSTABILITY POWER, MW, WITH THE PRESSURIZER PRESSURE AT 85 PSIA 46
TABLE 22. LEU CORE CD35 CHF RATIO AT FLOW INSTABILITY POWER WITH THE PRESSURIZER PRESSURE AT 60 PSIA 50
TABLE 23. LEU CORE CD35 CHF RATIO AT FLOW INSTABILITY POWER WITH THE PRESSURIZER PRESSURE AT 75 PSIA 50
TABLE 24. LEU CORE CD35 CHF RATIO AT FLOW INSTABILITY POWER WITH THE PRESSURIZER PRESSURE AT 85 PSIA 50
TABLE 25. LEU CORE CD35 CHF POWER, MW, WITH THE PRESSURIZER PRESSURE AT 60 PSIA.....51
TABLE 26. LEU CORE CD35 CHF POWER, MW, WITH THE PRESSURIZER PRESSURE AT 75 PSIA.....51
TABLE 27. LEU CORE CD35 CHF POWER, MW, WITH THE PRESSURIZER PRESSURE AT 85 PSIA.....51
TABLE 28. HEU CORE FLOW INSTABILITY WHEN THREE REACTOR PARAMETERS ARE AT THEIR LSSS VALUES.....55
TABLE 29. LEU CORE CD35 FLOW INSTABILITY WHEN THREE REACTOR PARAMETERS ARE AT THEIR LSSS VALUES .55
TABLE 30. COMPARISON OF FLOW INSTABILITY PREDICTIONS.....58
TABLE 31. COMPARISON OF CRITICAL HEAT FLUX PREDICTIONS.....60
TABLE 32. COMPARISON OF CHF RATIO = 2.0 PREDICTIONS FOR THE MOST LIMITING FLOW INSTABILITY CHANNEL 63
TABLE 33. HEU CORE HSR FLOW INSTABILITY WHEN THREE REACTOR PARAMETERS ARE AT THEIR LSSS VALUES ...66
TABLE 34. MARGINS TO FLOW INSTABILITY WHEN THREE REACTOR PARAMETERS ARE AT THEIR LSSS VALUES 66

TABLE A - 1. KEY SPIDER LOAD PARAMETERS AND RESULTS A.2

1. Geometry of the Fuel Elements

The three core designs that are analyzed are the existing highly-enriched uranium (HEU) design and two low-enriched uranium (LEU) designs. The first of the two LEU designs is the feasibility study design (FSD), which was initially investigated in September 2009.[1] Because of issues related to the manufacture of the fuel plates for this design, the FSD was replaced by the CD35 design. Since Reference 1 was issued, the thermal-hydraulic modeling and analysis has been refined and extended. It now includes more core states and the prediction of the onset of critical heat flux. Therefore, all three cores are analyzed and compared in this report.

Each of the three core designs has eight wedged-shaped fuel elements of identical design that are arranged in a circle, as shown in Figure 1. Each HEU element and each FSD element has 24 curved fuel plates that are parallel to the inner and outer circular boundaries of the annular reactor vessel. The CD35 element has 23 fuel plates. In all three core designs the fuel plates of each element are parallel to each other and separated by coolant channels, 23 internal coolant channels in the HEU and LEU FSD cores and 22 in the LEU CD35. In addition, each element has two end coolant channels, one in the narrow curved rectangular space between the inner pressure vessel wall and the innermost fuel plate and another one between the outmost fuel plate and the outer pressure vessel wall. Table 1 lists the channel thicknesses for the three core designs, with the first and last channel thicknesses highlighted in yellow. As shown, the HEU element has an 80 mil (1 mil = 0.001 inch) gap between adjacent plates. The FSD element has 92 mils between adjacent fuel plates. In the CD35 element the first four and the last four interior channels each have 93-mil gaps and the rest of the interior channels have 92-mil gaps. The gap thickness tolerance for all of the interior channels in all three element designs is ±8 mils.

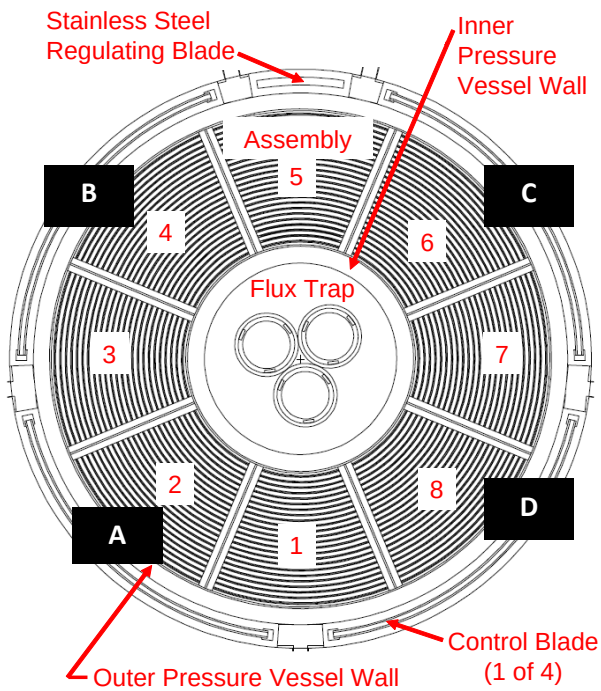

Figure 1. MURR Core Layout with Control Blades Identified

Because there are eight elements in each core, the HEU and LEU FSD cores have 8 × 25, or 200 hydraulically parallel coolant channels. The LEU CD35 core has 8 × 24, or 192 channels. Each coolant channel is 25.5 inches long. The flow enters the core from the top. The first 0.75 inches are unheated, the next 24 inches are fueled, and the last 0.75 inches are unheated. The flow area immediately ahead of the plates and immediately after them is formed between the inner and outer pressure vessel walls.

The outer diameter of the inner wall is 5.32 inches. The inner diameter of the outer wall is 11.8 inches. Thus, each of these flow areas is $\pi/4\ [(11.8\ \text{in})^2 - (5.32\ \text{in})^2]/(144\ \text{in}^2/\text{ft}^2) = 0.60507\ \text{ft}^2$. The element end fittings and support structures in the reactor vessel would moderately reduce this area. The coolant channel flow area of the HEU, FSD, and CD35 cores is 56.5, 63.7, and 61.4%, respectively, of this value. The maximum allowed surface roughness of each fuel plate is 63×10^{-6} inches.

Each element has two guide rollers on the top and two on the bottom of the element, as shown in Figure 2, which position the element between the inner and outer vessel walls and help guide the element into place while it is being inserted into the core. Table 2 provides values for the dimensions A, B, C1, D1, E1, C-L, D-L, and E-L that are shown in Figure 2. The insertion clearance produced by the difference between dimensions A and B must be large enough to permit the elements to be inserted and removed easily, yet small enough to limit the variability in the end channel thicknesses. The dimension A is deduced from the diameters of the inner and outer vessels, which are not changed as a result of core conversion. Since the existing HEU value of insertion clearance has functioned well in the past, the existing value and tolerance of B are maintained for the LEU cores.

Table 1. Nominal Coolant Channel Thicknesses (Channel 1 is at the inner wall of the vessel.)

	Nominal Channel Thickness, mils		
Channel	HEU	LEU FSD	LEU CD35
1	110	95	95.5
2	80	92	93
3			
4			
5			
6	80	92	92
7			
8			
9			
10			
11			
12			
13			
14			
15			
16			
17			
18			
19			
20	80	92	93
21			
22			
23			
24	80	92	95.5
25	90	95	

Dimension A in Figure 1 was deduced from the University of Missouri Drawing 554. In the drawing the inner diameter of the outer wall of the pressure vessel is given as 11.800±0.010 inches and the outer diameter of the inner wall of the vessel is given as 5.320±0.005 inches. If it is assumed that these two diameters are concentric, then the radial distance between the two circular vessel walls is half of the difference of the two diameters, or 3.240±0.0075 inches. Any eccentricity between the centers of the two circular vessel walls must be very small or element binding would be occurring where the two vessels walls are closest together. Also, neither the equivalent hydraulic diameter nor the total core flow area is affected by eccentricity. Therefore, the impact of such eccentricity on the minimum flow rate of either end channel or on any other channels also must be extremely small.

Dimension B was deduced from the Babcock and Wilcox Company Drawing 13000D, which is an assembly drawing of the HEU fuel element. The inner radius of the inner roller at either end of the element is 2.675±0.003 inches. The outer radius of the outer roller of either end is 5.885±0.003 inches. Therefore, the nominal value of dimension B is the difference of the two radii and the tolerance is the sum of the two equal tolerances, or 3.210±0.006 inches. It is assumed that the nominal 30-mil clearance in A – B is shared equally by the first and last coolant channels, thereby contributing ±15 mils to the tolerance for each.

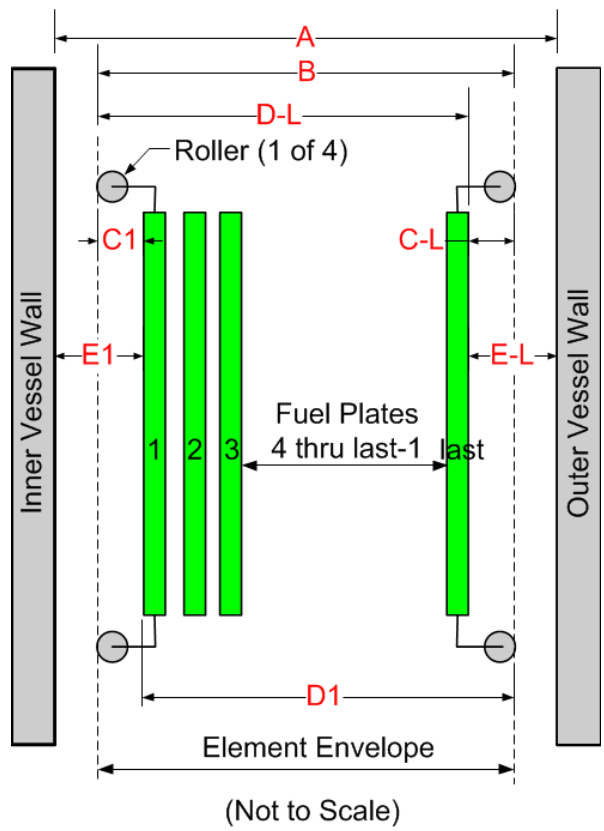

Figure 2. Thicknesses of Outer Channels

From the dimensions of fuel element subcomponents given in B&W drawings 13000E, 13005D, and 13006E, the inner radius of HEU plate 1 is 2.770 inches and the outer radius of HEU plate 24 is 5.810 inches, which agree with the radii given for plates 1 and 24 in the B&W 13005 drawing. Based on this review, the correct HEU dimensions for C1 and C-L are 0.095±0.007 and 0.075±0.010 inches, respectively. The nominal value for C1 and C-L is 0.080 inches for the LEU FSD fuel and 0.0805 for the CD35 fuel. The tolerances for the LEU CD35 core, which are to be determined, are expected to be and assumed to be the same as those for the HEU fuel.

In the thermal hydraulic analysis, the thicknesses of the end channels, E1 and E-L, are important. Thinning an end channel decreases its coolant flow and causes higher temperatures in its adjacent fuel plate. Thickening an end channel increases its flow and thereby reduces the flow to the other channels in the core. The most limiting configurations are the ones where one end channel is as small as possible and the other end channel is as large as possible. This would require shifting the element inward or outward so that both rollers on one side of the element contacts one of the vessel walls and minimizes the flow in one of the two end channels. Thus, for example, a potentially limiting configuration is one in which both of the inner rollers of each of the eight elements contact the inner vessel wall, thereby minimizing all of the eight E1 values and maximizing all of the eight E-L values.

Obviously, the smallest value for E1 occurs when the two inner rollers are against the inner vessel wall and C1 is the smallest that is allowed by its tolerance. Similarly, E-L is the smallest when the two outer rollers are against the outer vessel wall and C-L is the smallest that is allowed by its tolerance. The largest value of E-L, of course, occurs when the two inner rollers are against the inner vessel wall. Therefore, the dimension D-L, which is the distance from the inner roller at the inner edge of the

element envelope to the outer edge of the outermost plate, was introduced. As is obvious from Figure 2, the largest value of E-L is the maximum value of A allowed by the tolerances minus the smallest value of D-L allowed by its tolerance. Similarly, the largest value of E1 is the maximum value of A allowed by the tolerances minus the smallest value of D1 allowed by its tolerance.

Table 2. End Channel Dimensions

	Value, inches		
Dimension	**HEU**	**LEU FSD**	**LEU CD35**
A	3.240±0.0075		
B	3.210±0.006		
A − B	0.030±0.0135		
C1	0.095 ± 0.007	0.080 ± 0.007*	0.0805 ± 0.007*
C-L	0.075 ± 0.010	0.080 ± 0.010*	0.0805 ± 0.010*
D1	3.115±0.007	3.130±0.007	3.1295±0.007
D-L	3.135±0.010	3.130±0.010	3.1295±0.010
Min. E1**	0.088	0.073[+]	0.0735[+]
Nom. E1**	0.110	0.095[+]	0.0955
Max. E1**	0.1395	0.1245	0.1250
Min. E-L**	0.065	0.070[+]	0.0705[+]
Nom. E-L**	0.090	0.095[+]	0.0955
Max. E-L**	0.1225	0.1275	0.1280

*These tolerances are under investigation.

** The minimum values of E1 are the minimum values of C1 allowed by their tolerances. The nominal values of E1 are the nominal values of C1 increased by 0.015, which is half of the nominal value of the quantity A − B. The maximum values of E1 are the maximum value of A allowed by the tolerances minus the minimum value of D1 allowed by its tolerance. The minimum, nominal, and maximum values of EL are obtained in an analogous manner with C1 in the above three sentences replaced with CL, D1 replaced by D-L, and E1 replaces with E-L.

[+]These values are based on the C1 and C-L tolerances, which are under investigation.

As Figure 2 shows, the nominal value of D1 is the difference between the nominal values of B and C1. Similarly, the nominal value of D-L is the difference between the nominal values of B and C-L. The tolerances for D1 and D-L were obtained with the aid of B&W drawings 13000E and 13006E. The 0.007 inch tolerance for D1 is the sum of the 0.004 inch tolerance on the radial location of the smaller radius of the first (No. 1) fuel plate and the 0.003 inch tolerance on the radial location of the of the outer rollers at the element envelope. Similarly, the 0.010 tolerance on D-L is the sum of the 0.003 mil tolerance on the inner rollers at the element envelope and the 0.007 mil tolerance on the larger radius of the last (outermost) fuel plate. This tolerance is larger than the one for the first fuel plate because it is at the convex side of the fuel plate rather than the concave one. Since the reference points are at the concave side of the fuel plates, a tolerance on the additional fuel plate thickness is involved.

Table 2 shows the range of values possible for E1 and E-L for all three cores. When E1 is near its minimum value, E-L must be near its maximum value, and vice versa. The channel thickness tolerances are included in the thermal analysis of each core.

2. Core Configurations and Operating Conditions

For each of the three reactor cores, the core neutron physics analysis[2] considered 24 cases that together bound the worst thermal-hydraulic state for each core. These cases are summarized in Table 3 through Table 5. In these tables the cases appear in triplets, with the first case of each triplet having all four of the control blades fresh, the second case having only blades A and B fresh, and the third case having only blades B and C fresh. The upper 12 cases, the "A" cases, in each table have samples in the flux trap. The lower 12 cases, the "B" cases, have an empty flux trap.

Table 6 lists both the nominal and the limiting safety system settings (LSSS) reactor operating conditions for all three cores.

3. Thermal Criteria to Be Met

The two principal thermal criteria to be met are that flow instability and critical heat flux (CHF) must be avoided by maintaining a realistic margin to safety under all operating conditions. Either of these abnormal events can lead to a rapid increase in temperature and thereby cause fuel failure. The mechanism for flow instability is that subcooled boiling increases the hydraulic resistance in the channel, which diverts flow to the other parallel channels. The reduced flow leads to more boiling and more hydraulic resistance and thereby causes a rapid reduction in channel flow. This flow reduction excursion usually leads to CHF. When CHF occurs in this manner, the event is classified as a flow instability event rather than a CHF event. A CHF event is one where CHF occurs without a flow excursion. Correlations for predicting CHF are presented in section 6. These correlations are based on measurement in channels in which the channel flow rate is maintained. Typically, this would require taking measurements in a "stiff" single-channel system, which is by definition one in which channel flow rate is essentially insensitive to changes in channel hydraulic resistance. The distinction between a flow instability event and a CHF event is important because, in general, the uncertainty in the prediction of the channel power at which a CHF event occurs is much larger than that for the occurrence of a flow instability event.

Table 3. Summary of Power Distribution Evaluations – HEU Core

Core state that may bound power peaking				Element Burnup (MWd) at Beginning of Week						Inches withdrawn			
Case	Burnup State	Time (Days)	Flux Trap	X1 X5	X2 X6	X3 X7	X4 X8	Fresh Blades	Depleted Blades	Fresh Blades	Depleted Blades	Reg Blade	MCNP k-eff
1A	Fresh	0	Samples	0	0	0	0	A, B, C, D		12.911		10	0.99983
1A1	Fresh	0	Samples	0	0	0	0	A, B	C, D	10.307	11.307	10	1.00020
1A2	Fresh	0	Samples	0	0	0	0	B, C	A, D	10.466	11.466	10	1.00009
2A	Fresh	2	Samples	0	0	0	0	A, B, C, D		16.782		15	1.00017
2A1	Fresh	2	Samples	0	0	0	0	A, B	C, D	14.423	15.423	15	1.00002
2A2	Fresh	2	Samples	0	0	0	0	B, C	A, D	14.556	15.556	15	1.00014
3A	"Week 58"	0	Samples	0	81	65	142	A, B, C, D		17.809		10	1.00044
3A1	"Week 58"	0	Samples	0	81	65	142	A, B	C, D	15.473	16.473	10	0.99999
3A2	"Week 58"	0	Samples	0	81	65	142	B, C	A, D	15.536	16.536	10	0.99985
4A	"Week 58"	2	Samples	0	81	65	142	A, B, C, D		24.031		15	1.00020
4A1	"Week 58"	2	Samples	0	81	65	142	A, B	C, D	22.394	23.394	15	1.00014
4A2	"Week 58"	2	Samples	0	81	65	142	B, C	A, D	22.373	23.373	15	0.99993
1B	Fresh	0	Empty	0	0	0	0	A, B, C, D		13.295		10	0.99974
1B1	Fresh	0	Empty	0	0	0	0	A, B	C, D	10.694	11.694	10	1.00000
1B2	Fresh	0	Empty	0	0	0	0	B, C	A, D	10.873	11.873	10	1.00006
2B	Fresh	2	Empty	0	0	0	0	A, B, C, D		17.367		15	0.99985
2B1	Fresh	2	Empty	0	0	0	0	A, B	C, D	15.041	16.041	15	0.99993
2B2	Fresh	2	Empty	0	0	0	0	B, C	A, D	15.187	16.187	15	1.00006
3B	"Week 58"	0	Empty	0	81	65	142	A, B, C, D		18.380		10	0.99969
3B1	"Week 58"	0	Empty	0	81	65	142	A, B	C, D	16.125	17.125	10	1.00010
3B2	"Week 58"	0	Empty	0	81	65	142	B, C	A, D	16.216	17.216	10	0.99998
4B	"Week 58"	2	Empty	0	81	65	142	A, B, C, D		26.000		15	1.00029
4B1	"Week 58"	2	Empty	0	81	65	142	A, B	C, D	24.569	25.569	15	0.99988
4B2	"Week 58"	2	Empty	0	81	65	142	B, C	A, D	24.664	25.664	15	1.00016

"Samples" indicates a typical loading of samples in all three flux trap tubes
"Empty" indicates neither samples nor tubes in the flux trap (i.e., "empty island" configuration)
Full blade withdrawal is 26 inches

Table 4. Summary of Power Distribution Evaluations – FSD Core (LEU)

Core state that may bound power peaking				Element Burnup (MWd) at Beginning of Week						Inches withdrawn			
Case	Burnup State	Time (Days)	Flux Trap	X1 X5	X2 X6	X3 X7	X4 X8	Fresh Blades	Depleted Blades	Fresh Blades	Depleted Blades	Reg Blade	MCNP k-eff
5A	Fresh	0	Samples	0	0	0	0	A, B, C, D		12.267		10	1.00037
5A1	Fresh	0	Samples	0	0	0	0	A, B	C, D	9.590	10.590	10	1.00000
5A2	Fresh	0	Samples	0	0	0	0	B, C	A, D	9.749	10.749	10	0.99993
6A	Fresh	2	Samples	0	0	0	0	A, B, C, D		16.165		15	0.99998
6A1	Fresh	2	Samples	0	0	0	0	A, B	C, D	13.795	14.795	15	1.00014
6A2	Fresh	2	Samples	0	0	0	0	B, C	A, D	13.930	14.930	15	1.00004
7A	“Week 79”	0	Samples	0	116	97	199	A, B, C, D		17.020		10	1.00011
7A1	“Week 79”	0	Samples	0	116	97	199	A, B	C, D	14.679	15.679	10	1.00020
7A2	“Week 79”	0	Samples	0	116	97	199	B, C	A, D	14.705	15.705	10	0.99980
8A	“Week 79”	2	Samples	0	116	97	199	A, B, C, D		23.481		15	1.00027
8A1	“Week 79”	2	Samples	0	116	97	199	A, B	C, D	21.505	22.505	15	0.99991
8A2	“Week 79”	2	Samples	0	116	97	199	B, C	A, D	21.663	22.663	15	0.99988
5B	Fresh	0	Empty	0	0	0	0	A, B, C, D		12.647		10	0.99995
5B1	Fresh	0	Empty	0	0	0	0	A, B	C, D	9.966	10.966	10	0.99976
5B2	Fresh	0	Empty	0	0	0	0	B, C	A, D	10.166	11.166	10	1.00007
6B	Fresh	2	Empty	0	0	0	0	A, B, C, D		16.826		15	1.00021
6B1	Fresh	2	Empty	0	0	0	0	A, B	C, D	14.411	15.411	15	0.99993
6B2	Fresh	2	Empty	0	0	0	0	B, C	A, D	14.568	15.568	15	1.00000
7B	“Week 79”	0	Empty	0	116	97	199	A, B, C, D		17.632		10	1.00015
7B1	“Week 79”	0	Empty	0	116	97	199	A, B	C, D	15.283	16.283	10	1.00007
7B2	“Week 79”	0	Empty	0	116	97	199	B, C	A, D	15.396	16.396	10	1.00003
8B	“Week 79”	2	Empty	0	116	97	199	A, B, C, D		25.116		15	1.00049
8B1	“Week 79”	2	Empty	0	116	97	199	A, B	C, D	23.479	24.479	15	1.00009
8B2	“Week 79”	2	Empty	0	116	97	199	B, C	A, D	23.439	24.439	15	0.99987

“Samples” indicates a typical loading of samples in all three flux trap tubes
“Empty” indicates neither samples nor tubes in the flux trap (i.e., "empty island" configuration)
Full blade withdrawal is 26 inches

Table 5. Summary of Power Distribution Evaluations – CD35 Core (LEU)

Core state that may bound power peaking				Element Burnup (MWd) at Beginning of Week						Critical Blade Position (Inches withdrawn)			
Case	Burnup State	Time (Days)	Flux Trap	X1 X5	X2 X6	X3 X7	X4 X8	Fresh Blades	Depleted Blades	Fresh Blades	Depleted Blades	Reg Blade	MCNP k-eff
5A	Fresh	0	Samples	0	0	0	0	A, B, C, D		13.259		10	1.00016
5A1	Fresh	0	Samples	0	0	0	0	A, B	C, D	10.656	11.656	10	0.99993
5A2	Fresh	0	Samples	0	0	0	0	B, C	A, D	**10.814**	11.814	10	0.99999
6A	Fresh	2	Samples	0	0	0	0	A, B, C, D		17.193		15	0.99985
6A1	Fresh	2	Samples	0	0	0	0	A, B	C, D	14.912	15.912	15	1.00001
6A2	Fresh	2	Samples	0	0	0	0	B, C	A, D	**15.027**	16.027	15	0.99990
7A	"Week 76"	0	Samples	0	96	77	170	A, B, C, D		17.567		10	1.00008
7A1	"Week 76"	0	Samples	0	96	77	170	A, B	C, D	15.209	16.209	10	0.99975
7A2	"Week 76"	0	Samples	0	96	77	170	B, C	A, D	**15.351**	16.351	10	1.00014
8A	"Week 76"	2	Samples	0	96	77	170	A, B, C, D		24.314		15	1.00001
8A1	"Week 76"	2	Samples	0	96	77	170	A, B	C, D	22.765	23.765	15	1.00004
8A2	"Week 76"	2	Samples	0	96	77	170	B, C	A, D	**22.698**	23.698	15	0.99986
5B	Fresh	0	Empty	0	0	0	0	A, B, C, D		13.650		10	0.99998
5B1	Fresh	0	Empty	0	0	0	0	A, B	C, D	11.080	12.080	10	1.00003
5B2	Fresh	0	Empty	0	0	0	0	B, C	A, D	**11.258**	12.258	10	1.00009
6B	Fresh	2	Empty	0	0	0	0	A, B, C, D		17.891		15	0.99997
6B1	Fresh	2	Empty	0	0	0	0	A, B	C, D	15.580	16.580	15	0.99988
6B2	Fresh	2	Empty	0	0	0	0	B, C	A, D	**15.741**	16.741	15	1.00017
7B	"Week 76"	0	Empty	0	96	77	170	A, B, C, D		18.193		10	1.00013
7B1	"Week 76"	0	Empty	0	96	77	170	A, B	C, D	15.933	16.933	10	1.00012
7B2	"Week 76"	0	Empty	0	96	77	170	B, C	A, D	**16.030**	17.030	10	1.00003
8B	"Week 76"	2	Empty	0	96	77	170	A, B, C, D		26.000		15	0.99917
8B1	"Week 76"	2	Empty	0	96	77	170	A, B	C, D	25.621	26.000	15	0.99998
8B2	"Week 76"	2	Empty	0	96	77	170	B, C	A, D	**25.312**	26.000	15	0.99986

"Samples" indicates a typical loading of samples in all three flux trap tubes.
"Empty" indicates neither samples nor tubes in the flux trap (i.e., "empty island" configuration).
Full blade withdrawal is 26 inches.

Table 6. Reactor Operating Conditions

	Nominal		Limiting Safety System Settings (LSSS)	
	HEU	LEU (FSD & CD35)	HEU	LEU (FSD & CD35)
Reactor Power, MW	10.0	12.0	12.5	15.0
Pressurizer Pressure, psia	84		75	75
Temperature, °F	120		155	145
Flow (inlet), gpm	3800		3200	3300
Pressurizer Level, in.*	0		−16	−16

*Strictly speaking, this is a scram setpoint rather than an LSSS value.

4. Replication of the Existing HEU Steady-State Thermal Analysis

In 2011, Appendix F, *Safety Limit Analysis for the MURR*, of Addendum 4 of the MURR Hazards Summary Report, was revised and attached to a letter sent to the US NRC.[3] Appendix F was revised to correct an error found in the original analysis. The steady-state thermal-hydraulic analysis used in the production of the revised appendix was a collaborative effort between the MURR staff and the staff of the Argonne National Laboratory (ANL). Values of allowed reactor power were determined for 180 combinations of three pressurizer pressures, six coolant inlet temperatures, and ten reactor coolant flow rates. The revised Appendix F demonstrates that the existing model in the MURR SAR is well understood and can be easily duplicated.

5. Correlations for Predicting Flow Instability Power

The Whittle and Forgan correlation will be used to predict the margin to flow instability.[4] The form of the correlation used in the analysis is as follows:

$$\frac{T_{allowed}-T_{inlet}}{T_{sat}-T_{inlet}} = \frac{1}{1+\eta\frac{D_h}{L_h}} \tag{1}$$

where $T_{allowed}$ is the bulk coolant exit temperature at which flow instability is predicted to be initiated; T_{sat} is the coolant saturation temperature at the exit; T_{inlet} is the coolant inlet temperature; D_h and L_h are the heated diameter (4 times the flow area divided by the heated perimeter) and heated length of the channel, respectively; and η is an adjustable parameter, for which a value of 32.5 is used. Reference 5 performed a statistical analysis of the 74 applicable experiments in Reference 4 and found that there is a 95% confidence interval that 95% of the rectangular channel data measured by future Reference 4 type of measurements will not exceed an η value of 31.09. Thus, the 32.5 value of η is slightly larger than it needs to be to achieve these statistical parameters. The reactor power used in the thermal-hydraulic

analysis is adjusted until the lowest power that achieves flow instability in at least one coolant channel is found.

In the existing MURR Hazards Summary Report it is assumed that flow instability will not occur in a coolant channel if bulk boiling at the channel exit is avoided and each local value of heat flux is less than half of the corresponding value of critical heat flux as predicted by the Bernath correlation[6]. This two-part criterion is based on measured data reported by Croft[7] in 1964 for electrically-heated channels that were designed to simulate Advance Test Reactor (ATR) channels. Croft observed that in 0.094-inch thick rectangular channels, flow instability occurred when the heat flux at any axial location in the heated channel reached about 60% of the value of critical heat flux as predicted by the Bernath correlation for that location or bulk boiling occurred at the exit. Croft postulated that burnout occurred by a process referred to as "hydraulic instability or autocatalytic vapor binding" which was seen as a form of critical heat flux (CHF) that occurred prematurely. MURR chose to use a more restrictive value of 50% instead of 60%. Requiring a heat flux that is 50% of the CHF is the same as requiring a CHF ratio, i.e., ratio of CHF to heat flux, of 2.0.

Waters[8] also used tests in electrically heated channels to measure the onset of fuel burnout caused by flow instability in the Advanced Test Reactor (ATR). The ATR fuel elements are thermal-hydraulically similar to those in the MURR reactor. However, the ATR heated length is 48 inches, which is twice that of the MURR. Reference 9 showed that equation 1 with a value of η of 32.5 accurately predicts flow instability in the Croft and the Waters experiments.

A commonly used method of predicting flow instability is to assume that it occurs at the onset of significant voids as predicted by Saha and Zuber[10]. This can be written as:

$$q''_{allowed} = \begin{cases} 455\ \frac{k\,(T_{sat} - T_{bulk})}{D_e}, & \text{if } Pe \leq 70{,}000 \\ 0.0065\ G\ c_p\ (T_{sat} - T_{bulk}), & \text{if } Pe > 70{,}000 \end{cases} \tag{2}$$

where $q''_{allowed}$ is the maximum allowed heat flux, which is where the onset of significant voids occurs, k is the thermal conductivity of the coolant, T_{sat} is the saturation temperature, T_{bulk} is the bulk coolant temperature, D_e is the hydraulic diameter, G, is the mass flux, or flow per until area, Pe is the Peclet number, which is the product of the Reynolds and Prandtl numbers, and c_p is the specific heat capacity at constant pressure. Equation 2 is used to determine the allowed heat flux at each axial level of the channel. Flow instability is assumed to occur if at any level the heat flux exceeds the allowed heat flux. This correlation tends to be less limiting than equation 1.

It is instructive to compare the half-of-Bernath-CHF predictions and the equation 2 Saha-Zuber flow instability predictions with those obtained by equation 1. This is done in section 16a where the flow instability performance of the limiting channel, as predicted by the above three criteria, is compared, for the limiting case of each of the three cores.

6. Correlations for Predicting Critical Heat Flux

6a. Extended Groeneveld 2006

If flow instability is prevented or is assumed not to occur, the MURR core potentially could experience a subcooled CHF (critical quality X < 0). The calculations that follow explore this scenario. The recent subcooled critical heat flux (CHF) literature was searched and evaluated, and the Groeneveld 2006 CHF Table[11] with a new diameter correction[12], equation 3, was selected as the most reliable for predicting CHF in the MURR steady-state thermal-hydraulic analysis. The diameter correction in equation 3 (n = 0.312) was recommended by Celata (1994)[13], Hall and Mudawar (2000)[12], and finally by the exhaustive review of Tanase et al. (2009)[14] with Groeneveld as co-author. The first term in equation 3, $q_c(0.008,P,G,X)$, is obtained from a look-up table that is basically a normalized data bank of CHF for a vertical 0.008-m-diameter water-cooled tube. The 2006 table provides CHF values at 24 pressures, 20 mass fluxes, and 23 qualities, covering the ranges 1 to 210 bars pressure, 0 to 8000 kg/m^2-s mass flux, and -0.5 to 1.0 critical quality. The 2006 table is derived from a world-class database containing 33175 measured CHF data points, out of which 8394 "bad" data points due to flow instability or poorly performed experiments were not used. It is the combined database[11] created by the Atomic Energy of Canada, Limited (AECL), Canada, and the Institute of Physics and Power Engineering (IPPE), Russia. The RMS (root-mean-square) error reported by Groeneveld et al.[11] for subcooled CHF is 14.7% if the 2006 table is used with the DSM (direct substitution method), and 7.1% if the 2006 table is used with the HBM (heat balance method). The factor $(G/8000)^{0.376}$ in equation 3 uses $q_c(0.008,P,8000,X_0)$ and extends the application of the 2006 table to mass fluxes greater than 8000 kg/m^2-s, using the same mass flux-dependence of CHF as in the Hall-Mudawar subcooled correlation[12] (discussed below).

$$q_c(D,P,G,X_o) = \begin{cases} q_c(0.008,P,G,X_o)\left(\dfrac{0.008}{D}\right)^n & \text{if} \quad G \le 8000 \\ q_c(0.008,P,8000,X_o)\left(\dfrac{0.008}{D}\right)^n\left(\dfrac{G}{8000}\right)^{0.376} & \text{if} \quad G > 8000 \end{cases} \tag{3}$$

where

q_c = Critical heat flux, kW/m^2

n = 0.312

D = Diameter of the tube, m. As discussed below, it is in general the heated diameter of the channel, given by (4 x flow area/heated perimeter). Note that the heated diameter equals the tube diameter for a circular tube heated over the whole perimeter.

P = Coolant pressure, bar

G = Coolant mass flux in the channel, kg/m^2-s

X_o = Equilibrium quality at the CHF location (critical quality)

Range of application: $3 < D < 25$ mm , $L/D > 25$ for subcooled CHF, $T_i > 0.01$ °C,
$1000 < G < 30{,}000$ kg/m^2-s , $L/D > 50$ for saturated CHF, $-0.5 < X_o < 1.0$,
$1.0 \le P \le 210$ bar
L is the heated length.
T_i is inlet temperature.

As mentioned, this CHF prediction method was selected as the most reliable on the basis of our review and comparison of 12 recent CHF correlations subsequent to the Sudo-Kaminaga correlation[15] which is reported to be based on a mixture of CHF and flow instability test data. These correlations include the Hall-Mudawar (2000) [12,16] , Sarma (2006)[17,18], Kureta-Akimoto (2002)[19], Caira (1995)[20], Lombardi (1995)[21], and Yagov (1996)[22] correlations. The review found that in addition to the AECL-IPPE database[11], Hall and Mudawar[16,12] have assembled all the measured CHF data in the world literature dating back to 1949, have checked each data point by heat balance for error, have independently developed another world-class database containing 32544 data points (4860 subcooled CHF data), and, using the database, have assessed 82 subcooled CHF correlations and ranked them in the order of reliability (ranking the Bernath correlation[6] as 43rd). This database is called the Purdue University-Boiling and Two Phase Flow Laboratory (PU-BTPFL) database[16]. The Hall-Mudawar inlet conditions subcooled CHF correlation (H-M ICC), equation 4, is derived from this database. All other CHF correlations are based on medium-size (1000 to 3000 CHF data points) or smaller databases.

$$\frac{q_c(D_h, P, G, L_h, X_i^*)}{G\, h_{fg,o}} = \frac{C_1 \left(\dfrac{G^2 D_h}{\rho_f\, \sigma}\right)^{C_2} (\rho_f/\rho_g)^{C_3} \left[1 - C_4 (\rho_f/\rho_g)^{C_5} X_i^*\right]}{1 + 4 C_1 C_4 \left(\dfrac{G^2 D_h}{\rho_f\, \sigma}\right)^{C_2} (\rho_f/\rho_g)^{C_3 + C_5} (L_h/D_h)} \qquad \text{(RMS error = 14.3\%)} \qquad (4)$$

where
C_1, C_2, C_3, C_4, C_5 = 0.0722, –0.312, –0.644, 0.900, 0.724, respectively
L_h , D_h = Heated length and heated diameter, m
$G^2 D_h / (\rho_f\, \sigma)$ = Weber number
$h_{fg,o}$ = Heat of vaporization at the heated length exit (CHF location), kJ/kg
$h_{f,o}$ = Saturated liquid enthalpy at the heated length exit (CHF location), kJ/kg
h_i = Inlet enthalpy, kJ/kg
X_i = Inlet quality = $(h_i - h_{f,i})/h_{fg,i}$
X_i^* = Pseudo-inlet quality = $(h_i - h_{f,o})/h_{fg,o}$
ρ_f , ρ_g = Densities of saturated liquid and saturated vapor, kg/m^3
σ = Surface tension, N/m
Range of application: $0.25 \le D_h \le 15$ mm , $6 \le L/D_h \le 200$, $300 \le G \le 30{,}000$ kg/m^2-s ,
$1.0 \le P \le 200$ bar , $-2.0 \le X_i \le 0.0$, $-1.0 \le X_o \le 0.0$

The CHF correlation selection criterion used is: If these two world-class prediction methods (the H-M ICC and the 2006 table) closely agree, then both are equally the most reliable. These two CHF prediction methods were compared at six pressures (1, 5, 10, 20, 30, and 50 bar) for $-0.5 \le X \le 0$, $1000 \le G \le 8000$

kg/m^2-s, assuming three inlet temperatures 30, 50, and 70 °C. The heated length used in equation 4 for each CHF value in the 2006 table was found by heat balance. Figure 3 shows the comparison. The RMS difference between the two is 18%, 15.4%, 12.3%, 10.8%, 9.9%, 6.9% at the six pressures (1, 5, 10, 20, 30, and 50 bar); the maximum difference in CHF for $L_h/D_h > 15$ is 33%. Based on this close agreement between the two, each is considered to be equally the most reliable subcooled CHF prediction method. The comparison of the Groeneveld 2006 CHF Table with some correlations derived from medium-size CHF databases (e.g., the Caira[20], Lombardi[21], and Sarma[17,18] correlations) shown in Figure 4 adds further confidence to the reliability of the Groeneveld 2006 Table[11] and the H-M ICC[12].

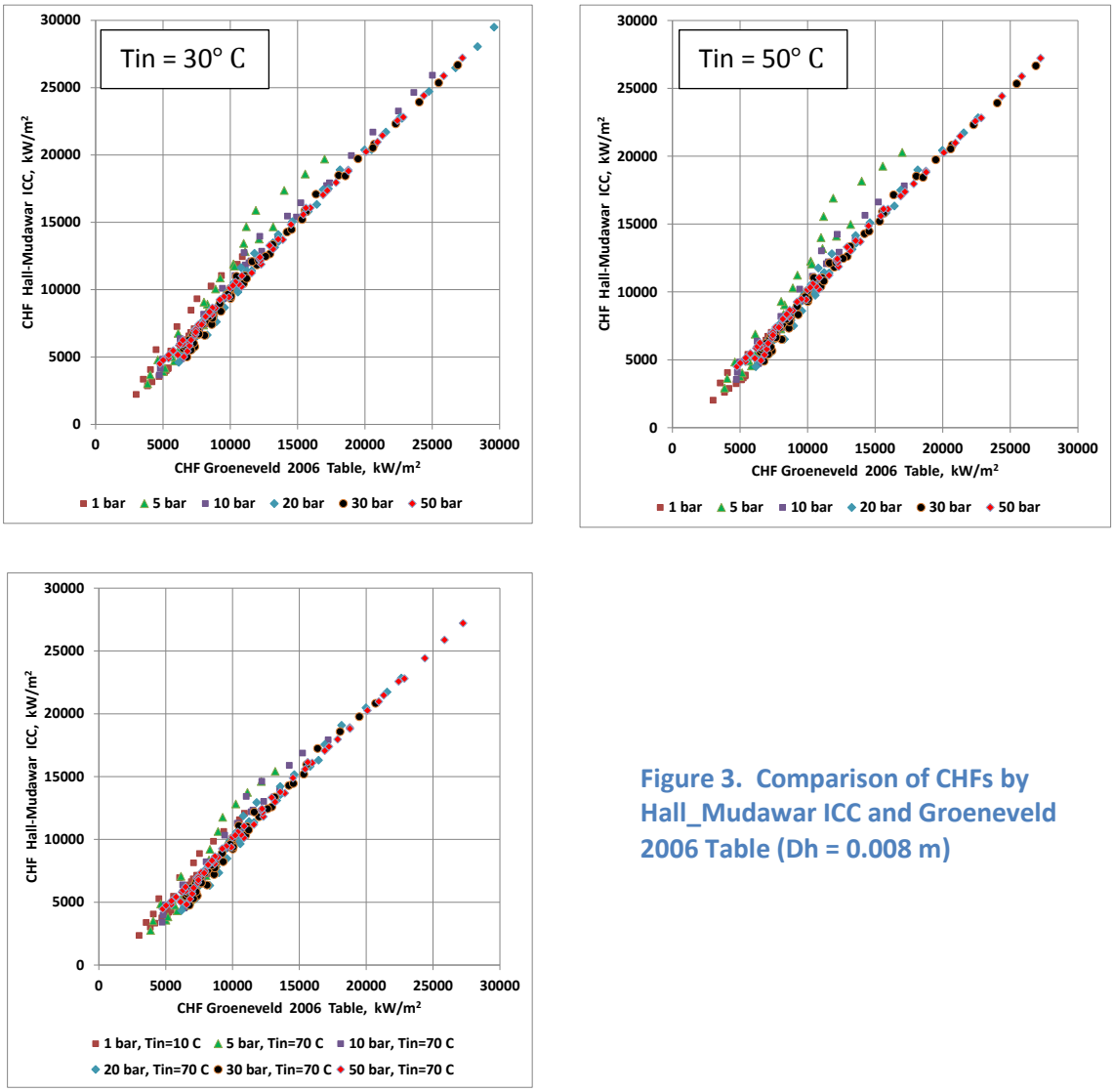

Figure 3. Comparison of CHFs by Hall_Mudawar ICC and Groeneveld 2006 Table (Dh = 0.008 m)

The AECL-IPPE and PU-BTPFL databases, the H-M ICC, and the Groeneveld 2006 Table are all developed for round tubes with uniform heat flux over the full wetted perimeter of the heated length. However, based on the works of Mishima and Nishihara (1987)[23] and Pioro et al.(1999)[24] with Groeneveld as co-author, these prediction methods are applicable to non-circular geometry at water velocities greater than approximately 2 m/s. In addition to this, based on the work of Zhang et al. (2007)[25] with Mudawar

as co-author, a dimensionless CHF correlation (developed originally for uniform heat flux on the full wetted perimeter) is applicable with acceptable accuracy to channels with heating on only part of the wetted perimeter if the heated diameter is used instead of the hydraulic diameter in the Weber number (but not in the Reynolds number). Therefore, by using the heated diameter instead of the tube diameter, both CHF prediction methods are applicable to non-circular geometries with heating on only part of the perimeter.

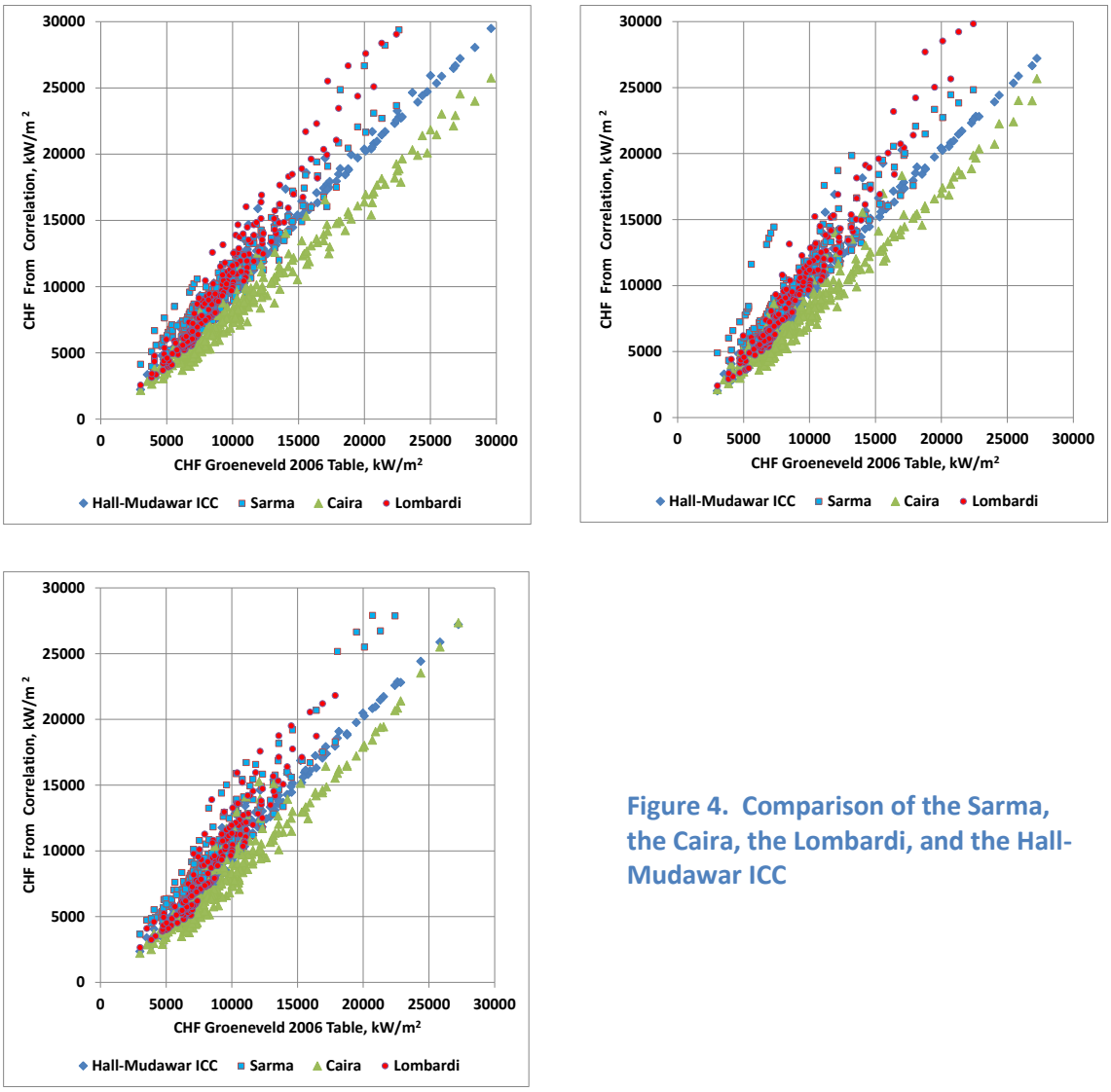

Figure 4. Comparison of the Sarma, the Caira, the Lombardi, and the Hall-Mudawar ICC

Based on the Hall-Mudawar outlet conditions correlation[12] , the Groeneveld 2006 Table is extended to a maximum mass flux (G) of 30,000 kg/m^2-s by multiplying the tabulated CHF at 8000 kg/m^2-s by a factor of $(G/8000)^{0.376}$. The subcooled CHF varies as $G^{0.376}$ in the Hall-Mudawar outlet conditions correlation, as $G^{0.4}$ in the Inasaka-Nariai correlation[26, 27], and as $G^{0.5}$ in the Celata correlation[28,29]. These three are outlet conditions correlations like the Groeneveld table. The recommended value, 0.376, for the exponent of G is the smallest and most conservative of the three values.

The Groeneveld 2006 Table, equation 3, is currently preferred over the Hall-Mudawar inlet conditions subcooled CHF correlation, equation 4, for use in the U.S. High-Power Research Reactor thermal-hydraulic analysis due to several considerations. These include (1) the ease of treating axially non-uniform heat flux and accounting for hot channel factors based on the local conditions hypothesis, (2) the fact that the Groeneveld table has been evaluated and revised three times at 10-year intervals since 1986 adds to its reliability, and (3) in addition to the subcooled CHF, the Groeneveld table also includes CHF for saturated conditions. The Hall-Mudawar correlation does not include saturated conditions.

6b. Bernath CHF Correlation

In assessing the margin to flow instability, the existing MURR SAR limits the local value of heat flux to half of the corresponding Bernath critical heat flux based on the local values of channel velocity, temperature, and channel exit pressure. Thus, the existing MURR HEU core flow instability criterion requires that the Bernath CHF ratio be no less than 2.0. The margin to CHF is described in Chapter 4 of the MURR SAR [30] in section 4.6.3, Safety Limit Analysis, in the middle of page 4-56, where this relationship is observed in asserting that a CHF ratio of at least 2.0 is maintained. (There, the term "departure from nucleate boiling", DNB, in used in place of the term "critical heat flux". For all practical purposes DNB is equivalent to CHF, and the two terms are used interchangeably here.) Below, in section 16d, the allowed CHF power based on the limiting channel, as predicted by both equation 3 and the Bernath CHF correlation, are compared for the limiting case of each of the three cores. The limiting channel is the one in which the extended Groeneveld 2006 CHF criterion predicts a CHF ratio of 1.0 to occur first. In addition, the Bernath CHF analysis is repeated to determine the power at which the minimum Bernath CHF ratio is 2.0. This power is significantly more than twice the power at which a Bernath CHF ratio of 1.0 is predicted to occur.

6c. Sudo and Kaminaga CHF Correlation

The CHF correlation of Sudo and Kaminago[15,31] is sometimes used in the assessment of CHF in research reactors. It is a relatively recent correlation that was developed for analyzing flow in rectangular research reactor channels. However, page 429 of Reference 15 indicates that in developing their CHF correlation, Sudo and Kaminaga included flow excursion data with CHF data. This is not a problem for reactors where CHF occurs at a lower power than does flow instability or where the flow instability power is at least twice the reactor LSSS power. However, in the MURR, flow instability is predicted to occur before CHF and the flow instability power is much less than twice the reactor power. For the limiting CD35 core configuration based on the use of equation 3, the margin to CHF based on the Sudo and Kaminaga correlation was also calculated. The power which at CHF is predicted to occur based on the Sudo and Kaminaga correlation is only 6.4% greater than the power at which equation 1 predicts flow instability to occur. Although fuel failure due to flow instability can be just as destructive as fuel failure due to CHF, there is a large difference from a regulatory perspective. Since it is deemed that flow

instability can be more accurately predicted than can CHF, the required safety margin to flow instability is much smaller than that to CHF.

7. Nusselt Number Correlation for Predicting Film Coefficient

The Dittus-Boelter Nusselt number correlation with an added factor of $(\mu_b/\mu_w)^{0.11}$, where μ_b is the viscosity of the coolant evaluated at the bulk coolant temperature and μ_w is the viscosity of the coolant evaluated at the wall temperature, was used in the analysis. The viscosity ratio factor is to account for the potentially large variation in coolant viscosity over the coolant channel cross section at a specific axial level. Thus, the Nusselt number, Nu, used in the analysis is:

$$\mathrm{Nu}=0.023\ \mathrm{Re}^{0.8}\mathrm{Pr}^{0.4}\left(\frac{\mu_b}{\mu_w}\right)^{0.11} \tag{5}$$

where Nu is defined as $h\ D_e / k$, Re is the Reynolds number, $\rho\ V\ D_e / \mu_b$, and Pr is the Prandtl number, $\mu_b\ c_p / k$. Here h is the film coefficient, ρ is the bulk coolant density, V is the mean coolant velocity over the flow cross section, and D_e is hydraulic diameter, c_p is specific heat capacity of the bulk coolant, and k is the thermal conductivity of the bulk coolant.

Although the film coefficient has a substantial effect on the temperatures within the fuel plate, it has only a second-order effect on flow instability and CHF. This is because it only affects how the power generated within a fuel plate is split between the two channels on either side of the fuel plate.

8. Hot Channel Factors

Hot channel factors are used in the thermal-hydraulic analyses in order to take into account the potential adverse effects of manufacturing tolerances and uncertainties in modeling on the quantities being predicted for safety analysis purposes. For example, a coolant channel may be thinner than its nominal value. A thinner channel would result in a lower coolant velocity than in a nominal channel. It would also have a lower flow rate due to both the lower velocity and the smaller flow area. The lower flow rate, in turn, would increase the channel bulk coolant temperature rise and could also reduce the film coefficient at the bounding fuel plate surfaces. In the analysis, separate hot channel factors are introduced for the effect on coolant velocity, for the effect on bulk coolant temperature rise, and for the effect on film coefficient. Each of these hot channel factors would have values greater than 1.0. The bulk coolant temperature rise and the film temperature rise would each be multiplied by their hot channel factors. The velocity would be divided by its hot channel factor. The hot channel factor is always used as a multiplicative factor or a divisor, depending on which choice represents an adverse effect.

Typically, a nominal analysis is performed first. Then the hot channel factors are applied to each channel individually. If instead, all of the channels were assumed to be simultaneously at the minimum thickness that their tolerances permit, much of the effect on flow would be masked. Since the total reactor flow rate is assumed to be a known value, narrowing all of the channels at the same time would not redirect flow away from any one channel. Much of the effect would appear as a greater core pressure drop and no change in channel flow rate. First a nominal analysis is performed in which the individual channel flow rates are determined with all channels assumed to be at their nominal thicknesses. Then the adverse effects on velocity, bulk coolant temperature, and fuel plate surface temperature are captured via three separate hot channel factors, which are applied to the velocities, bulk coolant temperature rises, and fuel plate surface temperature rises that are obtained in the nominal analysis.

8a. Local Hot Channel Factor Contributors

The five local contributors to hot channel factor that were considered in the analysis are:

- Fuel meat thickness and ^{235}U homogeneity (Local)
- ^{235}U fuel plate loading
- Power density
- Channel thickness
- Flow distribution

Each of these five contributors is a random effect that can affect one fuel plate or channel, without affecting another. This is to be contrasted with a global factor such as an uncertainty in film coefficient due to the choice of Nusselt number correlation, discussed later, which can adversely affect the film temperature rise at all fuel plate surfaces simultaneously. The first three contributors affect heat flux. The remaining two contributors affect channel flow rate.

<u>Fuel Meat Thickness and ^{235}U Homogeneity (Local)</u>

The combined effect of the local fuel meat thickness and ^{235}U homogeneity are measured together by the fuel plate manufacturer. Radiographs of every fuel plate are taken by sending gamma rays through the thickness of the entire fuel plate. The relative amount of uranium within a specified area is detected by how dark the area appears on the radiograph for the plate. The darkness of the area is compared to a standard, which is an absolute standard that is the same for each plate of the same nominal fuel meat thickness. This method of measurement combines the local effects of fuel meat thickness and uranium density. In Table 1 on p. iii of Reference 32 a tolerance value of ±20% is provided for the HEU fuel and ±15% for the LEU fuel. Both of these tolerance values are over a 0.50-inch diameter area. In the thermal analysis this tolerance has a direct effect on local heat flux, but essentially no effect on channel bulk coolant temperature rise.

^{235}U Fuel Plate Loading

There is a tolerance on the total ^{235}U fuel plate loading within a fuel plate, which is not a local or spot tolerance. Table 1 on p. iv of Reference 32 indicates that for the HEU fuel this tolerance is ±1%. The same location in Table 1 also provides values for the LEU FSD design, which differ plate by plate. The basis for these LEU values is a ±1 mil (1 mil = 0.001 inches) tolerance on the thickness of the fuel meat. This is shown in Figure 1 of the reference and in Table 1 on the top of p. iii of the reference. Thus, the fuel meat can be as much as 1 mil thicker than its nominal value over the entire fuel length. Hence, the fuel meat of plate 1 of the LEU FSD design, which is nominally 9 mils thick, can be between 8 and 10 mils thick. This represents a tolerance of ±1/9 = ±11%. Due to self-shielding effects, a tolerance of ±11% will cause less than ±11% variation in plate heat flux. This was studied with the MCNP code[33]. The results are provided in Table 7 and Table 8 for the LEU FSD and LEU CD35 designs, respectively. In the thermal analysis, the power overload fraction in percent was rounded up to the nearest whole percent, as indicated in these tables. Also, the results for plates 3 through 23 of the FSD design are based on MCNP analysis of plate 3. Similarly, the results for plates 4 through 22 of the CD35 design are based on MCNP analysis of plate 4. In the thermal analysis this tolerance has a direct effect on bulk coolant temperature rise. It has no effect on local heat flux, which is a local effect that is fully taken into account in the combined tolerance of the local fuel meat thickness and uranium homogeneity that is measured by radiography.

Table 7. LEU FSD Plate Overload Tolerance Fractions, %

Plate	Meat Thickness, mils	Overload Tolerance Fraction, %	
		Calculated	Used
1	9	7.1	8.0
2	12	6.0	6.0
3 - 23	18	2.6	3.0
24	17	3.6	4.0

Table 8. LEU CD35 Plate Overload Tolerance Fractions, %

Plate	Meat Thickness, mils	Overload Tolerance Fraction, %	
		Calculated	Used
1	9	8.5	9.0
2	12	6.2	7.0
3	16	5.4	6.0
4 - 22	20	3.4	4.0
23	17	3.9	4.0

Power Density

In spite of the considerable geometric and analytical detail that goes into determining the three-dimensional distribution of power throughout the core with the aid of the MCNP code,[2] there is some uncertainty in the calculated power density distribution. For the HEU core and for both LEU cores the power density tolerance is assumed to affect the values of heat flux by ±10%. This value is based on a combination of judgment and analysis. Part of this uncertainty is due to potential variations in the distribution of the fuel as allowed by fuel element manufacturing tolerances and clearances in the core to facilitate fuel element insertion and removal. In the MURR feasibility report[1] the effects of 0.008-inch changes in channel thicknesses and 0.015-inch movements of entire elements on individual fuel plate

powers were studied for the FSD core design and were found to be no more than about ±2%, which is well within the ±10% tolerance assumed.

Channel Thickness

Variations in channel thickness can be due to tolerance in the as-built fuel plate thickness, to fuel swelling and cladding oxidation, and to variations in the fuel plate spacing during fuel element manufacture. For thin rectangular channels for which the hydraulic diameter is approximately twice the channel thickness and where the flow is turbulent with friction factor approximated as, $f = Re^{-\alpha}$, where Re is Reynolds number, Reference 34 shows that the hot channel factor component for velocity, F_V, is:

$$F_V = \left(\frac{t_{nom_chan}}{t_{hot_chan}}\right)^{\frac{1+\alpha}{2-\alpha}} \tag{6}$$

where t_{nom_chan} is the nominal thickness of the channel and t_{hot_chan} is the minimum thickness of the channel. The Reynolds number exponent, α, is normally between 0.20 and 0.25 for turbulent flow. In the hydraulic analysis, 0.25 is used. Equation 6 is based on the perturbation in the flow rate of a single channel due to a decrease in channel thickness from t_{nom_chan} to t_{hot_chan} with no change in pressure drop between the inlet and outlet of the channel. , F_V, is the ratio of the velocity through the channel when the channel thickness is at its nominal value to the velocity through the channel when the channel thickness is at its minimum value.

Similarly, the ratio of the nominal channel flow rate to the hot channel flow rate, F_W, which is a hot channel factor component for flow rate, is the product of F_V and the ratio of the nominal channel flow area to the hot channel flow area, i.e., $t_{nom_chan} / t_{hot_chan}$. Hence,

$$F_W = \left(\frac{t_{nom_chan}}{t_{hot_chan}}\right)^{\frac{3}{2-\alpha}} \tag{7}$$

Reference 34 shows that the hot channel factor component for film coefficient, F_h, is:

$$F_h = \left(\frac{t_{nom_chan}}{t_{hot_chan}}\right)^{\frac{0.4+\alpha}{2-\alpha}} \tag{8}$$

This relationship is based on the Dittus-Boelter Nusselt number correlation.

Table 1 provides the nominal thickness of all of the channels for all three cores to be analyzed. All of the channels that are not end channels have a channel thickness tolerance of ±8 mils. The minimum channel thickness for the end channel nearest the flux trap (channel 1) is shown in Table 2 as “Min. E1”. Similarly, the minimum channel thickness for the end channel furthest from the flux trap is shown in Table 1 as “Min. E-L”. As can be seen from the values in Table 2, the minimum value of the end channel

nearest the flux trap is always 22 mils less than its nominal ("Nom. E1") value and the minimum value of the end channel furthest from the flux trap is always 25 mils less than its nominal ("Nom. E-L") value.

Flow Distribution

For a series of parallel channels all of equal thickness, slight variations in manufacturing that are not captured by the tolerances and other effects that are not captured by the analytical methods can lead to variations in flow among the channels. For example, the hydraulic analysis uses Moody friction factors that are obtained from the Colebrook equation and are a function of Reynolds number and relative roughness. The surface roughness is an empirically determined quantity and the Colebrook equation is a fit to empirical data. For the HEU core and for both LEU cores the uncertainty in flow rate due to uncertainty in flow distribution is assumed to be ±15%. This is based on judgment. The Oregon State University Hydro-Mechanical Fuel Test Facility (OSU-HMFTF) is to be used to measure individual channel flow rates and pressure drops in a full-scale mock-up of an LEU CD35 element for which the as-built channel thicknesses and fuel plate surface roughness can be accurately measured. A careful comparison of these measurements with predictions based on hydraulic fundamentals may provide guidance regarding the adequacy of the assumed ±15% tolerance.

Table 1 of Reference 32 near the bottom of page v indicates that the "Measured Flow Disparity with MURR Element" has a worst case flow reduction factor of 0.82 for the HEU fuel and 0.86 for the LEU (FSD) fuel. By definition, $(1/0.82 - 1) \times 100\% = 22\%$ and $(1/0.86 - 1) \times 100\% = 16\%$, should correspond to the ±15% flow distribution tolerance. However, the values in the Reference 32 table have been reassessed and ±15% is now the replacement value for both values of flow distribution tolerance.

8b. Evaluating and Combining Local Hot Channel Factor Components

Table 9 provides a sample hot channel factor calculation for channel 23 and plate 23 of the LEU CD35 core. Channel 23 is between fuel plates 22 and 23. The first column lists the local hot channel factors contributors. The second column lists the tolerance fractions. The 0.50 values in the third column represent the effect that the contributor has on the bulk coolant temperature rise. In the hot channel factor calculation, where there are two fuel plates bounding a channel, each is assumed to contribute equally to the channel bulk coolant temperature rise. This is to be contrasted with an end channel for which the single bounding fuel plate contributes 100% to the channel bulk coolant temperature rise. The remaining columns in the table list five hot channel factor components. These factor components, in order from left to right, are for the film temperature rise on the convex side of plate 22, the bulk coolant temperature rise of channel 23, the film temperature rise on the concave side of plate 23, the heat flux of plate 23, and the coolant velocity of channel 23.

Table 9. Sample Hot Channel Factor Calculation for Channel 23 and Plate 23 of the LEU CD35 Core

Local Contributor	Tolerance, Fraction	Effect on Bulk ΔT, Fraction	Plate 22 Film ΔT, F_{FILM}	Channel 23 Bulk ΔT, F_{BULK}	Plate 23 Film ΔT, F_{FILM}	Plate 23 Heat Flux, F_{FLUX}	Channel 23 Velocity, $F_{VELOCITY}$
Fuel Meat Thickness & ^{235}U Homogeneity (Local) for Plate 22	0.15		1.15				
Fuel Meat Thickness & ^{235}U Homogeneity (Local) for Plate 23	0.15				1.15	1.15	
^{235}U Loading for Plate 22	0.04	0.50		1.020			
^{235}U Loading for Plate 23	0.04	0.50		1.020			
Power Density for Plate 22	0.10	0.50	1.10	1.050			
Power Density for Plate 23	0.10	0.50		1.050	1.10	1.10	
Channel Thickness (See below.)			1.034	1.167	1.034		1.066
Flow Distribution	0.15		1.118	1.15	1.118		1.15
Uncertainties Combined Multiplicatively			**1.46**	**1.54**	**1.46**	**1.27**	**1.23**
Uncertainties Combined Statistically			1.22	1.24	1.22	1.18	1.16

Channel Thickness, mils	
Nominal Channel	93
Tolerance	8
Swelling & Oxide	0
Hot Channel	85
Thickness Ratio, Nominal/Hot	1.094

In the first column each of the first three contributors listed above, which are fuel meat thickness and ^{235}U homogeneity (local), ^{235}U fuel plate loading, and power density, appears twice, once for each of the two fuel plates that bound channel 23. A 15% increase in the power generated at a particular location of the fuel plate is assumed to cause a 15% increase in the local heat flux exiting both surfaces of the fuel plate. This will cause a 15% increase in the local film temperature rise on each side of the fuel plate. This explains the three 1.15 factors shown in the second and third rows of the table. Since a local variations in heat flux should have a negligible effect on the overall bulk coolant temperature rise, F_{BULK} is not impacted by this local 15% tolerance.

The ^{235}U loading and the power density contributors each increase the total power produced by each fuel plate. Therefore, they both increase the bulk coolant temperature rise. A 4% ^{235}U loading tolerance from one of two fuel plates that heat a channel causes a 2% increase in the coolant temperature rise. Hence, it contributes a factor of 1.02 to F_{BULK}. Similarly, a 10% power density tolerance contributes a factor of 1.05 to F_{BULK}. The power density increases the local heat flux in the same manner that the fuel meat thickness and ^{235}U homogeneity does and similarly impacts F_{FILM} and F_{FLUX}. However, the ^{235}U loading does not contribute to F_{FILM} and F_{FLUX}. The reason is, as explained earlier, that in the radiography measurements fuel meat thickness and uranium homogeneity is measured against an absolute standard that includes the effect of uranium loading. Thus, if a ^{235}U loading factor were included here, the effect of this tolerance would be included twice.

As shown in the small subsection at the bottom of Table 9, the nominal thickness of channel 23 is 93 mils and the tolerance is 8 mils. In this example there is no reduction in channel thickness due to fuel swelling or oxide buildup. Thus, the hot channel thickness is 93 – 8 mils, or 85 mils, and the ratio of the nominal channel thickness to the hot channel thickness is 93/85, or 1.094. This ratio is used in equations 6, 7, and 8 with an α of 0.25 to obtain components of $F_{VELOCITY}$, F_{BULK}, and F_{FILM}, respectively. As shown in the "Channel Thickness" row in the table, the component for $F_{VELOCITY}$ which is based on the equation for F_V, is 1.066, the one for F_{BULK}, which is based on the equation for F_W, is 1.167, and both of the ones for F_{FILM}, which is based on the equation for F_h, are 1.034.

Taken by itself, the flow distribution tolerance of 15% would cause the nominal values of velocity and flow rate to each be divided by a factor of 1.15. Dividing the flow rate by a factor of 1.15 increases the bulk coolant temperature rise by the same factor. Hence, in the "Flow Distribution" row of Table 9, F_{BULK} and $F_{VELOCITY}$ are each 1.15. The 1.118 factor in the same row for the two values of F_{FILM} is $1.15^{0.8}$. This is because in the Dittus-Boelter correlation for Nusselt number, the film coefficient is proportional to flow rate raised to the 0.8 power.

Accepted practice in the safety analysis of research reactors is to use a statistical combination of the hot channel factor components. The probability distributions used in the statistical combination permit the full range of the tolerances, including both the positive and the negative sides. This includes the possibility of one variable being near the most beneficial extreme of its tolerance while another is near its most adverse extreme. By contrast, the multiplicative combination of hot channel components can

be much more limiting than the statistical one because the multiplicative combination assumes that all of the hot channel factor contributors occur simultaneously at their most adverse extreme of their tolerances and that they occur at the most limiting location in the core.

For the statistical combination, the value of each component listed in Table 9 represents a specific number of standard deviations of the component's probability distribution function. These component probability distribution functions are to be combined. If all of these distribution functions are normally distributed and independent of each other and, in addition, the temperature rise, velocity, or heat flux being studied is formed as a product of terms, then the root-mean-square of the component errors is the same number of standard deviations for the combined probability distribution function. For example, for the combined tolerance fraction for F_{FILM} for the convex side of plate 22 in the LEU CD35 core, Table 9, is $[(1.15 - 1.00)^2 + (1.10 - 1.00)^2 + (1.034 - 1.000)^2 + (1.118 - 1.000)^2]^{1/2} = [0.15^2 + 0.10^2 + 0.034^2 + 0.118^2]^{1/2} = 0.22$. Therefore, the combined value of this F_{FILM} is 1 + 0.22, which is 1.22, as shown in Table 9. This is to be compared with its multiplicative counterpart. As the name implies, the multiplicative combination is the product of all of the contributing components, i.e., product of 1.15, 1.10, 1.034, and 1.118, which, as shown in Table 9, is 1.46.

For LEU core CD35, the combined components of F_{FILM} for the convex side of plates 22, of F_{FILM} for the concave side of plate 23, of F_{BULK} and $F_{VELOCITY}$ for channel 23, and of F_{FLUX} for plate 23 are shown near the bottom of Table 9 for both the multiplicative and statistical combination methods described above. The same methods were repeated for all of the fuel plates and all of the coolant channels of all three cores. Table 10 through Table 12 provide values of combined hot channel factor for the HEU, LEU FSD, and the LEU CD35 core, respectively, for the case of no fuel plate swelling or oxide growth. All of the rows in Table 10 for channels (or plates) 2 through 24 are identical.

The multiplicative combination of hot channel factor components is employed in the MURR Safety Analysis Report[30]. Using the multiplicative combination of hot channel factor components in the current analysis facilitates more direct comparisons between the earlier analysis and the current one. An important acceptance criterion for the LEU core that is to replace the HEU core is that the thermal safety margins for the replacement core must be comparable to or greater than those of the HEU core. The acceptability of the replacement core essentially would not be affected by the larger power margins that the statistical combination of hot channel factor components for the LEU core would predict, since the HEU core, which is the standard to be achieved, would also display larger power margins.

Table 10. Hot Channel Factors for the HEU Core (No Fuel Plate Swelling or Oxide Growth)

	Multiplicative Combination					Statistical Combination					
Channel (or Plate*)	F_{FILM} Left	F_{BULK}	F_{FILM} Right	F_{FLUX}	$F_{VELOCITY}$	F_{FILM} Left	F_{BULK}	F_{FILM} Right	F_{FLUX}	$F_{VELOCITY}$	Thickness Ratio
1	-	1.87	1.60	1.32	1.35	-	1.50	1.27	1.22	1.23	1.25
2	1.54	1.53	1.54	1.32	1.24	1.26	1.26	1.26	1.22	1.17	1.11
3	1.54	1.53	1.54	1.32	1.24	1.26	1.26	1.26	1.22	1.17	1.11
4	1.54	1.53	1.54	1.32	1.24	1.26	1.26	1.26	1.22	1.17	1.11
5	1.54	1.53	1.54	1.32	1.24	1.26	1.26	1.26	1.22	1.17	1.11
6	1.54	1.53	1.54	1.32	1.24	1.26	1.26	1.26	1.22	1.17	1.11
7	1.54	1.53	1.54	1.32	1.24	1.26	1.26	1.26	1.22	1.17	1.11
8	1.54	1.53	1.54	1.32	1.24	1.26	1.26	1.26	1.22	1.17	1.11
9	1.54	1.53	1.54	1.32	1.24	1.26	1.26	1.26	1.22	1.17	1.11
10	1.54	1.53	1.54	1.32	1.24	1.26	1.26	1.26	1.22	1.17	1.11
11	1.54	1.53	1.54	1.32	1.24	1.26	1.26	1.26	1.22	1.17	1.11
12	1.54	1.53	1.54	1.32	1.24	1.26	1.26	1.26	1.22	1.17	1.11
13	1.54	1.53	1.54	1.32	1.24	1.26	1.26	1.26	1.22	1.17	1.11
14	1.54	1.53	1.54	1.32	1.24	1.26	1.26	1.26	1.22	1.17	1.11
15	1.54	1.53	1.54	1.32	1.24	1.26	1.26	1.26	1.22	1.17	1.11
16	1.54	1.53	1.54	1.32	1.24	1.26	1.26	1.26	1.22	1.17	1.11
17	1.54	1.53	1.54	1.32	1.24	1.26	1.26	1.26	1.22	1.17	1.11
18	1.54	1.53	1.54	1.32	1.24	1.26	1.26	1.26	1.22	1.17	1.11
19	1.54	1.53	1.54	1.32	1.24	1.26	1.26	1.26	1.22	1.17	1.11
20	1.54	1.53	1.54	1.32	1.24	1.26	1.26	1.26	1.22	1.17	1.11
21	1.54	1.53	1.54	1.32	1.24	1.26	1.26	1.26	1.22	1.17	1.11
22	1.54	1.53	1.54	1.32	1.24	1.26	1.26	1.26	1.22	1.17	1.11
23	1.54	1.53	1.54	1.32	1.24	1.26	1.26	1.26	1.22	1.17	1.11
24	1.54	1.53	1.54	1.32	1.24	1.26	1.26	1.26	1.22	1.17	1.11
25	1.67	2.23	-	-	1.45	1.28	1.77	-	-	1.30	1.38

*"Plate" applies only to F_{FLUX}. ("Channel" applies to all other entries.)

Table 11. Hot Channel Factors for the LEU FSD Core (No Fuel Plate Swelling or Oxide Growth)

	Multiplicative Combination					Statistical Combination					
Channel (or Plate*)	F_{FILM} Left	F_{BULK}	F_{FILM} Right	F_{FLUX}	$F_{VELOCITY}$	F_{FILM} Left	F_{BULK}	F_{FILM} Right	F_{FLUX}	$F_{VELOCITY}$	Thickness Ratio
1	-	2.15	1.56	1.27	1.39	-	1.60	1.24	1.18	1.26	1.30
2	1.46	1.59	1.46	1.27	1.23	1.22	1.24	1.22	1.18	1.16	1.10
3	1.46	1.55	1.46	1.27	1.23	1.22	1.24	1.22	1.18	1.16	1.10
4	1.46	1.53	1.46	1.27	1.23	1.22	1.24	1.22	1.18	1.16	1.10
5	1.46	1.53	1.46	1.27	1.23	1.22	1.24	1.22	1.18	1.16	1.10
6	1.46	1.53	1.46	1.27	1.23	1.22	1.24	1.22	1.18	1.16	1.10
7	1.46	1.53	1.46	1.27	1.23	1.22	1.24	1.22	1.18	1.16	1.10
8	1.46	1.53	1.46	1.27	1.23	1.22	1.24	1.22	1.18	1.16	1.10
9	1.46	1.53	1.46	1.27	1.23	1.22	1.24	1.22	1.18	1.16	1.10
10	1.46	1.53	1.46	1.27	1.23	1.22	1.24	1.22	1.18	1.16	1.10
11	1.46	1.53	1.46	1.27	1.23	1.22	1.24	1.22	1.18	1.16	1.10
12	1.46	1.53	1.46	1.27	1.23	1.22	1.24	1.22	1.18	1.16	1.10
13	1.46	1.53	1.46	1.27	1.23	1.22	1.24	1.22	1.18	1.16	1.10
14	1.46	1.53	1.46	1.27	1.23	1.22	1.24	1.22	1.18	1.16	1.10
15	1.46	1.53	1.46	1.27	1.23	1.22	1.24	1.22	1.18	1.16	1.10
16	1.46	1.53	1.46	1.27	1.23	1.22	1.24	1.22	1.18	1.16	1.10
17	1.46	1.53	1.46	1.27	1.23	1.22	1.24	1.22	1.18	1.16	1.10
18	1.46	1.53	1.46	1.27	1.23	1.22	1.24	1.22	1.18	1.16	1.10
19	1.46	1.53	1.46	1.27	1.23	1.22	1.24	1.22	1.18	1.16	1.10
20	1.46	1.53	1.46	1.27	1.23	1.22	1.24	1.22	1.18	1.16	1.10
21	1.46	1.53	1.46	1.27	1.23	1.22	1.24	1.22	1.18	1.16	1.10
22	1.46	1.53	1.46	1.27	1.23	1.22	1.24	1.22	1.18	1.16	1.10
23	1.46	1.53	1.46	1.27	1.23	1.22	1.24	1.22	1.18	1.16	1.10
24	1.46	1.53	1.46	1.27	1.23	1.22	1.24	1.22	1.18	1.16	1.10
25	1.58	2.22	-	-	1.43	1.25	1.71	-	-	1.29	1.36

*"Plate" applies only to F_{FLUX}. ("Channel" applies to all other entries.)

Table 12. Hot Channel Factors for the LEU CD35 Core (No Fuel Plate Swelling or Oxide Growth)

	Multiplicative Combination					Statistical Combination					
Channel (or Plate*)	F_{FILM} Left	F_{BULK}	F_{FILM} Right	F_{FLUX}	$F_{VELOCITY}$	F_{FILM} Left	F_{BULK}	F_{FILM} Right	F_{FLUX}	$F_{VELOCITY}$	Thickness Ratio
1	-	2.16	1.56	1.27	1.39	-	1.60	1.24	1.18	1.25	1.30
2	1.46	1.60	1.46	1.27	1.23	1.22	1.24	1.22	1.18	1.16	1.09
3	1.46	1.58	1.46	1.27	1.23	1.22	1.24	1.22	1.18	1.16	1.09
4	1.46	1.55	1.46	1.27	1.23	1.22	1.24	1.22	1.18	1.16	1.09
5	1.46	1.54	1.46	1.27	1.23	1.22	1.24	1.22	1.18	1.16	1.09
6	1.46	1.54	1.46	1.27	1.23	1.22	1.24	1.22	1.18	1.16	1.10
7	1.46	1.54	1.46	1.27	1.23	1.22	1.24	1.22	1.18	1.16	1.10
8	1.46	1.54	1.46	1.27	1.23	1.22	1.24	1.22	1.18	1.16	1.10
9	1.46	1.54	1.46	1.27	1.23	1.22	1.24	1.22	1.18	1.16	1.10
10	1.46	1.54	1.46	1.27	1.23	1.22	1.24	1.22	1.18	1.16	1.10
11	1.46	1.54	1.46	1.27	1.23	1.22	1.24	1.22	1.18	1.16	1.10
12	1.46	1.54	1.46	1.27	1.23	1.22	1.24	1.22	1.18	1.16	1.10
13	1.46	1.54	1.46	1.27	1.23	1.22	1.24	1.22	1.18	1.16	1.10
14	1.46	1.54	1.46	1.27	1.23	1.22	1.24	1.22	1.18	1.16	1.10
15	1.46	1.54	1.46	1.27	1.23	1.22	1.24	1.22	1.18	1.16	1.10
16	1.46	1.54	1.46	1.27	1.23	1.22	1.24	1.22	1.18	1.16	1.10
17	1.46	1.54	1.46	1.27	1.23	1.22	1.24	1.22	1.18	1.16	1.10
18	1.46	1.54	1.46	1.27	1.23	1.22	1.24	1.22	1.18	1.16	1.10
19	1.46	1.54	1.46	1.27	1.23	1.22	1.24	1.22	1.18	1.16	1.10
20	1.46	1.54	1.46	1.27	1.23	1.22	1.24	1.22	1.18	1.16	1.09
21	1.46	1.54	1.46	1.27	1.23	1.22	1.24	1.22	1.18	1.16	1.09
22	1.46	1.54	1.46	1.27	1.23	1.22	1.24	1.22	1.18	1.16	1.09
23	1.46	1.54	1.46	1.27	1.23	1.22	1.24	1.22	1.18	1.16	1.09
24	1.58	2.21	-	-	1.43	1.25	1.71	-	-	1.28	1.35

*"Plate" applies only to F_{FLUX}. ("Channel" applies to all other entries.)

The statistical combination of hot channel factor components adds considerable complexity to the analysis. Each variable must have a probability distribution function associated with it. These distribution functions must be properly combined statistically. The channel that is found to be most limiting by this probabilistic approach must be shown to have an acceptably small probability of exceeding a safety limit. Since, in the realm of probability, this does not preclude the failure of another channel that perhaps is nearly as limiting, "acceptably small" may mean "very small". In spite of all of the difficulties associated with the statistical approach, it may be the preferred one. When the multiplicative approach, which implies that everything is simultaneously at its worst everywhere, shows a very small positive margin to a safety limit, or even a negative margin, the statistical approach, which permits a small probability of failure, may be the only acceptable option. Neither approach changes the actual margin to safety. This margin is what it is regardless of analytical methods.

Since the multiplicative approach was used in the existing MURR Safety Analysis Report[30] and the safety margins of the HEU core serve as a benchmark with which to gauge acceptability of the safety margins of the LEU cores, the multiplicative combination of hot channel factor components is used in the current analysis. Both the HEU core and the two LEU cores will be analyzed in the same manner with equivalent sets of assumptions that are appropriate for the particular core and are consistent among the three cores.

8c. Global Hot Channel Factors

In contrast to the just considered local hot channel factors, which are assumed to occur randomly, this section considers global, or systematic, hot channel factors. A prime example of a global hot channel factor is the one that arises in the film coefficient at the surface of the fuel plate. The uncertainty in the equation 5 Nusselt number correlation being employed to obtain the film coefficient can affect all fuel plate surfaces simultaneously. In the analysis, based on judgment, an uncertainty factor of 1.20 is applied to the film coefficient. Hence, the values of film coefficient, h, used in the analysis are obtained by dividing the value of h (predicted via equation 5) by 1.20.

The safety limiting values of power, flow rate, inlet temperature, and pressurizer pressure are additional examples of global factors. In the operation of the MURR reactor, the uncertainty in the measurement of these quantities is taken into consideration. For example, if the uncertainty in the inlet temperature is 5° C, the trip setting on inlet temperature is set at least 5° C lower than it would be if there was no uncertainty in the measurement of the inlet temperature. Hence, no uncertainty factors associated with these measured quantities are included in the analysis.

9. Pressure Drop from the Pressurizer to the Inlets of the Coolant Channels

Figure 5 shows a schematic representation of the reactor core inlet piping. The measured pressurizer pressure used in the operation of the reactor is the pressure of the nitrogen gas above the liquid surface in the pressurizer. This pressure is controlled and has a minimum LSSS value of 75 psia. Point 1 in Figure 5 is 608 feet and 6 inches above sea level. The flow in Loop A and the flow in Loop B are each always 25 gpm more than half of the core flow. Thus, in the figure where the total core flow rate is 3600 gpm, 1825 gpm enters from the left through Loop A and another 1825 gpm enters through Loop B. At point 2 50 gpm is extracted from the Loop A flow and goes to the deionizer. The deionizer flow remains constant at 50 gpm regardless of the core flow. At point 3 the remaining 1775 gpm of the Loop A flow merges with the 1825 gpm flow of Loop B to form the combined flow of 3600 gpm that goes through the core. Hence, the flow rate between points 2 and 3 is always 25 gpm less than half of the total core flow rate and the flow rate between points 3 and 4 is always the total core flow rate.

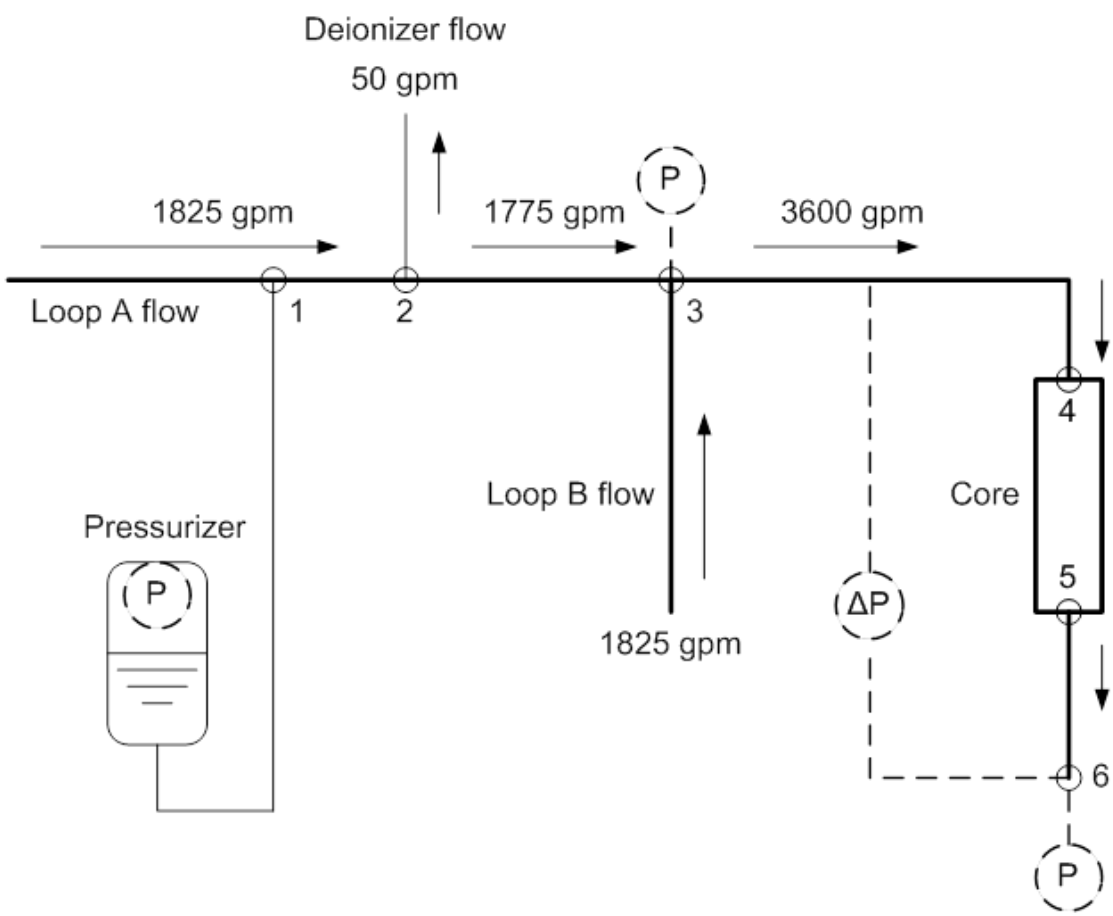

Figure 5. Schematic Representation of the Reactor Core Inlet Piping

As shown in Figure 5, the pressurizer is attached to a stagnant leg below Loop A. For the thermal-hydraulic analysis of the reactor core, the pressure at point 4, which is between the fuel plates and at the inlet to them, is needed. The pressure at point 1 is the pressurizer pressure reduced by the gravity head, ΔP_P, from the surface of the liquid water in the pressurizer to point 1, which is along Loop A. The Bernoulli equation, modified to include the hydraulic resistance from point 1 to 4, is used to determine the pressure drop from point 1 to point 4.

A zero-inch reading for the pressurizer liquid water level corresponds to 48 inches below point 1. If L is the amount in inches that the water level in the pressurizer is above the zero reading, then:

$$\Delta P_P = P_P - P_1 = \rho_P \times g \times (48 - L) \tag{9}$$

where P_P and P_1 are the pressure at the pressurizer water surface and point 1, respectively, ρ_P is the density of the liquid in the pressurizer and also in the pressurizer pipe leg leading to point 1, g is the acceleration due to gravity, 9.80665 m/s^2. Since the water in the stagnant leg leading from the pressurizer to Loop A is at 85° F, the density is 995.97 kg/m^3. The nominal value of L is zero inches. The primary charging pump starts adding water to the pressurizer when the pressurizer water level drops down to 6 inches below its nominal value. A low water-level scram is initiated at −16 inches.

The Bernoulli equation, modified to include the hydraulic resistance from point 1 to 4 is:

$$P_1 + \frac{\rho V_1^2}{2} + \rho g Z_1 = P_4 + \frac{\rho V_4^2}{2} + \rho g Z_4 + \Delta P_{HR} \tag{10}$$

where P is pressure, ρ is the density of the fluid between points 1 and 4, V is velocity, Z is elevation, ΔP_{HR} is the pressure drop due to the hydraulic resistance between points 1 and 4, and subscripts 1 and 4, of course, refer to points 1 and 4. The pressure drop due to the hydraulic resistance is an irrecoverable pressure loss caused by the pipes and fittings between points 1 and 4.

Equations 9 and 10 may be combined to eliminate P_1 and obtain:

$$P_4 = P_P - \rho_P\, g\,(48 - L) + \rho\, g\,(Z_1 - Z_4) - \frac{\rho(V_4^2 - V_1^2)}{2} - \Delta P_{HR} \tag{11}$$

$Z_1 - Z_4$ is 15.25 inches. The velocity at any point is the local volumetric flow rate in the pipe, divided by the local pipe flow area. Point 1 is in an 8-inch pipe that has a flow area of 0.34741 ft^2. The flow rate at point 4 is always the total core flow rate. The flow area at point 4 is the flow area inside the fueled region, which is 0.3419, 0.3856, and 0.3715 ft^2, for the HEU, LEU FSD, and LEU CD35 cores, respectively.

A set of relationships that define ΔP_{HR} were obtained by the MURR staff during March through May of 2011. They used hydraulic handbook data and analytical models that were calibrated with measurements on the MURR plant. Measurements were made on March 27, 2011 with the eight core fuel elements in the reactor vessel and the reactor operating at 10 MW. Measurements were also taken on March 28, 2011 with the eight core fuel elements out of the reactor vessel while the primary coolant system was operating. The locations where pressure measurements were made are indicated in Figure 5 by the letter "P" inside a dashed circle. The pressure difference, which is indicated in Figure 5 by "ΔP" inside a dashed circle, was also measured, along with coolant flow rates and temperatures.

The pressure drop ΔP_{HR} can be divided into three pressure drops, one from point 1 to point 2 of Figure 5, one from point 2 to point 3, and one from point 3 to point 4. Each of these three pressure drops is the sum of a pressure drop component that is characterized by friction, ΔP_f, at the walls of the pipes and another component, ΔP_K, that is characterized by form losses (often called "K-losses"). The value of ΔP_{HR} is the sum of these six pressure drop components.

From well-known hydraulic relationships for turbulent flow through pipes and fittings, one can derive the relationship for the pressure drop portion along each pipe segment that is characterized by friction at the walls of the pipes as:

$$\Delta P_f = \Delta P_{f0} \left(\frac{\rho}{\rho_0}\right)^{0.8} \left(\frac{Q}{Q_0}\right)^{1.8} \left(\frac{\mu}{\mu_0}\right)^{0.2} \tag{12}$$

where ΔP_{f0}, ρ_0, Q_0, and μ_0 are the pressure drop portion, density, volumetric flow rate, and viscosity for a reference temperature, T_0, and ΔP_f, ρ, Q, and μ are the corresponding quantities at any temperature, T. In a similar manner, one can derive the relationship for the pressure drop portion along each pipe segment that is characterized by form losses as:

$$\Delta P_K = \Delta P_{K0} \left(\frac{\rho}{\rho_0}\right)^{1.0} \left(\frac{Q}{Q_0}\right)^{2.0} \tag{13}$$

where ΔP_{K0}, ρ_0, and Q_0 are the pressure drop portion, density, and volumetric flow rate for a reference temperature, T_0,, and ΔP_K, ρ, and Q μ are the corresponding quantities at any temperature, T.

In equations 12 and 13, Q and Q_0 always correspond to the flow rate and reference flow rate, respectively, along the particular path. In the derivation of equation 12 it was assumed that friction factor is inversely proportional to the Reynolds raised to the 0.20 power. The data in Table 13 provide the frictional and non-frictional portions of ΔP_{HR} for each of the three path segments between points 1 and 4 for a reference temperature of 120° F and the reference flow rate indicated for each path segment in Table 13 and in Figure 5. As shown in Table 13, the frictional value of ΔP_f from point 2 to point 3 is 0. The values of density and viscosity at the reference temperature are 988.69 kg/m^3 and 0.00055725 Pa-s, respectively. Density and viscosity are essentially independent of pressure over the range of pressures of interest to the operation of the MURR reactor. 4.5 bar was assumed in obtaining ρ_0 and μ_0 and ρ_P in equation 9. Equation 11, with ΔP_{HR} obtained from equations 12 and 13 and data from Table 13, can be used to obtain P_4.

Table 13. Reference Hydraulic Conditions Used in Conjunction with Equations 12 and 13 to Determine ΔP_{HR}

Path Segment	T_0, °F	Q_0, gpm	Pressure Drop at T_0, psi	
			Frictional, ΔP_{f0} (Equation 12)	Non-frictional, ΔP_{K0} (Equation 13)
Point 1 to 2	120	1825	0.0913	4.500
Point 2 to 3	120	1775	0.0	0.2640
Point 3 to 4	120	3600	4.5551	0.8008

10. Fuel Plate Thermal Model

The HEU fuel plate has three layers – a fuel meat layer and an aluminum clad layer on either side. The LEU fuel plate has a similar design, but it has a layer of zirconium on each side of the fuel meat that forms a barrier between the fuel meat and the aluminum clad. While the fuel in being irradiated, a thin layer of oxide gradually forms on the heated surfaces of the clad and thickens with hours of irradiation time. Therefore, the HEU fuel plate is modeled as a five-layer solid consisting of a fuel meat layer, two aluminum layers, and two oxide layers. The LEU fuel plate is modeled as a seven-layer solid consisting of a fuel meat layer, two zirconium layers, two aluminum layers, and two oxide layers. All five layers of the HEU and all seven layers of the LEU fuel are modeled in the analysis. The fuel, zirconium, and aluminum layer thicknesses are explicitly modeled. The oxide layers are represented as thermal resistances that have no explicit thickness.

Table 14 lists the thermal conductivities of all of the fuel plate materials. Because the fuel meat thermal conductivity decreases with burnup, two values are provided for each fuel type, one for the fresh fuel and another for the fuel when it is ready for discharge. Between these two extremes, linear interpolation based on hours of operation is used. For each fuel element, the number of hours of operations is assumed to be directly proportional to the MWd of burnup. For example, each LEU CD35 element is assumed to have an operating power of 12 MW/8, or 1.5 MW. Its discharge burnup of 180 MWd is equal to 180 MWd / 1.5 MW × 24 hours/day = 2880 hours of operation. Table 15 provides the burnup in both MWd and hours of operation for each element of each case of each of the three cores that are used in the thermal analysis. The burnups in this table agree with those in Table 3 through Table 5 except for the last week of the cycle. In Table 3 through Table 5 all of the burnups are for the beginning of the week of the cycle. In Table 15 all of the burnups are for the beginning of the week except for the last week of the cycle, where the burnups (shown in red) are the discharge burnups.

Table 14. Thermal Conductivities of HEU and LEU Fuel Plate Materials, W/m-K

Material	Fresh (No Burnup)	At Maximum Burnup*
HEU Fuel Meat	40	30
LEU Fuel Meat	16.2	11.3
Zirconium Layer	19	
6061 Aluminum	150	
Oxide Layer	2.25	

*Maximum Burnup per Element:

HEU: 150 MWd = 2880 hours of irradiation time

LEU FSD Design: 208 MWd = 3328 hours of irradiation time

LEU CD35 Design: 180 MWd = 2880 hour of irradiation time

<u>HEU Thermal Conductivity</u>

The value of thermal conductivity for the fresh HEU fuel meat was obtained from Reference 35. In Table 4 on page 22 of this reference, the volume-% UAl_x of 35.4 was added to the percent porosity of 6 to

obtain a total value of 41.4. Then in Figure 8 on page 27 of the reference, at 41.4 Volume Percent (fuel + voids), the open square symbols indicate that the thermal conductivity is about 40 to 45 W/m-K. Therefore, 40 W/m-K was selected. Burnup tends to reduce the thermal conductivity of the fuel meat. A lower bound for the value of the high-burnup MURR HEU fuel of 30 W/m-K is based on the judgment of Reference 36.

Table 15. Element Burnup*
(X1 through X8 are elements 1 through 8, respectively.)

		Element Burnup (MWd)				Element Burnup (Hours of Operation)			
Fuel	**Case****	**X1, X5**	**X2, X6**	**X3, X7**	**X4, X8**	**X1, X5**	**X2, X6**	**X3, X7**	**X4, X8**
HEU	**1A**	0	0	0	0	0	0	0	0
	2A	0	0	0	0	0	0	0	0
	3A	0	81	65	150	0	1555.2	1248	2880
	4A	0	81	65	150	0	1555.2	1248	2880
	1B	0	0	0	0	0	0	0	0
	2B	0	0	0	0	0	0	0	0
	3B	0	81	65	150	0	1555.2	1248	2880
	4B	0	81	65	150	0	1555.2	1248	2880
LEU FSD	**5A**	0	0	0	0	0	0	0	0
	6A	0	0	0	0	0	0	0	0
	7A	0	116	97	208	0	1856	1552	3328
	8A	0	116	97	208	0	1856	1552	3328
	5B	0	0	0	0	0	0	0	0
	6B	0	0	0	0	0	0	0	0
	7B	0	116	97	208	0	1856	1552	3328
	8B	0	116	97	208	0	1856	1552	3328
LEU CD35	**5A**	0	0	0	0	0	0	0	0
	6A	0	0	0	0	0	0	0	0
	7A	0	96	77	180	0	1536	1232	2880
	8A	0	96	77	180	0	1536	1232	2880
	5B	0	0	0	0	0	0	0	0
	6B	0	0	0	0	0	0	0	0
	7B	0	96	77	180	0	1536	1232	2880
	8B	0	96	77	180	0	1536	1232	2880

*All values in the table that are shown in red represent the burnup at discharge. All of the other values represent the burnup at the beginning of the cycle.

** The burnup for 1A1 and 1A2 is the same as that for 1A. This is also true for 2A through 8B.

LEU Thermal Conductivity

The thermal conductivity of the fresh LEU fuel meat is based on equation 5 on page 7 of Reference 37, which is $\lambda_{U\text{-}10Mo}$ = (10.2 ± 0.688) + (3.51× 10^{-2} ± 1.61×10^{-3}) T, where $\lambda_{U\text{-}10Mo}$ is thermal conductivity in W/m-K and T is temperature in C. Nominal values of thermal conductivity at 100, 200, 250, and 300 °C are 13.71, 17.22, 18.97, and 20.73 W/m-K, respectively. Minimum values, i.e., at the lower end of the tolerance, at 100, 200, 250, and 300 °C, are 12.86, 16.21, 17.88, and 19.56 W/m-K, respectively. The

corresponding ratios of nominal to minimum values are 1.066, 1.062, 1.061, and 1.060. Values at the lower end of the tolerance are used in the analysis. The computer code that is used to execute the thermal analysis, PLTEMP/ANL[38], does not allow temperature-dependent thermal conductivity. The value of thermal conductivity used in the thermal analysis is 16.2 W/m-K, which corresponds to the low end of the tolerance at 200° C. Since thermal conductivity increases with temperature, if a higher fuel temperature were predicted based on this value of thermal conductivity, the predicted temperature would be higher than it actually would be. If the predicted value based on 16.2 W/m-K were less than 200° C, the predicted temperature would be lower than it otherwise would be, but this would not represent a safety issue because the fuel certainly must be able to withstand temperatures below 200° C without sustaining any damage or degradation.

The reduction in thermal conductivity due to irradiation of the LEU fuel is obtained from the plot of U-10Mo thermal conductivity at 200° C as a function of burnup that is given in Figure 6.5 on page 38 of Reference 39. The approximate maximum burnup for the LEU CD35 and FSD fuels is 35 and 37 × 10^{20} fissions/cc, respectively. The plot shows that the thermal conductivity at 0, 35, 37, and 40 × 10^{20} fissions/cc burnup is 17.8, 13.3, 13.0, and 12.4 W/m^2-K, respectively. Thus, the ratio of thermal conductivity of the irradiated fuel to that of the fresh (i.e., 0 fissions/cc) fuel for each of these four burnups is 1.00, 0.75, 0.73, and 0.70, respectively. For simplicity and to allow for the potential need to include burnup values up to 40 × 10^{20} fissions/cc, the thermal conductivity for the maximum burned LEU CD35 or FSD fuel is taken to be 0.70 × 16.2 W/m-K, or 11.3 W/m-K.

Zirconium Thermal Conductivity and Thicknesses of Clad and Fuel Meat

Values of the thermal conductivity of zirconium, Figure 6, can be found in Reference 40 (equation 8), which, for temperatures between 298 and 2000 K (24.85 to 1726.85 °C), recommends the equation $k = 8.8527 + 7.0820 \times 10^{-3}\,T + 2.5329 \times 10^{-6}\,T^2 + 2.9918 \times 10^{3}\,T^{-1}$, where T is temperature in K and k is thermal conductivity in W/m-C . At 100° C, k is 19.9 W/m-K and decreases monotonically to a minimum value of 18.954 W/m-K at 277.4° C and then monotonically increases and is 20.0 W/m-K at 550°C and 20.4 W/m-K at 600° C. It is no greater than 19.44 W/m-K between 150 and 450° C. Thus, the thermal conductivity of the zirconium layer is taken to be 19 W/m-K.

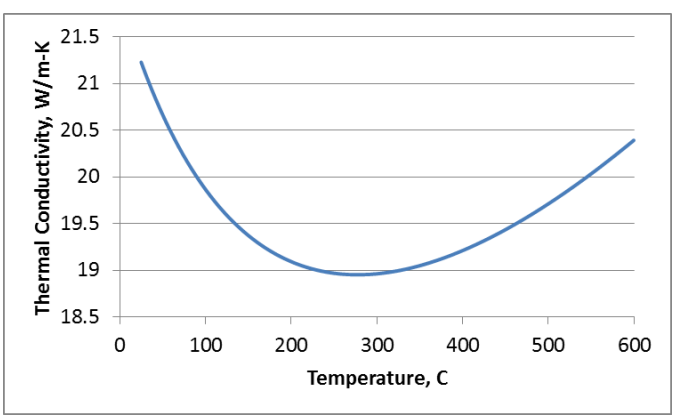

Figure 6. Thermal Conductivity of Zirconium

6061 Aluminum Thermal Conductivity

The two internet sites: http://www.efunda.com/materials/alloys/aluminum/show_aluminum.cfm?ID=AA_6061&show_prop=tc&Page_Title=Aluminum%20Alloy%20AA%206061 and http://www.engineersedge.com/properties_of_metals.htm provide the value of the thermal conductivity for the three tempers of aluminum 6061. The first shows that at 25° C the thermal conductivity is 180, 154, and 167 W/m-K for Treatment O, Treatment T4, and Treatment T6, respectively. The second provides the same values, but does not specify a temperature. Whatever heat treatment or temper the feedstock for the LEU clad has will probably be changed during the hipping process used to form the finished fuel plates. For simplicity 150 W/m-K was chosen for both the LEU and the HEU clad. This value is a round number close to, but lower than, the lowest of the three values for the three tempers.

Oxide Layer Thermal Conductivity and Thickness

The thermal resistance due to the buildup of oxide on the clad surface can influence the margins to flow instability and CHF because heat is transferred from one coolant channel to the next through the intervening fuel plate. (There is another way to view the same phenomenon. The coolant temperatures on either side of a fuel plate affect how the power exiting the two plate surfaces is divided between the two coolant channels.) This is a second-order effect that is most pronounced when the limiting channel is or is next to an end channel because this is the location where the temperature difference between two adjacent fuel channels is the greatest. For a 2-mil oxide layer on CD35 fuel plates with channel 23, which is next to the end channel, being the limiting one, flow instability power was found to be about 0.7% lower than when there was no oxide layer. The value for the thermal conductivity of the oxide, 2.25 W/m-K, was obtained from Reference 41. A maximum oxide thickness of about 1 mil at discharge burnup is expected for all three cores. In the analysis of flow instability and CHF the thermal resistance of the oxide layer was taken to be 0.

11. Channel Thickness Reduction Due to Fuel Plate Swelling and Oxide Buildup

The reduction in channel thickness due to fuel plate swelling and oxide buildup reduces the flow through the channel. This adversely affects the bulk coolant temperature rise and the film temperature rise at the surface of the fuel plate. Since the total core flow rate is controlled, the flow that is diverted from one channel must go to another channel. A bounding approach to the flow reduction in one channel could cause an overly optimistic assessment of the flow in the other channels. This problem is avoided by treating the channel thickness reduction as if it were the result of a local manufacturing tolerance, as described in section 8a.

For the HEU core the maximum reduction in channel thickness due to fuel plate swelling and oxide buildup for channels bounded by two fuel plates is assumed to be 10 mils. For the two LEU cores this

value was reduce to 8 mils to reflect expected fuel swelling and oxide growth. In the past, the actual channel thickness as burnup proceeds in the HEU core has been monitored with a 62-mil welding rod that was used as a gauge. This is 10 mils below the allowed minimum as-built HEU internal channel thickness. All observed channels thicknesses have been considerably above 62 mils. A similar monitoring approach will be used for the LEU CD35 core. For all three cores the reduction in end channel thickness is taken to be half of the internal channel values, i.e., 5 mils for the HEU and 4 mils for each of the two LEU cores. For the fresh fuel the channel thickness reduction due to fuel plate swelling and oxidation buildup is assumed to be zero. Analogous to the modeling of fuel thermal conductivity as a function of burnup, the channel thickness reduction is assumed to be linearly proportional to burnup, as defined in Table 15.

The narrowing of the coolant channel due to fuel plate swelling and oxide buildup is represented in the modeling as an additional reduction in the channel thickness and is included with the reduction in channel thickness due to manufacturing tolerances. For example, in the representation of thickness at the bottom lower left of Table 9, "Swelling & Oxide" is listed as 0 mils. If there were 8 mils of fuel plate swelling and oxide growth, this value would be 8 mils and the hot channel thickness would be 93 – 8 – 8 mils, or 77 mils instead of the 85 mils shown. Then the thickness ratio would be 93/77, or 1.208. This value would be used in place of 1.094 (= 93/85) in the "channel thickness" row to find the four hot channel factor component values. This approach would provide correct results for the multiplicatively combined hot channel factor values near the bottom of the table. However, the statistically combined results would require a slightly different treatment since the reduction in channel thickness due to fuel plate swelling and oxide growth is not a randomly occurring event. When it exists, it is assumed to exist regardless of how the hot channel factor components are combined. For example, as shown in Table 9 in the (Channel Thickness, F_{BULK}) cell, 8 mils of channel reduction by itself from any cause would increase the channel bulk coolant temperature rise by a factor of 1.167. Thus, for the statistical combination, the total F_{BULK} including 8 mils fuel plate swelling and oxide growth in addition to 8 mils of manufacturing tolerance would be the 1.24 value shown near the bottom of the table increased by a factor of 1.167, or 1.44. This is slightly greater that the 1.42 value that would have been obtained if the 8 mils of fuel plate swelling and oxide growth were merely added to the 8 mils due to manufacturing tolerance and treated as part of a randomly occurring change in channel thickness.

12. The PLTEMP/ANL Code[38]

The PLTEMP/ANL code is the primary thermal-hydraulic computational tool that is used in evaluating the margins to flow instability and critical heat flux during steady-state operation. It is capable of modeling all of the MURR fuel elements at one time and considering all of the fuel plates and coolant channels of each element simultaneously. In the PLTEMP/ANL code the only coupling between parallel elements is hydraulic.

The code divides the axial length of the core into a series of parallel axial layers and predicts the temperatures and heat fluxes of each layer. The code considers the thermal boundary conditions in the channel on each side of a fuel plate in determining the fraction of the power emanating from each face of the fuel plate. This can be particularly important when the channel on one side of a fuel plate is much cooler than the channel on the other side, such as may occur in the end channels of an element.

The code includes a hot channel factor on bulk coolant temperature rise for each channel of each element. It also includes a hot channel factor on film temperature rise, i.e., from bulk coolant to fuel plate surface, for each heated surface of each fuel plate. There is also a hot channel factor on heat flux for each fuel plate in the core. A global hot channel factor on the Nusselt correlation, which is used in determining the local values of film coefficient, is also included. The code does not include a hot channel factor on coolant velocity, $F_{VELOCITY}$, for the CHF models used in the analysis.

The code can explicitly represent the axial power distribution of each fuel plate. Although not used in the current analysis, the code also allows the fuel meat of each fuel plate to be subdivided into vertical strips, so that the axial power distribution for each strip can be explicitly represented. Since the MURR LEU core has thin rectangular channels with large aspect ratios, the strip-wise variations in power can be extremely significant to the thermal-hydraulic performance of the core. The code does not include thermal conduction from one axial layer to the next or one vertical strip to the next. Within each axial level of each strip the heat transfer from the fuel meat to the bulk coolant is assumed to be one dimensional with the thermal conductance from the fuel plate surface to the adjacent bulk coolant represented by a film coefficient. Equation 5 is one of the Nusselt number (or film coefficient) correlations included in the code. An unheated vertical strip can also be included at the ends of the channel, before the first and after the last heated vertical strip of each channel. There is an adjustable user-input parameter that allows for coolant mixing between adjacent strips to be set to no mixing, complete mixing, or anything in between.

The code has a hydraulic model that predicts the coolant flow rate of each channel in the core. The pressure drop, ΔP, across the length of each coolant channel is the same for all of the channels and is represented as $(f_i\ L/D_i + K) \times \rho_i\ V_i^2/2$, where f_i is the Moody friction factor for channel i, L is the length of the channel, D_i is the hydraulic diameter of channel i, ρ_i the coolant density of channel i, V_i is the bulk coolant velocity of channel i based on ρ_i. The ρ_i, V_i, and Reynolds number are evaluated at the average of the coolant channel inlet and outlet temperatures. A single value of K is used to represent the sum of the inlet and outlet form-loss values and is applied to all coolant channels in the element, uniformly along the heated length of the element. If ΔP is known, then a value of V_i can be determined for each coolant channel in the core. Because the flow area of each channel is known, the total core flow rate for a given value of ΔP can be determined. The code has a search capability which allows the assumed pressure drop across the reactor to be adjusted until the total flow rate through the reactor is predicted to be the desired value. This, in effect, allows the total core flow rate to be a user-specified input.

The flow rate of each strip of a channel is assumed to be linearly proportional to the width of the strip. For each vertical strip of each heated coolant channel in the core, the PLTEMP/ANL code can calculate

the flow instability ratio (FIR), which is the ratio of the allowed bulk coolant temperature rise based on equation 1 to the calculated bulk coolant temperature rise. The code has a search capability to automatically adjust the reactor power until the minimum value of FIR among all strips in the core is a particular value that is specified by code input. Similarly, the code has the ability to calculate the critical heat flux ratio for each of the two heat transfer surfaces of each axial level of each strip of each plate of each element in the core and to adjust the core power until a specified value of minimum CHF ratio is achieved. The extended Groeneveld 2006 CHF correlation, equation 3, is represented in the code. The Sudo and Kaminaga[15,31] and the Bernath[6] CHF correlations are also represented.

Several verification and validation works done for previous versions of the PLTEMP/ANL code have been compiled in a single volume.[42]

13. Application of the PLTEMP/ANL Code to the MURR Cores

A separate PLTEMP/ANL model was developed for each of the three cores. Each model explicitly and simultaneously represented all coolant channels and all fuel plates of all eight elements of each core. The heated width of each fuel plate was represented as a single vertical strip and was not subdivided into smaller strips. However, a single unheated strip on each side of the heated strip was modeled. Thus, each coolant channel was represented as three adjoining subchannels. In the model it was assumed that there is no mixing among these three subchannels. Hence, it was assumed that none of the power that is deposited in the fuel meat is shared with either of the two unheated edge subchannels.

The heated length of the core was subdivided into 24 horizontal sublayers. This was done to match the axial power distributions provided by the core neutron physics analysis[2]. The core neutron physics analysis also subdivided each fuel meat into nine vertical strips. Although the code can explicitly represent this fine structure, it assumes that there is no heat conduction between adjacent strips. Moreover, the appropriate value of the factor that controls coolant mixing among the strip subchannels of a coolant channel is not provided in the code user's guide and must be specified by the user.

Rather than represent each strip, the PLTEMP/ANL model for each MURR core used multipliers on the local hot channel factor to account for the more severe thermal conditions of the limiting strip. For each of the nine heated strips of each fuel plate, the ratio of the average heat flux in a strip to the average heat flux for the entire heated width of the fuel plate was determined. (Here, in the determination of average heat fluxes in a strip, half of the power of each fuel plate strip was assumed to exit each strip face.) The largest ratio for each plate was identified and incorporated into the three local hot channel factors, F_{FLUX}, F_{FILM}, and F_{BULK}. Thus, the value of F_{FLUX}, and the two values of F_{FILM} for each fuel plate was multiplied by the largest of the fuel plate's nine heat flux ratios. For each internal coolant channel, the value of F_{BULK} was multiplied by the average of the ratios for the two bounding fuel plates. For each end channel F_{BULK} was multiplied by this ratio for the one bounding fuel plate. The hot channel factors listed

in Table 10 through Table 12 do not include these heat-flux ratio multipliers. Thus, in the PLTEMP/ANL model, the multiplicatively-combined channel-by-channel and plate-by-plate hot channel factors provided in Table 10 through Table 12 were multiplied by these ratios to predict an upper bound for the thermal conditions of the most limiting strip of each channel and to also include the reductions in channel thickness due to fuel plate swelling and clad surface oxidation, as described in section 11.

Because the code does not include a hot channel factor on coolant velocity, $F_{VELOCITY}$, this effect is investigated separately in section 16f. This factor has no effect on the margin to flow instability that is predicted by equation 1 because velocity does not appear in this equation. However, it does have an effect on CHF as predicted by equation 3 because mass flux, G, is the product of density and velocity. A reduction in velocity will reduce the predicted CHF value.

As indicated in Table 9, one of the two contributors to $F_{VELOCITY}$ is channel thickness tolerance. Although reducing the channel thickness has an adverse effect on velocity, which adversely impacts flow rate and bulk coolant and film temperature rises, the reduced channel thickness also has a beneficial effect on CHF that is not included in the PLTEMP/ANL code model. As equation 3 indicates, CHF is proportional to the heated diameter, D, to the −0.312 power. Since D is directly proportional to the channel thickness, the reduction in channel thickness that is represented in the hot channel factors has beneficial effect that is not included in the PLTEMP/ANL analysis. Therefore, in section 16f it is demonstrated that when $F_{VELOCITY}$ and the reduction in channel thickness are taken together any residual adverse effect, if it exists, is acceptably small. Moreover, the heated diameter appears in the flow instability equation, equation 1, as D_h. A reduction in D_h causes an increase in the margin to flow instability. This beneficial effect is assessed in section 16b. The ratio of the nominal channel thickness to the hot channel thickness, which is equal to the ratio of the nominal and the hot heated channel diameters, is listed in the last column of Table 10 for all of the channels of the HEU core and in the last columns of Table 11 and Table 12 for the channels of the other two cores. These ratios do not include any reduction in hot channel thickness due to fuel plate swelling or oxide growth, which was included where applicable.

Core neutron physics calculations showed that 6.0% of the reactor power generated by the HEU core is deposited outside of the primary system. Hence, the power represented in the PLTEMP/ANL model is only 94% of the reactor power. Therefore, for the HEU core, all PLTEMP/ANL values of power obtained by the code were divided by 0.940 before being inserted in the tables of results provided later. Similarly, for the LEU FSD and CD35 cores, 4.1 and 3.6% of the reactor power, respectively, is deposited outside the primary system. According, the PLTEMP/ANL powers for the FSD core were divided by 0.959 and the ones for the CD35 core were divided by 0.964.

Although a small fraction of the power deposited in the primary system may be deposited beyond the fuel meat, for all three cores all of the primary system power was assumed to be deposited in the fuel meat. This assumption, which is the most limiting one, has no effect on flow instability that is based on equation 1 because the exit bulk coolant temperature is unaffected by how the power is distributed within the channel. However, depositing a small fraction of the power in the coolant would diminish the local heat flux accordingly and slightly improve the margins to CHF.

The Moody friction factors used in the hydraulic analysis are a function of the relative roughness and the Reynolds number. The relative roughness is the absolute roughness divided by the hydraulic diameter. The absolute roughness has a maximum value of 63e-6 inches. The hydraulic diameter of the 24 channels for the fresh CD35 element is between 4.495e-3 and 4.745e-3 m, with an overall value (4 times total flow area divided by total wetted perimeter) of 4.565e-3 m. These values are based on nominal dimensions. This average diameter was used in determining a relative roughness, of 63e-6 inches × 0.0254 m/inch / 4.565 × 10^{-3} m, or 3.5× 10^{-4}. Similarly, the hydraulic diameter for the FSD core is 4.546 × 10^{-3} m and the relative roughness is 3.5 × 10^{-4}, and for HEU core the hydraulic diameter is 4.020 × 10^{-3} m and the relative roughness is 4.0 × 10^{-4}.

As indicated in section 1, the total coolant flow area between the fuel plates is about 60% of that above and below the core. The flow area contraction into the core and the flow area expansion after the core each produce an irrecoverable pressure drop. The inlet irrecoverable pressure drop is already included in the pressure drop model presented in section 9, specifically in the values of ΔP_K from point 3 to 4. A reduction in pressure that occurs at the outlet from the fuel plate, which is beyond the fuel region, can have no effect on the thermal performance of the fuel. However, the presence of these hydraulic resistances at the inlet and outlet of each channel tends to have a flow straightening effect in that they reduce the differences in bulk coolant velocities among the coolant channels.

After careful consideration, the combined values of the inlet and outlet form losses, i.e., combined K value used in the PLTEMP/ANL model were set zero. The K values that would apply were determined. Based on Reference 43, for a sudden contraction from flow area A_1 to flow area A_2, where the inlet to the smaller area is sharp, i.e., square-edged rather than rounded, the K-loss value, $K_{contract}$, for Reynolds number greater than 10^4 can be approximated by:

$$K_{contract}=0.5\left(1-\frac{A_2}{A_1}\right)^{0.75} \tag{14}$$

For the CD35 core, A_2/A_1 is 0.614, as given in section 1. Thus, the inlet K is 0.5 × $(1 – 0.614)^{0.75}$ = 0.24. Since the leading edges of the fuel plates are rounded, this value could be an order of magnitude smaller. It is well known that for a sudden expansion from flow area A_2 to flow area A_1, the K-loss value, $K_{expansion}$, is given by:

$$K_{expansion}=\left(1-\frac{A_2}{A_1}\right)^{2} \tag{15}$$

Thus, the outlet K is $(1 – 0.614)^2$ = 0.15. The K values should be compared to the corresponding friction factor resistance, f L/D, where f is the friction factor and L and D are the channel length and hydraulic diameter, respectively. f L/D is about 2.8 at the LSSS flow.

The potential for the flow straightening effect was investigated by examining the velocity distribution among channels with the combined value of K in the PLTEMP/ANL model set to zero and with it set to 0.24 + 0.15, or 0.39. In the PLTEMP/ANL model the channel velocities are calculated without the inclusion of local hot channel factors. For a combined K value of 0 in element 8 of the CD35 core 8A, at the LSSS conditions (3300 gpm) the 24 coolant channels have velocities between a minimum of 6.001 m/s and a maximum of 6.200 m/s. The average of the 24 values is 6.053 m/s. The other 7 elements for this case of this core and all eight elements for all other cases of this core should produce essentially the same results. This case was rerun with a combined K value of 0.39. The range of the coolant channel velocities was between 6.008 and 6.181 m/s. The average was 6.054 m/s. In both cases the first channel to achieve flow instability was channel 23 of element 8. In the K = 0.39 case the flow rate in this channel was 0.19% below that in the K = 0 case. This flow reduction should cause a 0.19% reduction in flow instability power. However, the flow instability power in the K = 0.39 case was 1.00% less than in the K = 0 case. The additional 0.81% reduction is due to the 0.070 bar pressure drop in the K = 0.39 case. The 0.19% potential error in the limiting channel flow rate is certainly acceptable when compared with the 15% local flow distribution hot channel factor.

14. Results

Table 16 lists the power at which flow instability and the power at which CHF is predicted to first occur for each of the 24 cases of the HEU core considered in the core neutron physics analysis. The minimum flow instability power, 14.61 MW (in red bold), occurs in case 3B2. As indicated at the bottom of the table, this power is 2.11 MW above the LSSS power of 12.5 MW. It occurs in channel 2 of element 1. This channel is bounded by two fuel plates and is the second closest to the flux trap. (The closest channel is an end channel.) Table 16 also shows the minimum CHF ratio at each flow instability power. The location of the minimum CHF ratio need not occur in the same channel or elements as the location of the minimum flow instability power. As indicated in bold red, the minimum CHF ratio is 2.421. The minimum CHF power, 29.88 MW (in red bold), occurs in case 1B1. This is the minimum power at which a CHF ratio of 1.0 occurs. It occurs in the end channel nearest the flux trap on the concave side of the first fuel plate at level 19 of element 7. Since the 24-inch heated length is divided into twenty-four 1-inch intervals, the physical location where CHF is predicted to first occur is 19 inches below the top of the heated section.

Table 17 and Table 18, which are arranged analogous to Table 16, list the flow instability and CHF powers and CHF ratio at the flow instability powers for the LEU FSD and LEU CD35 designs, respectively. The LEU LSSS power is 15.0 MW. The flow instability powers for these two cores are 2.12 and 2.10 MW above this LSSS value for the FSD and CD35 cores, respectively. These margins are within 0.01 MW of the flow instability safety margin of the HEU core. The HEU flow instability power is 1.169 times its LSSS power. The LEU FSD and LEU CD35 flow instability powers are 1.141 and 1.140, respectively, times their LSSS powers. As indicated in bold red, the minimum CHF ratio at the flow instability power is 2.082 and 2.024 for the LEU FSD and LEU CD35 cores, respectively.

In the HEU core both flow instability and CHF first occurs in a fresh element. In both LEU cores flow instability first occurs in the channel between the two fuel plates furthest from the flux trap. In the LEU FSD core this element that has 97 MWd of burnup of a total discharge burnup of 208 MWd. In the LEU CD35 core this element is at the discharge burnup of 180 MWd. For the two LEU cores, CHF first occurs in a fresh element in the end channel furthest from the flux trap which, of course, is on the convex side of the last fuel plate.

Of the 24 LEU CD35 cases considered in Table 18, case 8A1 produced the lowest flow instability power. For this case the PLTEMP/ANL (eight-element) model was used to perform a parametric study in which pressurizer pressure, core inlet temperature, and core inlet flow rate were varied. The corresponding flow instability powers were obtained. The pressurizer level was maintained at its minimum value of −16 inches throughout the study. Table 19 shows the results for a pressurizer pressure of 60 psia. The first column shows the six inlet temperatures in the study. The first row of numbers shows the 11 flow rates in the study. Table 20 and Table 21 show the corresponding results and at the same inlet temperature and flow rates for pressurizer pressures of 75 and 85 psia, respectively. The results of Table 19 through Table 21 are plotted in Figure 7 through Figure 9, respectively.

For each value of flow instability power provided in Table 19 through Table 21 the corresponding value of CHF ratio is provided in the same location in Table 22, Table 23, and Table 24, respectively. In each of these three CHF ratio tables, the minimum CHF ratio occurs at the lowest inlet temperature (120° F) and the highest flow rate (4000 gpm). The lowest CHF ratio, 2.140, is at 85 psia.

Of the 24 LEU CD35 cases considered in Table 18, case 7A1 produced the lowest critical heat flux power. A parametric CHF study that is analogous to the parametric flow instability study was performed with the pressurizer level also maintained at −16 inches. The results are presented in Table 25 through Table 27 and in Figure 10 through Figure 12.

The LSSS values for the four reactor parameters, pressurizer pressure, inlet temperature, inlet flow rate, and reactor power are shown in Table 6 for both the HEU and LEU cores. In the results presented above, the first three of these parameters have been constrained to their LSSS values and the power at which flow instability is predicted to occur has been obtained with the aid of the PLTEMP/ANL code. This can be thought of as a constrained mathematical problem with three independent variables and one dependent one. If power and two of the other three reactor parameters are constrained to their LSSS values, then it is possible, via a series of trial-and-error PLTEMP/ANL code solutions to determine the allowed value of the remaining variable. In all cases the pressurizer level would be maintained at its minimum value of −16 inches. Table 28 shows the results for these four constrained problems for case 3B2 of the HEU core. In each case in Table 28, the independent variable is shown in red and the other three are at their LSSS values and shown in black.

In Case 1 of Table 28 reactor power is the independent variable and is 14.61 MW, as shown in Table 16 for core configuration case 3B2. All four cases in the table are based on this core configuration. In Case

2 inlet temperature is the independent variable. In Case 3 inlet flow rate is the independent value. These definitions of Cases 1 through 3 correspond to Cases 1 through 3, respectively, as defined on page H-2 of Appendix H, *Bases for Limiting Safety System Settings for Model I and II Operation*, of Addendum 4 of the MURR Hazards Summary Report, which was revised and attached to a 2011 letter sent to the US NRC[3]. In Case 4 pressurizer pressure is the independent variable. The last column of Table 28 provides the CHF ratio at the reactor conditions for the case. Table 29 provides the analogous results for case 8A1 of the LEU core CD35. All of the CHF ratios in both Table 28 and Table 29 are greater than 2.0.

Table 16. Reactor Flow Instability and Critical Heat Flux Ratios and Powers (MW) for the HEU Core
(All other reactor operating conditions are at the LSSS Values – 155° F inlet temperature, 3200 gpm based on the inlet density, and 75 psia at the pressurizer. The pressurizer level is at −16 inches.)

	Flow Instability				Critical Heat Flux			
Case	Power	Element	Channel	CHFR*	Power	Element	Plate**	Axial Level
1A	16.15	2	2	2.456	32.47	2	+1	20
1A1	15.46	7	2	2.545	32.26	7	-1	20
1A2	15.61	1	2	2.555	32.25	2	+1	19
2A	16.79	5	2	2.545	35.14	2	+1	19
2A1	16.26	7	2	2.593	34.73	7	-1	17
2A2	16.44	1	2	2.606	34.76	1	-1	19
3A	15.60	5	2	2.567	33.31	5	+1	18
3A1	15.59	1	2	2.615	33.17	1	+1	18
3A2	15.26	1	2	2.655	32.83	1	+1	18
4A	16.40	5	2	2.674	36.58	5	+1	17
4A1	16.40	1	2	2.743	36.35	1	+24	17
4A2	16.32	1	2	2.731	36.50	1	+1	17
1B	15.46	5	2	**2.421**	30.62	5	-1	20
1B1	14.83	7	2	2.474	**29.88**	7	-1	19
1B2	15.00	1	2	2.482	30.36	1	-1	19
2B	16.16	5	2	2.517	33.12	5	-1	19
2B1	15.66	7	2	2.594	32.77	7	-1	19
2B2	15.80	1	2	2.581	33.01	1	-1	18
3B	15.04	5	2	2.567	31.40	1	+1	19
3B1	14.84	1	2	2.623	31.24	1	-1	19
3B2	**14.61**	1	2	2.618	30.84	1	-1	19
4B	15.82	1	2	2.797	35.11	1	+1	17
4B1	15.76	1	2	2.798	35.02	1	-1	17
4B2	15.74	1	2	2.813	35.34	1	-1	17
Min. Ratio	1.169			2.421	2.390			
Margin, MW	2.11				14.88			

*CHF ratio at the flow instability power, based on the extended Groeneveld 2006 CHF Table, equation 3

** A "−" sign implies that the location is at the concave side of the fuel plate. A "+" sign Implies that the location is at the convex side of the fuel plate.

Table 17. Reactor Flow Instability and Critical Heat Flux Ratios and Powers (MW) for the LEU FSD Core
(All other reactor operating conditions are at the LSSS Values – 145° F inlet temperature, 3300 gpm based on the inlet density, and 75 psia at the pressurizer. The pressurizer level is at –16 inches.)

	Flow Instability				Critical Heat Flux			
Case	Power	Element	Channel	CHFR*	Power	Element	Plate**	Axial Level
5A	18.48	3	3	2.243	33.09	2	-3	24
5A1	17.84	7	3	2.156	31.79	8	+24	20
5A2	17.87	2	3	2.145	31.78	8	+24	20
6A	19.25	2	3	2.159	33.87	8	+24	19
6A1	18.82	7	3	**2.082**	31.57	6	+24	18
6A2	18.82	1	3	2.119	32.25	8	+24	18
7A	18.22	8	4	2.237	32.68	1	+24	19
7A1	17.55	8	4	2.188	**30.55**	1	+24	19
7A2	17.60	8	4	2.227	31.04	1	+24	18
8A	18.19	1	24	2.385	33.83	1	+24	16
8A1	**17.12**	7	24	2.455	32.35	1	+24	17
8A2	17.19	1	24	2.488	32.77	1	+24	16
5B	17.85	5	3	2.321	32.94	4	-3	24
5B1	17.14	7	3	2.222	31.65	6	+24	20
5B2	17.28	1	3	2.250	31.86	8	+24	20
6B	18.77	7	3	2.248	33.92	8	+24	19
6B1	18.11	7	3	2.194	31.88	6	+24	18
6B2	18.33	1	3	2.191	32.22	8	+24	19
7B	17.65	8	4	2.357	33.05	1	+24	18
7B1	17.16	8	4	2.255	30.82	1	+24	18
7B2	17.23	1	3	2.281	30.89	1	+24	18
8B	17.92	6	24	2.496	34.45	1	+24	15
8B1	17.31	6	24	2.488	33.21	1	+24	17
8B2	17.28	8	24	2.571	33.65	1	+24	17
Min. Ratio	1.141			2.082	2.037			
Margin, MW	2.12				15.55			

*CHF ratio at the flow instability power, based on the extended Groeneveld 2006 CHF Table, equation 3

** A "–" sign implies that the location is at the concave side of the fuel plate. A "+" sign Implies that the location is at the convex side of the fuel plate.

Table 18. Reactor Flow Instability and Critical Heat Flux Ratios and Powers (MW) for the LEU CD35 Core (All other reactor operating conditions are at the LSSS Values – 145° F inlet temperature, 3300 gpm based on the inlet density, and 75 psia at the pressurizer. The pressurizer level is at –16 inches.)

	Flow Instability				Critical Heat Flux			
Case	Power	Element	Channel	CHFR*	Power	Element	Plate**	Axial Level
5A	19.63	5	4	2.107	34.85	8	+23	20
5A1	18.91	8	4	**2.024**	31.73	6	+23	20
5A2	18.86	1	4	2.053	31.94	8	+23	20
6A	20.57	2	4	2.053	34.77	6	+23	19
6A1	18.79	6	23	2.130	32.04	6	+23	18
6A2	19.05	8	23	2.152	32.57	8	+23	18
7A	18.57	8	4	2.293	34.23	1	+23	18
7A1	17.99	6	23	2.166	**31.26**	1	+23	18
7A2	17.95	8	23	2.231	31.61	1	+23	18
8A	17.87	8	23	2.557	34.98	1	+23	16
8A1	**17.10**	8	23	2.581	33.50	1	+23	17
8A2	17.15	8	23	2.595	33.61	1	+23	16
5B	19.19	4	3	2.172	34.93	6	+23	20
5B1	18.32	7	4	2.098	31.91	6	+23	19
5B2	18.56	2	4	2.084	31.76	8	+23	20
6B	19.99	5	3	2.158	34.89	6	+23	18
6B1	18.73	6	23	2.179	32.52	6	+23	17
6B2	18.94	8	23	2.217	33.09	8	+23	18
7B	18.17	4	4	2.346	33.88	1	+23	18
7B1	17.65	8	4	2.225	31.38	1	+23	18
7B2	17.58	8	4	2.319	31.85	1	+23	18
8B	17.56	8	23	2.634	35.06	1	+23	15
8B1	17.37	6	23	2.667	34.99	1	+23	16
8B2	17.25	8	23	2.670	34.60	1	+23	16
Min. Ratio	1.140			2.024	2.08			
Margin, MW	2.10				16.26			

*CHF ratio at the flow instability power, based on the extended Groeneveld 2006 CHF Table, equation 3

** A "–" sign implies that the location is at the concave side of the fuel plate. A "+" sign Implies that the location is at the convex side of the fuel plate.

Table 19. LEU Core CD35 Flow Instability Power, MW, with the Pressurizer Pressure at 60 psia

Reactor Inlet Water Conditions											
Temp	Flow Rate (GPM)										
°F	400	800	1200	1600	2000	2400	2800	3200	3300	3600	4000
120	2.57	5.05	7.45	9.75	11.93	13.96	15.79	17.39	17.74	18.68	19.57
140	2.27	4.45	6.55	8.56	10.46	12.20	13.76	15.09	15.38	16.13	16.78
145	2.19	4.30	6.33	8.27	10.09	11.76	13.25	14.51	14.79	15.49	16.09
160	1.96	3.84	5.66	7.38	8.98	10.45	11.73	12.79	13.02	13.57	13.99
180	1.66	3.24	4.77	6.20	7.52	8.70	9.71	10.50	10.65	11.01	11.18
200	1.36	2.65	3.88	5.02	6.06	6.96	7.69	8.22	8.31	8.47	8.39

Table 20. LEU Core CD35 Flow Instability Power, MW, with the Pressurizer Pressure at 75 psia

Reactor Inlet Water Conditions											
Temp	Flow Rate (GPM)										
°F	400	800	1200	1600	2000	2400	2800	3200	3300	3600	4000
120	2.80	5.50	8.14	10.69	13.14	15.47	17.64	19.63	20.09	21.39	22.87
140	2.49	4.90	7.24	9.50	11.66	13.70	15.59	17.30	17.70	18.80	20.02
145	2.42	4.75	7.02	9.20	11.29	13.26	15.08	16.72	**17.10**	18.15	19.31
160	2.19	4.30	6.34	8.31	10.18	11.93	13.55	14.98	15.31	16.21	17.17
180	1.88	3.70	5.45	7.12	8.71	10.18	11.51	12.67	12.93	13.63	14.33
200	1.58	3.10	4.56	5.95	7.24	8.43	9.48	10.37	10.56	11.05	11.50

Table 21. LEU Core CD35 Flow Instability Power, MW, with the Pressurizer Pressure at 85 psia

Reactor Inlet Water Conditions											
Temp	Flow Rate (GPM)										
°F	400	800	1200	1600	2000	2400	2800	3200	3300	3600	4000
120	2.93	5.77	8.54	11.23	13.83	16.32	18.68	20.87	21.38	22.87	24.62
140	2.63	5.17	7.64	10.04	12.35	14.55	16.62	18.53	18.98	20.26	21.75
145	2.55	5.01	7.41	9.74	11.98	14.11	16.10	17.95	18.38	19.61	21.03
160	2.32	4.56	6.74	8.84	10.86	12.78	14.57	16.20	16.58	17.65	18.88
180	2.02	3.96	5.84	7.66	9.39	11.01	12.52	13.87	14.19	15.05	16.02
200	1.71	3.36	4.95	6.47	7.92	9.26	10.48	11.56	11.81	12.47	13.17

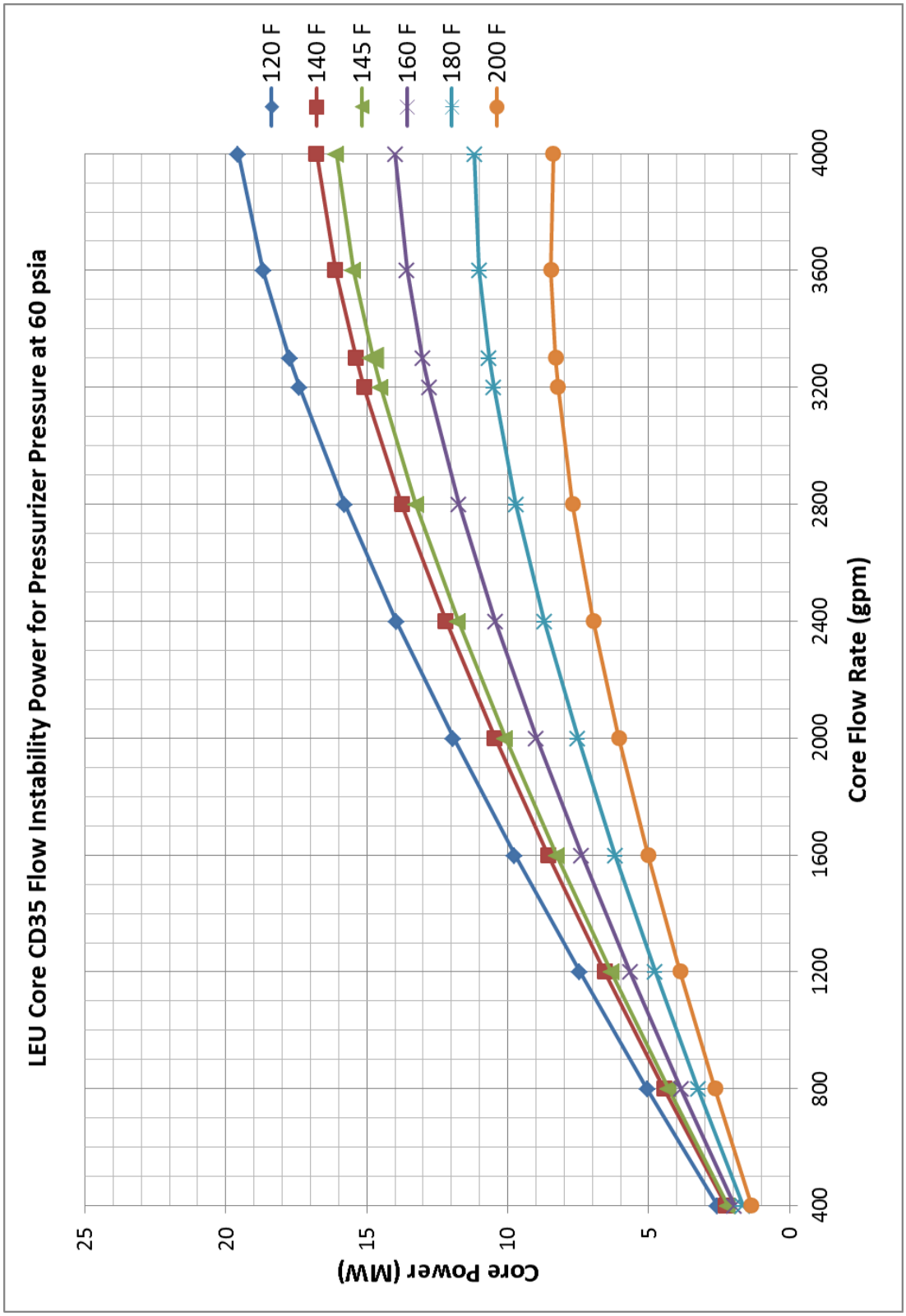

Figure 7. LEU Core CD35 Flow Instability Power for Pressurizer Pressure at 60 psia

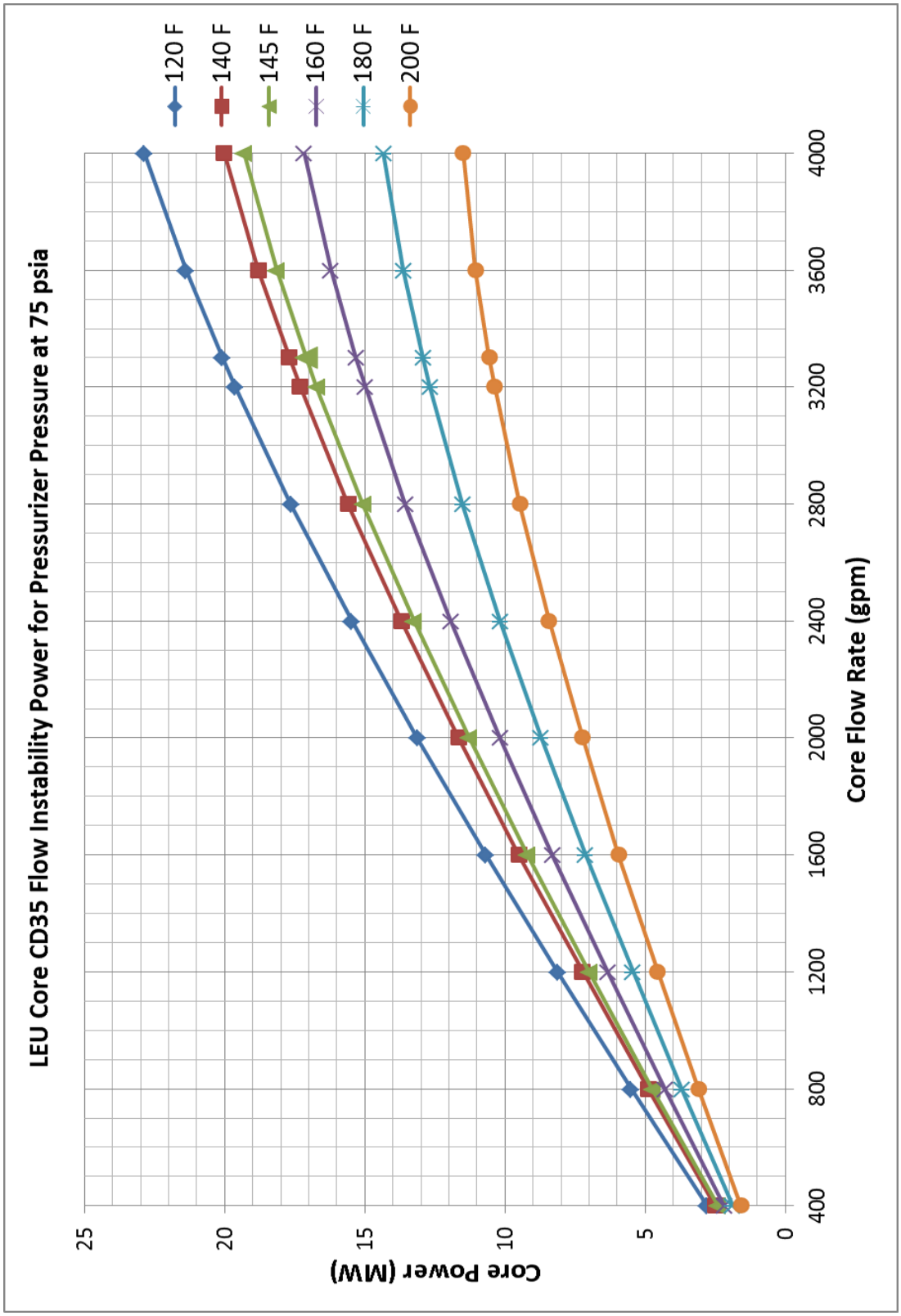

Figure 8. LEU Core CD35 Flow Instability Power for Pressurizer Pressure at 75 psia

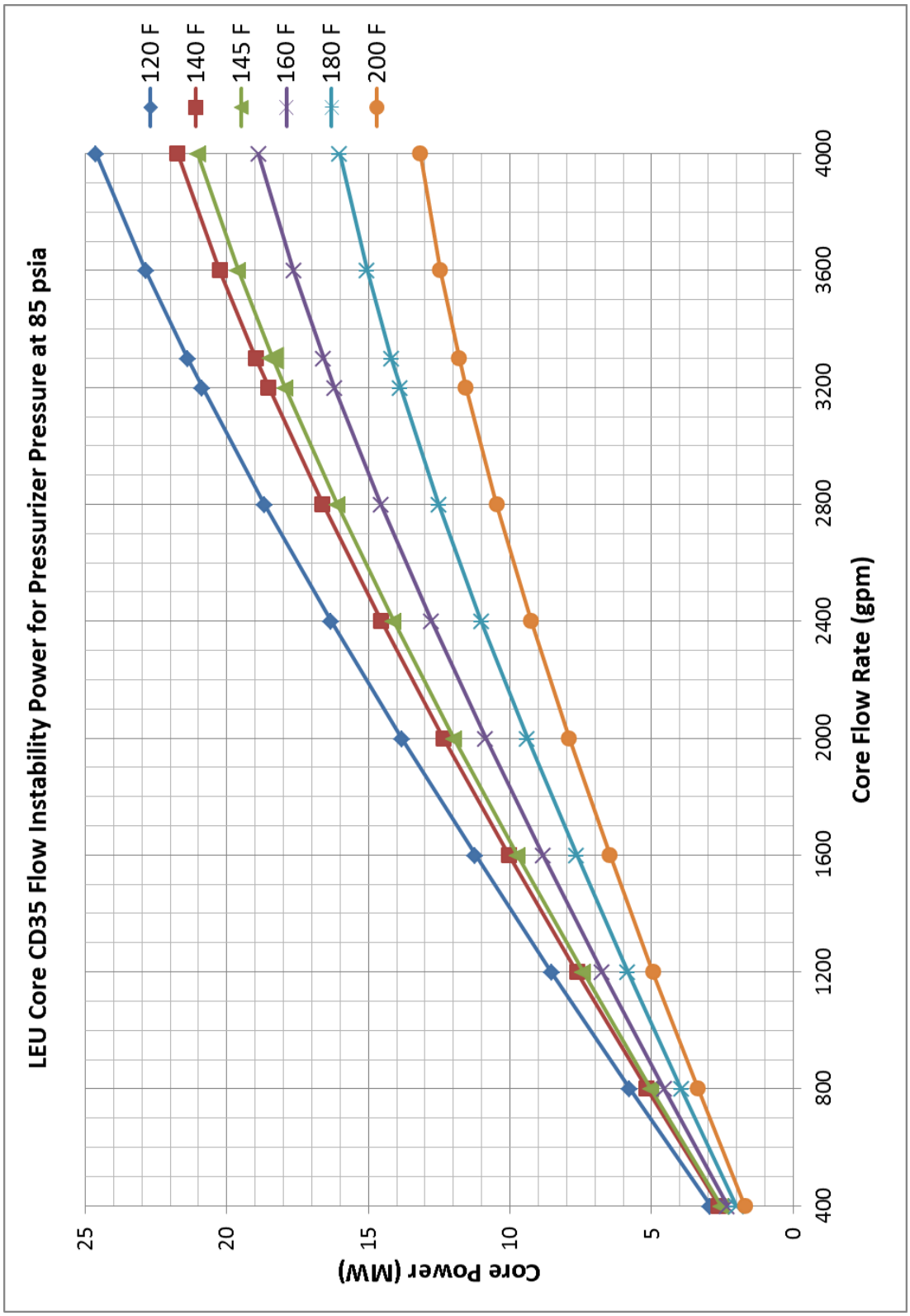

Figure 9. LEU Core CD35 Flow Instability Power for Pressurizer Pressure at 85 psia

Table 22. LEU Core CD35 CHF Ratio at Flow Instability Power with the Pressurizer Pressure at 60 psia

Reactor Inlet Water Conditions											
Temp	Flow Rate (GPM)										
°F	400	800	1200	1600	2000	2400	2800	3200	3300	3600	4000
120	7.959	5.739	4.575	3.694	3.111	2.850	2.636	2.537	2.526	2.503	2.465
140	8.409	6.147	4.911	3.990	3.388	3.136	2.904	2.762	2.744	2.690	2.637
145	8.574	6.263	4.995	4.055	3.451	3.201	2.969	2.822	2.803	2.744	2.691
160	9.280	6.677	5.292	4.284	3.673	3.427	3.200	3.038	3.014	2.942	2.891
180	10.545	7.423	5.829	4.700	4.071	3.841	3.625	3.442	3.414	3.325	3.277
200	12.354	8.512	6.616	5.319	4.649	4.464	4.272	4.079	4.044	3.940	3.981

Table 23. LEU Core CD35 CHF Ratio at Flow Instability Power with the Pressurizer Pressure at 75 psia

Reactor Inlet Water Conditions											
Temp	Flow Rate (GPM)										
°F	400	800	1200	1600	2000	2400	2800	3200	3300	3600	4000
120	7.956	5.563	4.450	3.585	2.981	2.719	2.488	2.353	2.332	2.282	2.233
140	8.087	5.906	4.777	3.875	3.228	2.953	2.707	2.546	2.524	2.477	2.436
145	8.190	6.008	4.876	3.961	3.302	3.022	2.772	2.604	2.581	2.534	2.477
160	8.658	6.359	5.198	4.243	3.555	3.254	2.986	2.781	2.751	2.684	2.622
180	9.677	6.985	5.655	4.612	3.900	3.581	3.300	3.071	3.036	2.958	2.890
200	11.080	7.864	6.291	5.128	4.377	4.052	3.750	3.494	3.453	3.359	3.293

Table 24. LEU Core CD35 CHF Ratio at Flow Instability Power with the Pressurizer Pressure at 85 psia

Reactor Inlet Water Conditions											
Temp	Flow Rate (GPM)										
°F	400	800	1200	1600	2000	2400	2800	3200	3300	3600	4000
120	8.024	5.477	4.383	3.527	2.912	2.655	2.431	2.279	2.254	2.194	2.140
140	8.160	5.798	4.677	3.788	3.138	2.864	2.624	2.445	2.417	2.355	2.306
145	8.207	5.892	4.764	3.865	3.204	2.925	2.681	2.493	2.465	2.403	2.355
160	8.529	6.217	5.066	4.130	3.433	3.134	2.879	2.666	2.634	2.564	2.502
180	9.361	6.788	5.524	4.513	3.788	3.456	3.172	2.921	2.880	2.801	2.733
200	10.600	7.585	6.104	4.981	4.217	3.861	3.549	3.270	3.224	3.133	3.066

Table 25. LEU Core CD35 CHF Power, MW, with the Pressurizer Pressure at 60 psia

Reactor Inlet Water Conditions											
Temp	Flow Rate (GPM)										
°F	400	800	1200	1600	2000	2400	2800	3200	3300	3600	4000
120	9.76	15.76	19.38	21.69	24.46	27.65	29.97	31.58	31.78	32.39	32.98
140	9.36	15.10	18.42	20.60	23.03	26.06	28.22	29.44	29.63	29.99	30.39
145	9.26	14.93	18.18	20.31	22.68	25.67	27.83	29.03	29.24	29.58	29.93
160	9.01	14.42	17.55	19.46	21.64	24.52	26.69	27.82	28.08	28.38	28.57
180	8.76	13.88	16.74	18.61	20.28	22.99	25.14	26.21	26.54	26.82	26.80
200	8.51	13.25	15.91	17.78	19.27	21.44	23.17	24.23	24.51	25.06	25.01

Table 26. LEU Core CD35 CHF Power, MW, with the Pressurizer Pressure at 75 psia

Reactor Inlet Water Conditions											
Temp	Flow Rate (GPM)										
°F	400	800	1200	1600	2000	2400	2800	3200	3300	3600	4000
120	10.30	16.80	20.73	23.47	26.60	29.89	31.98	33.57	34.02	35.30	36.74
140	9.89	16.12	19.71	22.30	25.11	28.09	29.92	31.52	31.91	32.85	34.04
145	9.79	15.95	19.45	22.07	24.75	27.71	29.46	30.90	**31.26**	32.33	33.34
160	9.51	15.46	18.71	21.21	23.72	26.58	28.33	29.44	29.73	30.52	31.39
180	9.14	14.89	17.93	20.15	22.29	25.08	26.86	27.76	28.06	28.84	29.64
200	8.81	14.28	17.04	19.24	21.06	23.56	25.44	26.08	26.38	27.16	27.91

Table 27. LEU Core CD35 CHF Power, MW, with the Pressurizer Pressure at 85 psia

Reactor Inlet Water Conditions											
Temp	Flow Rate (GPM)										
°F	400	800	1200	1600	2000	2400	2800	3200	3300	3600	4000
120	10.85	17.43	21.58	24.53	27.74	31.06	32.96	34.97	35.50	37.12	38.97
140	10.59	16.70	20.52	23.31	26.26	29.20	31.21	32.74	33.13	34.37	35.80
145	10.49	16.52	20.27	23.06	25.89	28.82	30.64	32.18	32.62	33.91	35.21
160	10.21	16.06	19.49	22.27	24.80	27.71	29.27	30.44	30.81	32.00	33.36
180	9.97	15.48	18.66	21.12	23.42	26.23	27.82	28.70	28.99	29.99	31.12
200	9.77	14.87	17.83	20.16	22.10	24.75	26.42	26.98	27.27	28.18	29.31

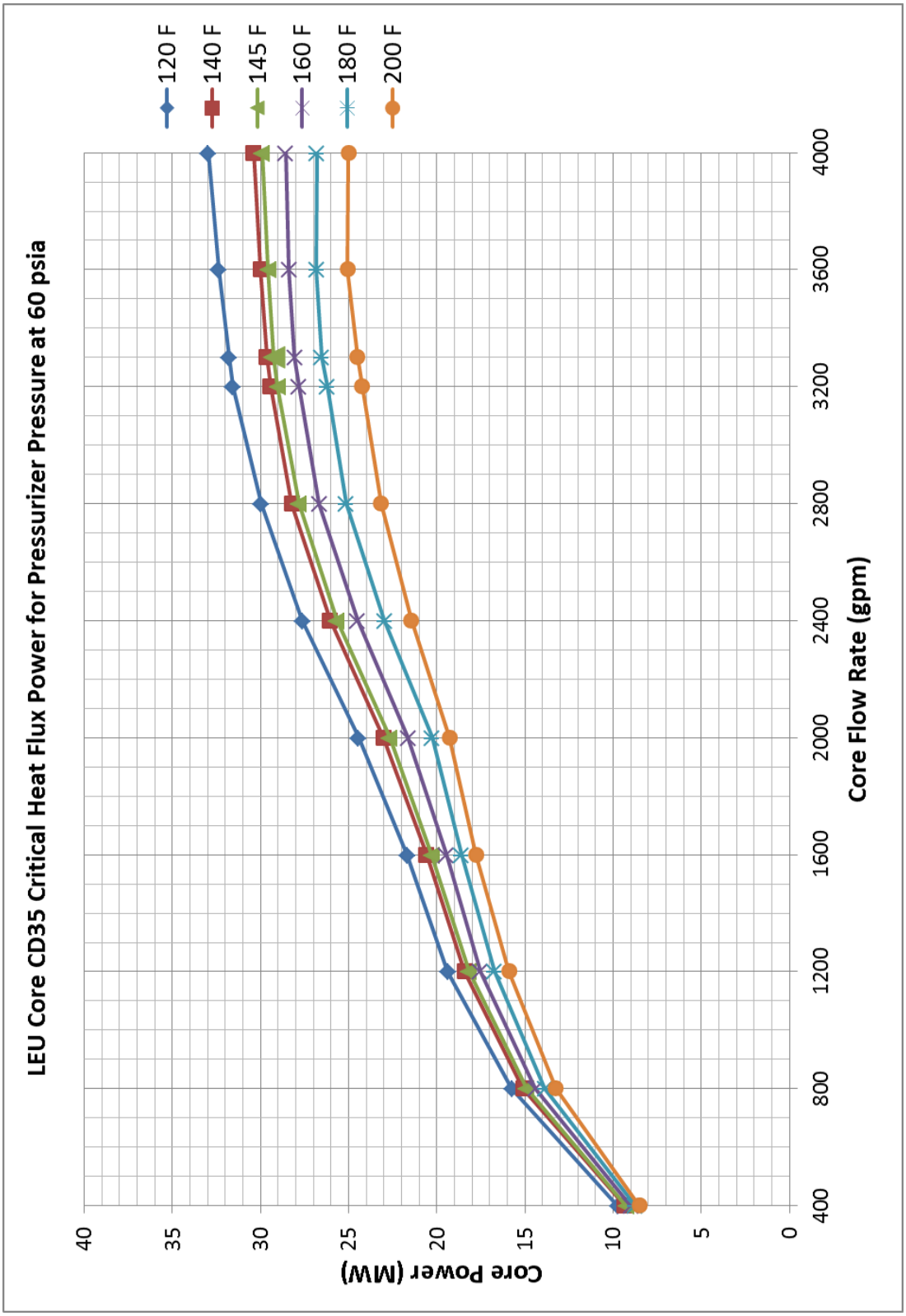

Figure 10. LEU Core CD35 Critical Heat Flux Power for Pressurizer Pressure at 60 psia

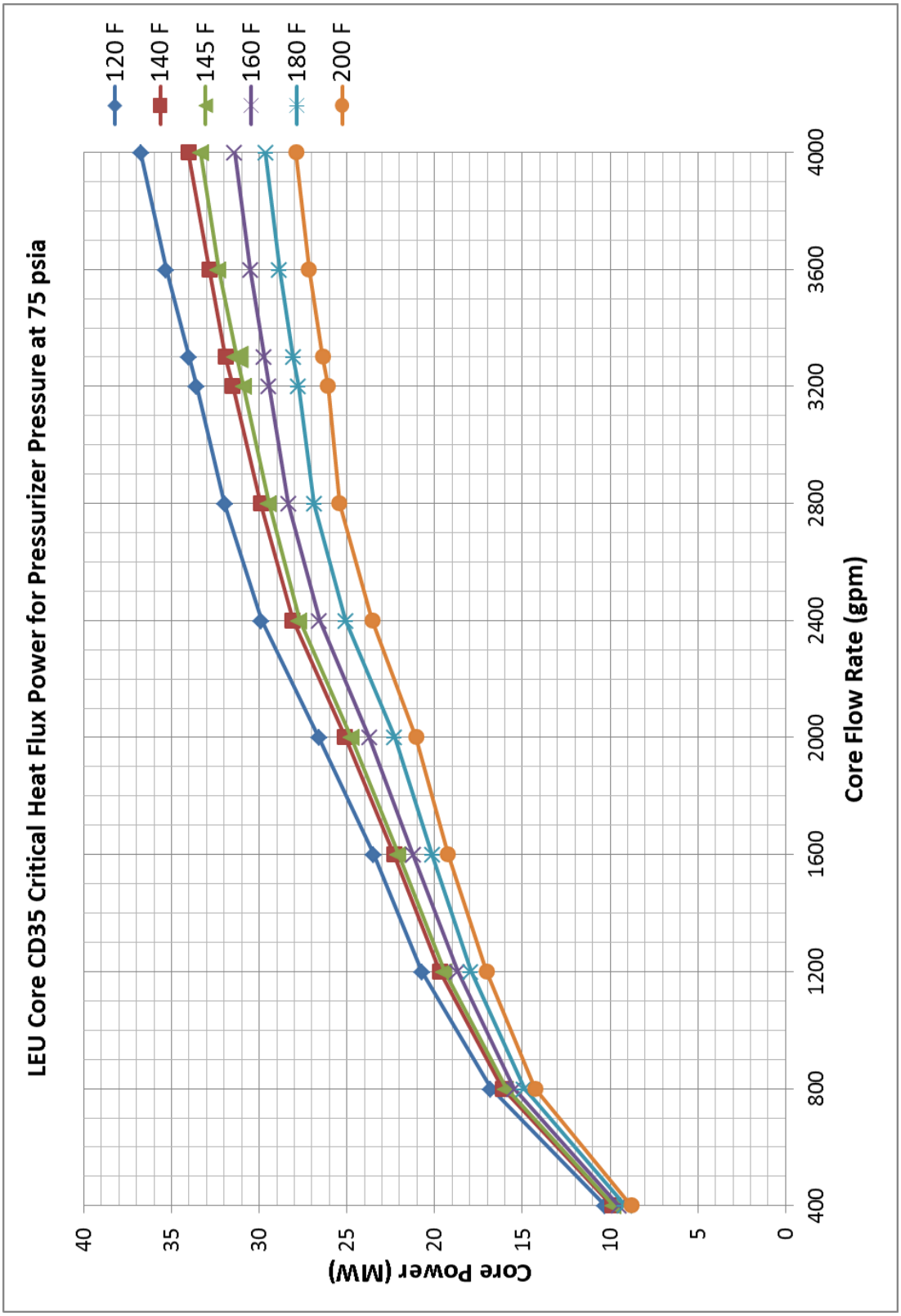

Figure 11. LEU Core CD35 Critical Heat Flux Power for Pressurizer Pressure at 75 psia

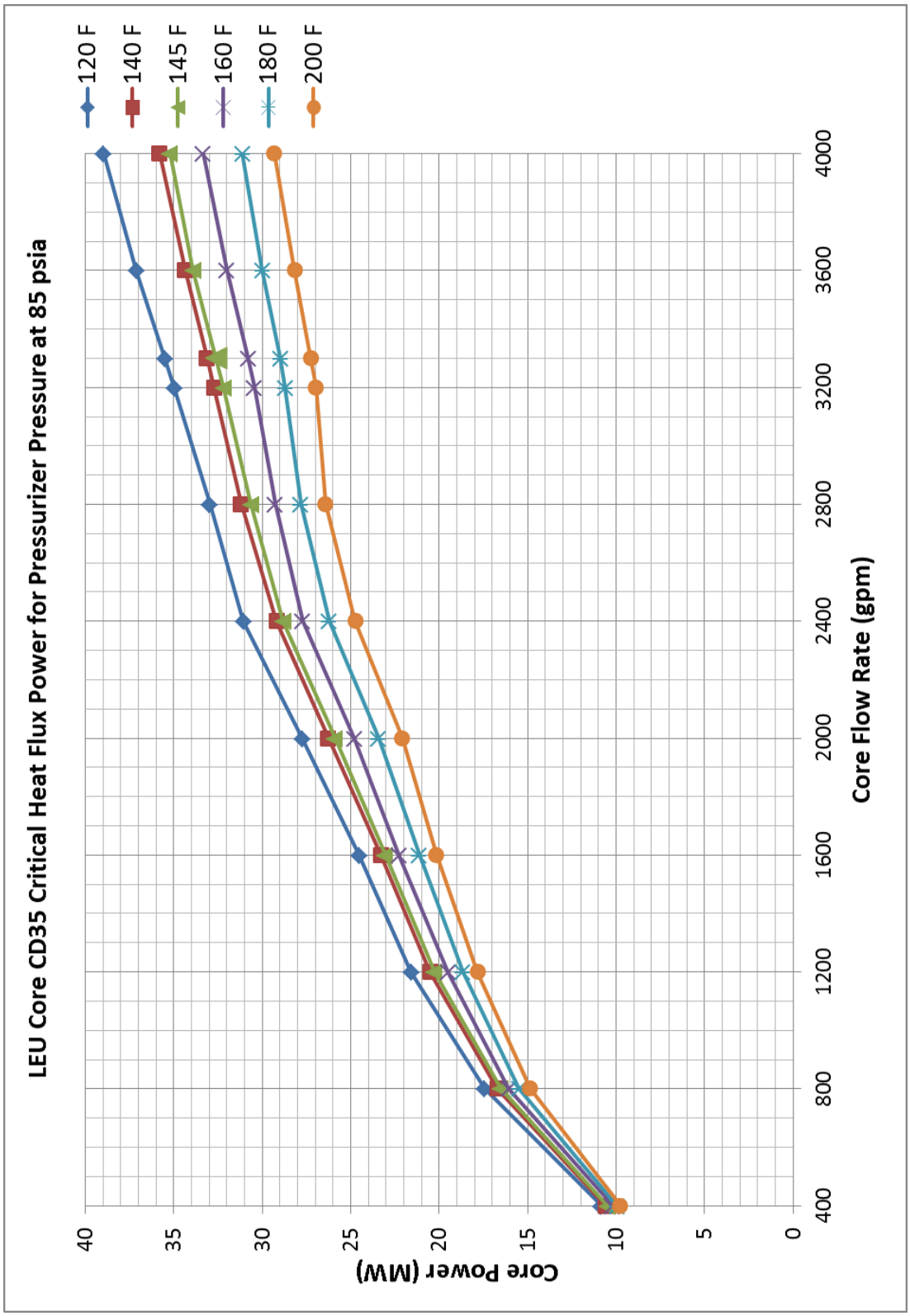

Figure 12. LEU Core CD35 Critical Heat Flux Power for Pressurizer Pressure at 85 psia

Table 28. HEU Core Flow Instability When Three Reactor Parameters Are at Their LSSS Values

MURR HSR* Appendix H Case	Pressurizer Pressure, psia	Inlet Flow, gpm	Inlet Temperature, F	Reactor Power, MW	CHF Ratio at These Conditions
1	75	3200	155	**14.61**	2.618
2	75	3200	**174.1**	12.50	2.882
3	75	**2580**	155	12.50	2.762
4**	**60.70**	3200	155	12.50	2.895

*Hazards Summary Report

**Case 4 is not defined in the MURR Hazards Summary Report.

Table 29. LEU Core CD35 Flow Instability When Three Reactor Parameters Are at Their LSSS Values

MURR HSR* Appendix H Case	Pressurizer Pressure, psia	Inlet Flow, gpm	Inlet Temperature, F	Reactor Power, MW	CHF Ratio at These Conditions
1	75	3300	145	**17.10**	2.581
2	75	3300	**162.6**	15.00	2.783
3	75	**2780**	145	15.00	2.783
4**	**61.20**	3300	145	15.00	2.779

*Hazards Summary Report

**Case 4 is not defined in the MURR Hazards Summary Report.

15. Verification of the PLTEMP/ANL Results

In order to independently verify the results of the PLTEMP/ANL analysis, a separate thermal model of a single channel was developed and implemented on a computer spreadsheet as a checker program. For a few selected PLTEMP/ANL cases the channel that was identified as limiting was analyzed with this specially-developed checker program. These cases include the limiting flow instability power case and the limiting CHF power case for each of the three cores. Their allowed powers are shown in red bold in Table 16 through Table 18.

Some of the inputs to the checker program are copied directly from the PLTEMP/ANL output. These include the channel flow rate, the axial distribution of pressure, and the level-by-level fraction of fuel plate nodal power that exits each face of each fuel plate. This fraction is typically about 0.5 since about half of the power generated in a fuel plate leaves from each face. However for the first and the last fuel plate, a highly asymmetric thermal boundary can cause as much as about 55% of the power at some axial levels to go into the end channel.

Some of the inputs to the checker code are taken directly from their original sources. The power produced in each axial level of each plate that bound the channel is taken from its source, which provides values for each level in watts. This source also provides the strip-wise peak heat flux ratio for each fuel plate. As described in section 13, this ratio was obtained in the core neutron physics analysis by subdividing the heated region of the fuel plate into nine vertical strips and dividing the average heat flux of each strip by the average heat flux taken over all nine strips. The hot channel factors of Table 10 through Table 12, with appropriate adjustments to include reductions in channel thicknesses due to burnup, are also inputs to the checker code.

The checker program calculates the axial distribution of channel bulk coolant temperature. For each heated surface it also calculates the axial distributions of surface temperature, film coefficient based on equation 5, heat flux, critical heat flux based on both equation 3 (the extended Groeneveld 2006 Table) and the Bernath CHF correlation[6], and the CHF ratio for each correlation. The program also determines the margin to flow instability based on equation 1 (Whittle and Forgan), equation 2 (Saha -Zuber), and the criterion that requires a Bernath CHF ratio of 2.0.

Although not used for flow instability or CHF analysis, the checker program replicates the fuel plate thermal model of section 10. For each axial level it provides the fuel plate temperature rises through the oxide, aluminum and the zirconium layers, the interface temperatures between adjacent layers, and the peak fuel temperature.

Quantities in the PLTEMP/ANL output that are to be verified by the checker program are copied from the PLTEMP/ANL output. The program explicitly and directly compares the quantities it calculates with their PLTEMP/ANL counterparts by displaying ratios for quantities such as heat fluxes and film coefficients and differences for quantities such as temperatures.

A considerable amount of output must be extracted from PLTEMP/ANL outputs. A typical PLTEMP/ANL output may contain about 200,000 lines. Therefore, another computer program, “pltemp_hotchan_analyzer”, was developed in the Python language to read the PLTEMP/ANL output file and to assemble the required input data for the checker program in a text file of about 40 lines. This text file is electronically copied and pasted to cells in the checker program spreadsheet. Cells in the checker program that need this data are directly linked to, i.e., equated with, the cells that were copied from the checker program output.

16. Discussion

16a Comparison of PLTEMP/ANL Flow Instability Predictions with the Checker Program Results for Three Flow Instability Correlations

The flow instability results presented in Table 16 through Table 18 are based on the Whittle and Forgan relationship, equation 1. The checker program, which is described in the previous section, was used to compare the flow instability predictions of equation 1, with those of the Saha-Zuber relation, equation 2, and the Bernath-CHF-ratio-of-2.0 relationship, which is identified in section 5. In the checker program the reactor power is multiplied by a "checker program factor", which was adjusted via the built-in solver in the computer spreadsheet until flow instability was predicted to occur by either equation 1, or the Saha-Zuber relationship, equation 2, or by a minimum Bernath CHF ratio of 2.0. A value of 1.0 for this factor implies perfect agreement with the PLTEMP/ANL (equation 1) prediction. The middle part of Table 30 compares this factor for each of the three flow instability criteria considered. The PLTEMP/ANL limiting case and location for each of the three MURR core types are shown in the upper part of the table, along with the LSSS values of reactor power.

All of the Whittle and Forgan checker program factors shown in the table are within 0.5% of 1.0. This demonstrates that the checker program results are in very close agreement with the PLTEMP/ANL results, as they should be. The Saha-Zuber values of the factors are about 5 to 8% larger than those for Whittle and Forgan ones. This demonstrates that equation 1 predicted lower allowed flow instability powers than equation 2 predicted. For the LEU FSD core the Bernath CHFR = 2.0 factor is 0.994, which agrees with the Whittle and Forgan factor to within less than 1%. For the HEU and LEU CD35 cores the Bernath CHFR = 2.0 criterion predicts a few percent greater power than is predicted by equation 1. These results also show that replacing equation 1 with the Bernath CHFR = 2.0 criterion causes a 3.2% ([1.037/1.0049 – 1] × 100%) improvement in the HEU flow instability margin and about an 7.6% improvement in the LEU CD35 one, resulting in a relative gain of about 4.4% of the LEU CD35 performance relative to that for the HEU core.

A second requirement of the Bernath flow instability criterion is that the power also be limited to the power at which bulk boiling occurs at the exit. For all of the Table 30 cases, a Bernath CHF ratio of 2.0 was always reached before bulk boiling occurred at the exit of the channel.

Although only the limiting channel of the limiting case of each core was considered in Table 30, the comparison should be indicative of what would have been obtained if the complete analysis were performed for each of the three criteria. The Table 30 comparison also serves to increase confidence in the use of the PLTEMP/ANL results in predicting minimum safety margins.

Table 30. Comparison of Flow Instability Predictions for the Most Limiting Channel

	HEU	LEU CD35	LEU FSD
LSSS Power, MW	12.5	15.0	15.0
PLTEMP/ANL Power, MW*	14.61	17.10	17.12
Limiting Case & Location			
Case	3B2	8A1	8A1
Element	1	8	7
Channel	2	23	24
Checker Program Factor**			
Whittle & Forgan, Eq. 1	1.0049	1.0038	1.0031
Saha-Zuber, Eq. 2	1.058	1.097	1.085
Bernath CHFR = 2.0	1.037	1.080	0.994
Heated Diameter Reduction Factor	1.11	1.21	1.15
Checker Program Factor Based on Whittle & Forgan, Eq. 1, with the Heated Diameter Reduction Factor Included	1.024	1.041	1.031
PLTEMP/ANL Power, MW, Adjusted to Include Effect of Heated Diameter Reduction Factor	14.89	17.73	17.60

*These values are the total reactor power, including the power that is deposited outside of the primary system.

**1.0 corresponds to the PLTEMP power.

16b. Beneficial Effect of Reduced Channel Thickness on the Margin to Flow Instability

As indicated in section 13, the reduction in channel thickness due to geometric tolerances and fuel plate swelling and oxide growth reduces the channel flow rate and has an adverse effect on the margin to flow instability, which is included in the PLTEMP/ANL analysis. However, the reduction in channel thickness has an accompanying beneficial effect that is not included in the PLTEMP/ANL analysis. Decreasing the channel thickness, decreases the heated diameter, D_h in equation 1, and improves the margin to flow instability. The checker program was used to assess the effect of this beneficial effect on the limiting channel for the limiting case of each of the three cores. The results of this assessment are provided in the bottom part of Table 30. The heated diameter reduction factor is the ratio of the nominal channel thickness to the hot channel thickness. For channel 2 of the HEU core for a fresh element, this factor is 80 mils / 72 mils, 1.11. In the checker program for the HEU core, the value of the heated diameter in equation 1 was divided by 1.11. The solver built into the checker program was used

to find the value of the multiplier on reactor power that caused flow instability to be predicted in the channel. As shown at the bottom of Table 30, the value is 1.024. This is to be compared with the 1.0049 value shown in the middle of the table and obtained when the heated diameter was not reduced. Hence, when the reduction in the heated diameter due to the reduction in channel thickness is included, the allowed power of 14.61 MW that is predicted by the PLTEMP/ANL code for the HEU core is increased by a factor of 1.024/1.0049 (= 1.0190) to 14.89 MW, as indicated in the last row of the table. The table also shows that the corresponding improvement factors for the LEU CD35 and LEU FSD cores are 1.041/1.0038 (= 1.0371) and 1.031/1.0031 (= 1.0278), respectively. Hence, when these improvement factors are taken into account, the 17.10 MW power for the LEU CD35 core becomes 17.73 MW and the 17.12 MW power for the LEU FSD core becomes 17.60 MW, as indicated in the last row of the table.

16c. Effect of Mixing Along the Width of the Coolant Channel

For all of the PLTEMP/ANL results in Table 16 through Table 18 it was assumed that only the coolant that was adjacent to the fuel meat removes heat. The coolant in the two unheated edges of each coolant channel was assumed to enter and exit the core at the inlet temperature. Had perfect mixing across the entire width of each channel been assumed, the predicted flow instability and CHF powers would have been greater. For the limiting channel in the LEU CD35 case shown in Table 30, for example, if perfect mixing were assumed instead of no mixing, the allowed flow instability power would have been 3.5% greater.

Although no mixing was assumed in the current analysis, perfect mixing was assumed in the Reference 9 analysis, where the measurements of Croft[7] and those of Waters[8] were compared with PLTEMP/ANL predictions that employed equation 1. The closest of these measured tests to the MURR channel thicknesses are those for the 94-mil thick channel tests by Croft. For those ten electrically heated tests, PLTEMP/ANL predicted that flow instability would occur between about 91.2 and 108.8% of the measured power. The average of the 10 values is 101.4 %. In these tests the channel width was 2.10 inches, of which the middle 2.0 inches was heated. Had no mixing been assumed, as was done for the current analysis, these percentages would have been multiplied by 2.00/2.10 and would have ranged from 86.9 to 103.6% with an average of 96.6%, indicating that PLTEMP/ANL would have predicted flow instability on average to occur at 96.6% of the power measured in these 10 electrically heated experiments.

16d. Comparison of PLTEMP/ANL CHF Predictions with the Checker Program Results for Two CHF Correlations

All of the CHF results presented in Table 16 through Table 18 are based on the extended Groeneveld 2006 relation, equation 3. The checker program was used to compare the CHF predictions of this correlation with that of the Bernath correlation, which was used as a CHF criterion in the MURR SAR[30]. This comparison is shown in Table 31, which is similar to Table 30 in organization. Analogous to the flow instability analysis for Table 30, the checker program factor, which multiplies the value of reactor power, was adjusted to achieve the desired values of CHF ratio.

Table 31. Comparison of Critical Heat Flux Predictions for the Most Limiting Channel

	HEU	LEU CD35	LEU FSD
LSSS Power, MW	12.5	15.0	15.0
PLTEMP/ANL Power, MW*	29.88	31.26	30.55
Limiting Case & Location			
Case	1B1	7A1	7A1
Element	7	1	1
Channel	1	24	25
Plate	1	23	24
Side of Plate	concave	convex	convex
Level	19	18	19
Checker Program Factor**			
Extended Groeneveld 2006	0.9957 (19)[+]	0.9998 (18)	1.0003 (19)
Bernath (CHFR = 1.0)	0.926 (19)	0.814 (24)	0.804 (24)
2 × Bernath CHFR = 2.0	1.111 (18)	1.003 (18)	0.999 (19)
Velocity Hot Channel Factor, $F_{VELOCITY}$	1.35	1.43	1.43
Heated Diameter Reduction Factor	1.25	1.35	1.36
Checker Program Factor Based on Extended Groeneveld 2006, Eq. 3, with the Above Two Factors Included	0.9790 (19)	0.9948 (18)	0.9918 (19)
PLTEMP/ANL Power, MW, Adjusted to Include Effect of Above Two Factors	29.38	31.10	30.29

*These values are the total reactor power, including the power that is deposited outside of the primary system.

**1.0 corresponds to the PLTEMP power.

[+]The number in parentheses is the level at which CHF is predicted to occur first. Since all of the channels are end channels, each has only one heated surface.

All of the extended Groeneveld 2006 checker program factors shown in the middle part of Table 31 are within 0.5% of 1.0. This demonstrates that the checker program results are in very close agreement

with the PLTEMP/ANL results, as they should be. The Bernath (CHFR = 1.0) results in the table were obtained by increasing the checker program power factor until the minimum CHF ratio in the channel was predicted to be 1.0 by the Bernath correlation.

16e. Critical Heat Flux Ratio and Critical Heat Flux Power

For every axial location within the heated width of every coolant channel of every fuel element, the value of CHF is predicted by the extended Groeneveld 2006 CHF correlation, equation 3. This CHF is entirely a function of local coolant conditions and channel geometry. Values of heated surface temperature and heat flux are not part of equation 3 or the Bernath CHF correlation. The ratio of CHF to heat flux at a particular spot on a fuel plate surface is the CHF ratio at that spot. In the PLTEMP/ANL analysis this ratio is calculated at every axial level of every fuel plate surface within the core. Hot channel factors and variations in heat flux along the widths of the fuel plates are taken into account in these calculations. The minimum of all of the numerous values of CHF ratio is the minimum CHF ratio. A minimum CHF ratio that is greater than 1.0 implies that at every location within the core the heat flux at which CHF is predicted to occur is greater than the heat flux at that location. Hence, a CHF ratio greater than 1.0 implies that CHF did not occur. The reactor power at which the minimum CHF ratio is 1.0 is the lowest power that is predicted to cause CHF. This is referred to as the CHF power.

Some analytical schemes cannot predict the CHF power. For example, in the analysis of transients the values of CHF can only be calculated for the transient conditions that are predicted. Also, since boiling is an inherently transient phenomenon that may be preceded by flow instability, some computer analysis codes that simulate the details of boiling well cannot predict the conditions at which CHF occurs had other boiling phenomena not interceded. PLTEMP/ANL does not have these limitations because it is a steady state code and its hydraulic model assumes that the coolant is always a single-phase liquid.

At least, in part, due to the obstacles to predicting the CHF power, regulatory acceptance criteria could include a value for the minimum CHF ratio, rather than a specific margin to the CHF power. Reference 44, which uses the term “departure from nucleate boiling” in place of the term “critical heat flux”, states that acceptable thermal-hydraulic design criteria could include a departure from nucleate boiling ratio of no less than 2 in any fuel channel. From a combination of page 4-27 and page 23 of Appendix 18.1, this can be interpreted to mean that a minimum CHF ratio should be no less than 2 for an HEU core. Page 23 of Appendix 18.1 specifies that either 1) there be no significant decrease in the safety margins of the HEU core in the LEU core or 2) that under certain circumstances that are required to accommodate the conversion from HEU to LEU, the safety margins can be reduced, but the minimum CHF ratio should be at least 2.0.

For the Groeneveld and Bernath CHF correlations, the CHF power is less than half of the reactor power at which a minimum CHF ratio of 2.0 occurs. This is because doubling the power at which a minimum CHF ratio of 2.0 occurs not only essentially doubles the values of heat flux, but also reduces the values of CHF. This reduction is due to the increased values of coolant quality (and coolant temperature under

subcooled conditions) which accompany greater reactor power. Thus, while heat fluxes are being increased, the corresponding values of CHF are being reduced.

The checker program was used to determine the power at which a CHF ratio of 2.0 was achieved in the CHF limiting channel of the LEU CD35 core with the extended Groeneveld 2006 CHF. The predicted power is 19.2 MW. Double this value is 38.4 MW. However, the checker program shows that a CHF ratio of 1.0 is achieved at only 31.3 MW, which is essentially the PLTEMP/ANL value and significantly smaller than 38.4 MW.

In the MURR HEU SAR a CHF ratio of 2.0 based on the Bernath CHF correlation was used to show both an acceptable margin to flow instability and an acceptable margin to CHF. This method of predicting flow instability was suggested by Croft[7] with a CHF ratio of 1/0.60 for 94-mil channels and adopted by MURR with the more stringent CHF ratio of 1/0.50. The middle portion of Table 31 includes results for a Bernath CHF ratio of 2.0. Here the row is labeled "2 × Bernath CHFR = 2.0". For the LEU CD35 core, for example, a Bernath CHF ratio of 2.0 was achieved at 0.5017 times the PLTEMP/ANL power of 31.26 MW, or at 15.7 MW. Double this is 31.4 MW. In Table 31, double 0.5017, or 1.003, is shown for the LEU CD35 core in the "2 × Bernath CHFR = 2.0" row. 1.003 is to be compared with the 0.814 value in the table for a Bernath CHF ratio of 1.0.

In experiments that measure the onset of CHF, there is no way to measure part of the way to CHF. The experiments are carried all of the way to CHF. Thus, finding the power at which PLTEMP/ANL predicts CHF to occur, i.e., a minimum CHF ratio of 1.0, is the more accurate and reliable method of determining the margin to CHF in megawatts. Hence, plots and tables of CHF power are provided in addition to the values of CHF ratio that are needed to show that a CHF ratio of at least 2.0 is maintained.

16f. The Combined Effect of the Hot Channel Factor for Velocity and the Beneficial Effect of the Reduced Channel Thickness on the Margin to CHF

The bottom portion of Table 31 is analogous to the bottom portion of Table 30. Table 31 shows the velocity hot channel factor and the heated diameter reduction factor for the limiting CHF channel of the limiting case of each of the three cores. These results show that when the adverse effect of the reduction in velocity or mass flux, G in equation 3, is coupled with the beneficial effect of the reduction in the heated diameter D of equation 3, the checker program power multiplication factor is 0.9790 for the HEU core. This is to be compared with the 0.9957 value that was obtained when the additional factors were not included. Hence, when these additional factors are included the HEU CHF power of 29.88 MW is multiplied by a factor of 0.9790/0.9957 (= 0.9832) and becomes 29.38 MW. Similarly, the LEU CD35 CHF power of 31.26 MW is multiplied by a factor of 0.9948/0.9998 (= 0.9950) and becomes 31.10 MW. The LEU FSD CHF power of 30.55 MW is multiplied by a factor of 0.9918/1.0003 (= 0.9915) and becomes 30.29 MW. Thus, the reduction in CHF power is 1.68% ([1 – 0.9832] × 100%) for the HEU core and 0.50% and 0.85% for the LEU CD35 and LEU FSD cores, respectively.

The three PLTEMP/ANL flow instability cases shown in Table 30, which represent the three cores, were rerun with the criterion that the CHF ratio be 2.0. Then the checker program was used in a manner analogous to Table 31 to produce Table 32, which is the same in structure as Table 31 except that it does not have Bernath CHF results. Table 32 shows that for each core for the channel that produced the CHF ratio of 2.0, the checker program agrees with the PLTEMP/ANL results to within a few tenths of a percent. The powers shown in the second row of the table, which correspond to a CHF ratio of 2.0, are greater than the corresponding flow instability powers of the second row of Table 30. The bottom row of the table shows that when the effects of velocity hot channel factor and the beneficial effect of the reduced channel thickness on CHF are taken together, the reactor power at which a CHF ratio of 2.0 occurs is still greater that the corresponding flow instability power, as provided in the last row of Table 30.

Table 32. Comparison of CHF Ratio = 2.0 Predictions for the Most Limiting Flow Instability Channel

	HEU	LEU CD35	LEU FSD
LSSS Power, MW	12.5	15.0	15.0
PLTEMP/ANL Power, MW*	18.65	20.79	20.01
Limiting Case & Location			
Case	3B2	8A1	8A1
Element	1	1	1
Channel	1	24	25
Plate	1	23	24
Side of Plate	concave	convex	convex
Level	16	15	16
Checker Program Factor**			
Extended Groeneveld 2006	0.9974 (16)[+]	0.9960 (17)	0.9989 (17)
Velocity Hot Channel Factor, $F_{VELOCITY}$	1.35	1.43	1.43
Heated Diameter Reduction Factor	1.25	1.35	1.36
Checker Program Factor Based on Extended Groeneveld 2006, Eq. 3, with the Above Two Factors Included	0.9270 (16)	0.9738 (16)	0.9729 (16)
PLTEMP/ANL Power, MW, Adjusted to Include Effect of Above Two Factors	17.33	20.33	19.49

*These values are the total reactor power, including the power that is deposited outside of the primary system.

**1.0 corresponds to the PLTEMP power.

[+]The number in parentheses is the level at which CHF is predicted to occur first. Since all of the channels are end channels, each has only one heated surface.

16g. Predictions Made with the Sudo and Kaminaga CHF Correlation[15,31]

As indicated in section 6c, the Sudo and Kaminaga correlation[15,31] was used to predict CHF for the limiting LEU CD35 core case. The PLTEMP/ANL analysis for case 7A1 at the LSSS conditions of flow rate, inlet temperature, and pressurizer pressure and level was repeated with the Sudo and Kaminaga CHF correlation used in place of the extended Groeneveld 2006 CHF correlation. Using the PLTEMP/ANL code here was much easier than adding the very complex Sudo and Kaminaga CHF correlation to the checker program. The Sudo and Kaminaga correlation predicted CHF to occur first in channel 23 of element 1 at level 16 of the concave side of plate 23 at a reactor power of 18.19 MW. As noted in section 6c, this is only 6.4% greater than the flow instability power obtained with equation 1 and is probably due to Sudo and Kaminaga including flow instability data with CHF data in forming their CHF correlation.

16h. Flow Instability Power Envelope for the LEU CD35 Core

The results of Table 19 through Table 21, which are plotted in Figure 7 through Figure 9, define an envelope. Reactor operation within the region defined by this envelope precludes flow instability. The coordinate point defined by the LSSS values for pressurizer pressure (75 psia) , core inlet temperature (145° F) , core inlet flow rate (3300 gpm), and reactor power (15 MW) is a safe distance from this envelope. Every point on the envelope violates one or more of these four LSSS values.

It is helpful to the reactor operator to have this envelope clearly defined. Appendix F, *Safety Limit Analysis for the MURR*, of Addendum 4 of the MURR Hazards Summary Report, which is attached to Reference 3, provides a similar envelope for the HEU core. In the unlikely event that an LSSS value is violated, the envelope can be used to assess the potential for core damage. For the HEU core this envelope is the power at which flow instability is predicted to occur when all hot channel factors are included in the analysis. It also provides the values of safety limit power as defined by the MURR Technical Specifications.

Analogous to the HEU core, the flow instability envelope defined by Table 19 through Table 21 can be used to define the values of safety limit powers for the CD35 core. Since every point on this envelope has a CHF ratio greater than 2.0, as indicated by Table 22 through Table 24, it also meets the CHF requirement of Reference 44. In addition, a comparison of every value of flow instability power in Table 19 through Table 21 with its CHF power counterpart in Table 25 through Table 27 shows that at each point the CHF power is considerably greater than the flow instability power. In the comparison the smallest ratio of CHF power (i.e., the power at which a CHF ratio of 1.0 occurs) to flow instability power occurs at 85 psia, 120° F, and 4000 gpm and is 1.58. Since the flow instability powers were calculated for the 8A1 case, which is the worst for flow instability, and the CHF powers were calculated for the 7A1 case, which is the worst for CHF power, had the 8A1 case been used to predict both the flow instability power and the CHF power, the margin to CHF power probably would have been even larger.

The flow instability power envelope is based on analysis of steady-state conditions. A rapid reactor transient, such as a protected loss-of-flow accident or a protected reactivity-insertion accident, that causes reactor operation outside the safe region defined by the envelope may not cause any reactor damage if the duration is very short, i.e., in the seconds or fraction of a second range. This is because the heat capacitance of the fuel and, to a lesser extent, the heat capacitance of the coolant, may keep clad surface temperatures and heat fluxes sufficiently low. Heat capacitance is always a mitigating factor. Each point on the trajectory of a transient can be no more severe than its steady-state counterpart.

The plots in Figure 7 through Figure 9 show a decreasing slope with increasing flow, which implies a decreasing power-to-flow ratio and a decreasing bulk coolant temperature rise with increasing flow. The reason that this happens can be inferred by close examination of equation 1. The numerator on the left side of the equation is the bulk coolant temperature rise. This value must decrease with increasing flow because the denominator is decreasing with increasing flow. The denominator is decreasing as the flow increases because the pressure drop from the pressurizer to the core exit is increasing with flow. This larger pressure drop, of course, causes a lower core outlet pressure. A lower core outlet pressure causes a lower saturation temperature at the exit of the core, which, in turn, reduces the denominator on the left side of equation 1. In Figure 7, the curve for 60 psia at the pressurizer and a core inlet temperature of 200° F shows that increasing the flow rate from 3600 to 4000 gpm causes the flow instability power to decrease instead of increase. Thus, increasing the flow rate beyond a certain point can be detrimental.

16i. Margin to Flow Instability Relative to LSSS Values

It is instructive to compare the margins to flow instability for the HEU and LEU CD35 cores provided in Table 28 and Table 29 with those provided for the HEU core in Appendix H of Addendum 4 of the MURR Hazards Summary Report, which was revised and attached to a 2011 letter sent to the US NRC[3]. Table 33, which is based on the MURR Hazards Summary Report, is analogous to Table 28. The values for the independent variables in Table 33 for Cases 1 through 3 were taken from this report. The pressurizer pressure of Case 4 was obtained with the aid of the analytical model that was used to analyze the other three cases in the table. All values of flow instability in Table 33 are based on the assumption that flow instability occurs when either the CHF ratio based on the Bernath CHF correlation[6] is 2.0 or bulk boiling occurs at the channel exit, whichever occurs first. In all cases a CHF ratio of 2.0 occurred first. The CHF ratios provided in the last column are all 2.0 because they are also based on the Bernath CHF correlation.

Table 34 compares the margins to flow instability in the MURR Hazards Summary Report, Table 33, with those predicted in the current analysis for the HEU and LEU CD35 cores, Table 28 and Table 29, respectively. For example, in Table 34 the power margin to flow instability (Case 1) for the LEU CD35 core is 2.10 MW because the flow instability power is 17.10 MW, which is 2.10 MW greater than the 15.0 MW LSSS power. As explained in section 16b, when the effect of the heated diameter reduction

factor is included in the power calculation, the allowed flow instability power predicted by the PLTEMP/ANL code is increased to 14.89 MW for the HEU core and to 17.73 MW for the LEU CD35 core. The results of these increased values are shown in parentheses in Table 34. Thus, the value in parentheses for the current analysis of the HEU core is the same as the power margin from the MURR Hazards Summary Report. The value in parentheses for the LEU CD35 core is greater than the one in parentheses for the current analysis of the HEU core. Although the inlet temperature, flow rate, and pressure margins shown in Table 34 are the smallest for the LEU CD35 core, they are substantial and certainly large enough to account for instrument measurement uncertainty bands and to permit safe operation of the reactor without a significant risk of spurious scrams.

Table 33. HEU Core HSR Flow Instability When Three Reactor Parameters Are at Their LSSS Values

MURR HSR* Appendix H Case	Pressurizer Pressure, psia	Inlet Flow, gpm	Inlet Temperature, F	Reactor Power, MW	CHF Ratio at These Conditions
1	75	3200	155	**14.894**	2.0
2	75	3200	**187.7**	12.50	2.0
3	75	**2469**	155	12.50	2.0
4**	**58.13**	3200	155	12.50	2.0

*Hazards Summary Report

**Case 4 is not defined in the MURR Hazards Summary Report.

Table 34. Margins to Flow Instability When Three Reactor Parameters Are at Their LSSS Values

MURR HSR* Appendix H Case	Dependent Parameter	MURR HSR*	Current HEU Analysis	LEU CD35
1	Power, MW	2.39	2.11 (2.39)**	2.10 (2.73)**
2	Inlet Temp. °F	32.7	19.1	17.6
3	Flow, gpm	731	620	520
4+	Pressure, psi	16.87	14.30	13.80

*Hazards Summary Report

**The values in parentheses include the adjustment in power to include the effect of the heated diameter reduction factor, as explained in section 16b.

+Case 4 is not defined in the MURR Hazards Summary Report.

17. Summary and Conclusions

The existing HEU core, the LEU Reference 1 feasibility study design (FSD) core, and the LEU CD35 core, which is the proposed LEU core that is to replace the HEU core, were evaluated with the aid of the steady-state PLTEMP/ANL code[38] to determine margins to flow instability and critical heat flux. The LEU FSD core design was developed before the LEU CD35 design. Subsequent issues related to fuel plate fabrication produced the need for the LEU CD35 core. The core neutron physics analysis[2] considered 24 cases for each core. These cases, which are summarized in Table 3 through Table 5, for the HEU, the LEU FSD, and the LEU CD35 cores, respectively, collectively bound the worst thermal hydraulic state for each core. All 24 cases were analyzed for each core. The PLTEMP/ANL model of each case explicitly modeled all eight fuel elements of the MURR core.

The axial power distribution of each plate of each case of each core was explicitly modeled. The variation in heat flux along the width of each fuel plate was also represented in the model. This took into account the higher heat fluxes due to power peaking near the vertical edges of the fuel meats.

The reduction in channel thicknesses due to both fuel plate swelling and surface oxidation were included as a function of burnup in the PLTEMP/ANL models.

The models used hot channel factors to take into account the potential adverse effects of manufacturing tolerances and modeling uncertainties. The random hot channel factors were combined multiplicatively. This approach assumes that the worst conditions occur simultaneously at the most limiting location in the core. This approach to combining hot channel factors, which is more bounding than the statistical approach, was chosen, in part, because it was used in the MURR SAR[30].

The Whittle and Forgan relationship[4], equation 1, with the parameter η set to 32.5 was used to predict flow instability. Critical heat flux correlations were studied in depth, section 6, where an extended form of the Groeneveld 2006 CHF Table, equation 3, is recommended. This correlation was used in the current analysis.

A separate computer spreadsheet program, section 15, was developed and used to verify the PLTEMP/ANL predictions for the limiting channel of selected cases. These selected cases include the limiting flow instability case and the limiting CHF power case of each of the three cores. The separate single-channel spreadsheet model was also used to investigate the predictions of additional flow instability and CHF correlations. The two additional flow instability correlations considered in this manner are the Saha-Zuber correlation for onset of significant voids, equation 2, and the Bernath-CHF-ratio-of-2.0 correlation. The Bernath-CHF-ratio-of-2.0 correlation was used in the existing MURR SAR and included in the Reference 3 submittal to the U.S. NRC. The Saha-Zuber correlation was found to predict a greater margin to flow instability than did equation 1. The Bernath-CHF-ratio-of-2.0 correlation showed a larger flow instability margin for the HEU and LEU CD35 cores and less than a 1% smaller margin for the LEU FSD core than did equation 1. The additional CHF correlation that was

evaluated via the single-channel model was the Bernath correlation, which was used in the existing MURR SAR[30].

The full PLTEMP/ANL model of the limiting case of the LEU CD35 core was also used to predict the margin to CHF based on the Sudo and Kaminaga CHF Correlation[15,31]. The predicted CHF power was only 18.19 MW, which is only 6.4% greater than the flow instability power predicted with equation 1 and is considerably less than the 31.26 MW predicted with the recommended extended Groeneveld 2006 CHF Table correlation. It is believed that the cause of the large discrepancy between the recommended and the Sudo and Kaminaga correlations is that Sudo and Kaminaga include flow instability data in the development of their CHF correlation.

The flow instability and CHF powers, with all hot channel factors included, for the 24 cases for each HEU core can be found in Table 16, where the allowed powers for the most limiting flow instability case and the most limiting CHF power case are shown in bold red and are 14.61 MW and 29.88 MW, respectively. For each value of flow instability power shown in the table, the value of minimum CHF ratio at that power is also shown. The smallest of the 24 values of minimum CHF ratio is shown in bold red. The corresponding results for the LEU FSD core are shown in Table 17, where the most limiting flow instability case has an allowed power of 17.12 MW and the most limiting CHF case has an allowed power of 30.55 MW. The results for LEU CD35 core are shown in Table 18, where the most limiting flow instability case has an allowed power of 17.10 MW and the most limiting CHF case has an allowed power of 31.26 MW. For all three cores, the pressurizer pressure, core inlet temperature, and core flow rate were set at their LSSS values. These values for the HEU core are 75 psia, 155° F, and 3200 gpm, respectively. For the two LEU cores the LSSS pressurizer pressure value is the same as in the HEU core, but the core inlet temperature value is 145° F and the core flow rate value is 3300 gpm. For all three cores the pressurizer level was set at its scram setpoint of −16 inches. In each of the three tables the minimum CHF ratio for each value of flow instability power is greater than 2.0. Thus, avoiding flow instability is a more restrictive requirement than is avoiding CHF.

For the HEU core with all hot channel factors included, the allowed flow instability power of 14.61 MW is 2.11 MW above its LSSS power of 12.5 MW. For the proposed LEU CD35 core the corresponding allowed power of 17.10 MW is 2.10 MW above its LSSS power of 15.0 MW. Thus, both the HEU core and its proposed LEU replacement have essentially the same margin to flow instability. Similarly, the FSD core, with its allowed flow instability power of 17.12 MW, has a 2.12 MW margin to its 15.0 MW LSSS power.

The value of CHF power, with all hot channel factors included, presented in Table 16 through Table 18 for the three cores are the values at which CHF is predicted to first occur. These values were obtained from the PLTEMP/ANL code analysis by adjusting the reactor power to a value at which CHF was predicted to first occur. As the tables show, the minimum HEU CHF power is 29.88 MW, the minimum LEU FSD CHF power is 30.55 MW, and the minimum LEU CD35 CHF power is 31.26 MW. These results provide further proof that all three cores have sufficient margin to CHF under steady-state operating conditions.

For the most limiting CD35 flow instability case in Table 18, a parametric study of flow instability power as a function of pressurizer pressure, core inlet temperature, and core inlet flow was performed using the full PLTEMP/ANL model. The results for all 198 parametric cases are shown in Table 19 through Table 21, and in Figure 7 through Figure 9. For the most limiting CD35 CHF case in Table 18, an analogous CHF parametric study was performed. The parametric CHF results are shown in Table 25 through Table 27 and in Figure 10 through Figure 12.

Analyses were performed with aid of the PLTEMP/ANL code in which three of the four reactor parameters, pressurizer pressure, inlet temperature, inlet flow rate, and reactor power, were constrained at their LSSS values and the value of the fourth at which the onset of flow instability occurs was obtained. This was done for the HEU and LEU CD35 cores, Table 28 and Table 29, respectively. The corresponding results from the analysis of the MURR Hazards Summary Report for the HEU core are provided in Table 33. For each of the four reactor parameters, pressurizer pressure, inlet temperature, inlet flow rate, and reactor power, the margin between the LSSS value and the onset of flow instability is summarized in Table 34 to compare the MURR Hazards Summary Report analysis of the HEU core to the current analyses of both the HEU and LEU CD35 cores.

In conclusion, the proposed LEU CD35 core design has acceptable flow instability and CHF safety margins, as does the LEU FSD core design, which was subsequently abandoned due to issues of fuel plate manufacture. For both of the LEU cores, the power margin to flow instability relative to the LSSS power is essentially the same as that for the HEU core and all values of CHF ratio evaluated at the values of flow instability power are greater than 2.0.

References:

1. J. C. McKibben, et al., *Feasibility Analyses for HEU to LEU Fuel Conversion of the University of Missouri Research Reactor (MURR)*, TDR-0125, September 30, 2009.
2. J. Stillman, et al., *Technical Basis in Support of the Conversion of the University of Missouri Research Reactor (MURR) Core from Highly-Enriched to Low-Enriched Uranium – Core Neutron Physics*, ANL/RERTR/TM-12-30, Argonne National Laboratory, September 2012.
3. Letter, Ralph A. Butler to U.S. Nuclear Regulatory Commission, Washington, DC, Docket 50-186, University of Missouri-Columbia Research Reactor, Amended Facility License R-103, August 19, 2011.
4. R. H. Whittle and R. Forgan, "A Correlation for the Minima in the Pressure Drop Versus Flow-Rate Curves for Sub-Cooled Water Flowing in Narrow Heated Channels," *Nuclear Engineering and Design*, 1967, pp. 89-99.
5. A. P. Olson, "Analysis of Flow Excursion Experiments Relevant to Research Reactors," The 2006 International Meeting on Reduced Enrichment for Research and Test Reactors, October 29-November 3, 2006, Cape Town, South Africa, http://www.rertr.anl.gov/RERTR28/PDF/S7-2_Olson.pdf.

6. Louis Bernath, "A Theory of Local-Boiling Burnout and Its Application to Existing Data," Chemical Engineering Progress Symposium, Series No. 30, Volume 56, pp. 95-116 (1960).
7. M. W. Croft, Advanced Test Reactor Burnout Heat Transfer Tests, USAEC Report IDO-24465, ATR-FE-102, Ca-2, Babcock & Wilcox Company, January 1964.
8. E. D. Waters, Heat Transfer Experiments for the Advanced Test Reactor, USAEC Report BNWL-216, UC-80, Reactor Technology (TID-4500) Pacific Northwest Laboratory, Richland, Washington, May 1966.
9. E. E. Feldman, *Comparison of the PLTEMP Code Flow Instability Predictions with Measurements Made with Electrically Heated Channels for the Advanced Test Reactor*, ANL/RERTR/TM-11-23**,** Nuclear Engineering Division, Argonne National Laboratory, June 9, 2011.
10. P. Saha and N. Zuber, "Point of Net Vapor Generation and Vapor Void Fraction in Subcooled Boiling," Heat Transfer 1974, Vol VI., 5th IHTC, Tokyo, 1974, pp. 175-179.
11. D. C. Groeneveld, J. Q. Shan, A. Z. Vasic, L. K. H. Leung, A. Durmayaz, J. Yang, S. C. Cheng, and A. Tanase, "The 2006 CHF Look-up Table," Nucl. Eng. and Design, Vol. 237, pp. 1909-1922 (2007).
12. D. D. Hall and I. Mudawar, "Critical Heat Flux for Water Flow in Tubes – II. Subcooled CHF Correlations," Intern. J. Heat and Mass Transfer, Vol. 43, pp. 2605-2640 (2000).
13. G. P. Celata, M. Cumo, and A. Mariani, "The Effect of the Tube Diameter on the Critical Heat Flux in Subcooled Flow Boiling," Intern. J. of Heat and Mass Transfer, Vol. 39, pp. 1755-1757 (1996).
14. A. Tanase, S. C. Cheng, D. C. Groeneveld, and J. Q. Shan, "Diameter Effect on Critical Heat Flux," Nucl. Eng. Des., Vol. 239, pp. 289-294 (2009).
15. Y. Sudo and M. Kaminaga, "A New CHF Correlation Scheme Proposed for Vertical Rectangular Channels Heated From Both Sides in Nuclear Research Reactors," *Trans. of the ASME, J. Heat Transfer*, Vol. 115, pp. 426-434 (1993).
16. D. D. Hall and I. Mudawar, "Critical Heat Flux for Water Flow in Tubes – I. Compilation and Assessment of World CHF Data," Intern. J. Heat and Mass Transfer, Vol. 43, pp. 2573-2604 (2000).
17. P. K. Sarma, V. Srinivas, K. V. Sharma, V. D. Rao, and G. P. Celata, "A Correlation to Evaluate Critical Heat Flux in Small Diameter Tubes under Subcooled Conditions of Coolant," Intern. J. of Heat and Mass Transfer, Vol. 49, pp. 42-51 (2006).
18. V. Srinivas, Department of Mechanical Engineering, GITAM Institute of Technology, Visakhapatnam, India, private communication (March 2, 2012).
19. M. Kureta and H. Akimoto, "Critical Heat Flux Correlation for Subcooled Boiling Flow in Narrow Channels," Intern. J. Heat and Mass Transfer, Vol. 45, pp. 4107-4115 (2002).
20. M. Caira, G. Caruso, and A. Naviglio, "A Correlation to Predict CHF in Subcooled Flow Boiling," Intern. Communications in Heat and Mass Transfer, Vol. 22, pp. 35-45 (1995).
21. C. Lombardi, "A Formal Approach for the Prediction of the Critical Heat Flux in Subcooled Water," Proceedings of the 7th International Meeting on Nuclear Reactor Thermal-Hydraulics: NURETH-7, NUREG/CP-0142, Vol. 4, US Nuclear Regulatory Commission, Washington, DC, pp. 2506-2518 (1995).
22. V. V. Yagov, V. A. Puzin, and L. A. Sukomel, "The Approximate Model for Critical Heat Flux under Subcooled Flow Boling Conditions," 2nd European Thermal Sciences and 14th UIT National Heat Transfer Conference, G. P. Celata, P. D. Marco, and A. Mariani (Editors), Edizioni ETS, Pisa, Italy, Vol. 1, pp. 483-490 (1996).
23. K. Mishima and H. Nishihara, "Effect of Channel Geometry on Critical Heat Flux for Low Pressure Water," Intern. J. Heat and Mass Transfer, Vol. 30, pp. 1169-1182 (1987).

24. I. L. Pioro, S. C. Cheng, D. C. Groeneveld, A. Z. Vasic, S. Pinchon, and G. Chen, "Experimental Study of the Effect of Non-circular Flow Geometry on the Critical Heat Flux," Nucl. Eng. and Design, Vol. 187, pp. 339-362 (1999).
25. H. Zhang, I. Mudawar, and M. M. Hasan, "Assessment of Dimensionless CHF Correlations for Subcooled Flow Boiling in Microgravity and Earth gravity," Intern. J. Heat and Mass Transfer, Vol. 50, pp. 4568-4580 (2007).
26. F. Inasaka and H. Nariai, "Evaluation of Subcooled Critical Heat Flux Correlations for Tubes with and without Internal Twisted Tapes," Nucl. Eng. and Design, Vol. 163, pp. 225-239 (1996).
27. W. Zhang, T. Hibiki, K. Mishima, and Y. Mi, "Correlation of Critical Heat Flux for Flow Boiling of Water in Mini-channels," Int. J. Heat and Mass Transfer, Vol. 49, pp. 1058-1072 (2006).
28. G. P. Celata, M. Cumo, and A. Mariani, "Assessment of Correlations and Models for the Prediction of CHF in Water Subcooled Flow Boiling," Intern. J. of Heat and Mass Transfer, Vol. 37, pp. 237-255 (1994).
29. G. P. Celata, ENEA, Thermal Process Engineering Division, Anguillarese, Rome, Italy, private communication (February 1, 2012).
30. University of Missouri Research Reactor Safety Analysis Report, Chapter 4, Reactor Description, submitted to the U.S. Nuclear Regulatory Commission in 2006.
31. M. Kaminaga, K. Yamamoto, and Y. Sudo, "Improvement of Critical Heat Flux Correlation for Research Reactors using Plate-Type Fuel," *J. Nuclear Science and Technology*, Vol. 35, pp. 943-951 (1998).
32. L. Foyto, et al., *Preliminary Safety Analysis Report, Methodologies and Scenarios for LEU Fuel Conversion of the University of Missouri Research Reactor (MURR)*, No. 128, Columbia, Missouri 65211, August 2011.
33. X-5 Monte Carlo Team, "MCNP-A General Monte Carlo N-Particle Transport Code, Version 5 Volume I, II and III," LA-UR-03-1987/LA-CP-03-0245/LA-CP-03-0284, Los Alamos National Laboratory (2003).
34. W. L. Woodruff, Evaluation and Selection of Hot Channel (Peaking) Factors for Research Reactor Applications, ANL/RERTR/TM-28, RERTR Program, Argonne National Laboratory, Argonne, Illinois, February 1997 [http://www.rertr.anl.gov/METHODS/TM28.pdf].
35. J. E. Matos and J. L. Snelgrove, "Selected Thermal Properties and Uranium Density Relations for Alloy, Aluminide, Oxide, and Silicide Fuel," *Research Reactor Core Conversion Guidebook*, IAEA-TECDOC-643, Volume 4: Fuels Appendices I-1.1, IAEA, Vienna, Austria, 1992, pp. 13-29.
36. Personal communication with Gerard Hofman on February 13, 2009.
37. D. E. Burkes, G. S. Mickum, D. M. Wachs, *Thermophysical Properties of U-10Mo Alloy*, INL/EXT-10-19373, November 2010, Idaho National Laboratory, http://www.inl.gov/technicalpublications/Documents/4702554.pdf.
38. Arne P. Olson and Kalimullah, *A User's Guide to the PLTEMP/ANL Code*, Version 4.1, ANL/RERTR/TM-11-22, Nuclear Engineering Division, Argonne National Laboratory, April 6, 2011. (This version is the last formal release of the code. A newer version, V4.2bta, of April 2, 2012 was used in the analysis because it has the extended Groeneveld 2006 CHF correlation that is described in Section 6a.)
39. J. Rest, Y. S. Kim, G. L. Hofman, M. K. Meyer, and S. L. Hayes, *U-Mo Fuels Handbook*, Version 1.0, ANL-09/31, Argonne National Laboratory, June 2006.
40. J. K. Fink and L. Leibowitz, "Thermal conductivity of zirconium," *Journal of Materials*, 226 (1995) 44-50.

41. J. C. Griess, H. C. Savage, and J. L. English, *Effect of Heat Flux on the Corrosion of Aluminum by Water. Part IV. Tests Relative to the Advanced Test Reactor and Correlation with Previous Results*, ORNL-3541, Oak Ridge National Laboratory, Oak Ridge, Tennessee, February 1964.
42. M. Kalimullah, A.P. Olson, E.E. Feldman, N. Hanan and B. Dionne, *Verification and Validation of the PLTEMP/ANL Code for Thermal-Hydraulic Analysis of Experimental and Test Reactors*, ANL/RERTR/TM-11-37, Rev. 0, Nuclear Engineering Division, Argonne National Laboratory, Argonne, Illinois, July 30, 2011.
43. I. E. Idelchik, *Handbook of Hydraulic Resistance*, Second Edition, Hemisphere Publishing Corporation, New York, 1986, pp. 149-151.
44. *Guidelines for Preparing and Reviewing Applications for the Licensing of Non-Power Reactors, Standard Review Plan and Acceptance Criteria*, NUREG-1537, Part 2, February 1996.

Appendix A. Load on the Grid Plate (Spider)

The weight of an HEU element (in air) is 6.25 kg. The weight of an LEU CD35 element (in air) is double this value. Thus, a MURR core of eight LEU CD35 elements weighs 100 kg (220 pounds) compared to 50 kg (110 pounds) for an HEU core. However, when the hydraulic forces due to the coolant flow through the core are taken into account, the maximum load on the MURR grid plate, or "spider", for the LEU CD35 core is considerably less than for the HEU core. The reduction in load for the LEU CD35 core is due to the lower friction pressure drop through the LEU CD35 elements. The reduction in load will be quantified with the aid of the integral form of the momentum equation.

Figure A - 1 shows the model that is used for the analysis. An annular control volume is drawn to contain the eight 32.5-inch-long elements and the spider. The top of the control volume is drawn sufficiently above the eight elements and the bottom of the control volume is drawn sufficiently below the bottom of the spider so that the top and bottom flow areas and velocities are the same. (In this analysis, the relatively small reduction in flow area that is needed to form small horizontal surfaces to support the circular edges of the spider is ignored.) The two cylindrical boundaries of the control volume are the cylindrical interior surfaces of the reactor vessel walls.

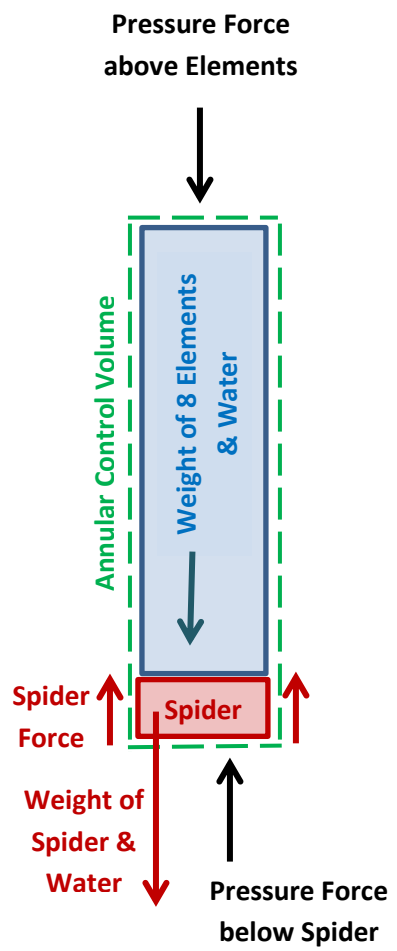

Figure A - 1. Spider Load Model

The shear and pressure forces acting on the surface of the control volume are:

S1. The pressure force above the elements at the top of the control volume.

S2. The pressure force below the spider at the bottom of the control volume.

S3. The spider force, as indicated by the two upward red arrows, which is the force that supports the spider where it contacts ledges in the walls of the reactor vessels.

S4. Fluid viscous forces at the reactor vessel walls, which are in the upward direction but not shown in Figure A - 1. These forces are due to the coolant viscous shear stresses at the reactor vessel walls.

The body forces, which are due to gravity, acting on the control volume are:

B1. The weight of the eight fuel elements (in air).

B2. The weight of the water within the control volume above the spider, including the water within the fuel elements.

B3. The weight of the spider (in air).

B4. The weight of the water in the control volume that is within and below the spider.

The force that the spider puts on the control volume, S3 listed above, is accompanied by an equal and opposite force, or load, on the spider, which is what is being sought from this analysis.

For a steady-state process, the governing equation, which was can be obtained from a fluid dynamics textbook[A.A.1], is:

$$\vec{F_s} + \int_{C.V.} \vec{B} d\vartheta = \int_{C.S.} \vec{V} \rho (\vec{V} \cdot d\vec{A}) \qquad (A.1)$$

where $\vec{F_s}$ is the sum of the surface forces acting on the control volume, $\vec{B}$ is the body force per unit volume acting on the control volume, C.V. is the control volume, $d\vartheta$ is infinitesimal volume, $\vec{V}$ is velocity, and ρ is density. The vector quantity $d\vec{A}$ is an infinitesimal area dA on the control surface whose normal or perpendicular vector is pointing in the outward direction relative to the control volume surface. Only the vertical or z component of equation A.1 is needed for the current analysis. In the application of this equation, the positive direction of z is in the downward direction. The first term represents the sum of the forces acting on the surface of the control volume, including those due to pressure and shear stress. The second term is an integral of all of the body forces, such as gravity, within the control volume. The third term represents the momentum flux term and is integrated over the surface of the control volume. This term arises because equation A.1 is applied to a fixed volume in space rather than a fixed mass.

For the analysis it will be assumed that the flow rate through the reactor core is at the normal operating value of 3750 gpm. Increasing the core flow rate increases the load on the spider more for an HEU core than it does for an LEU CD35 core and thereby makes the comparison more favorable for the LEU CD35 core. It will be assumed that the reactor has a coolant inlet temperature of 120° F and that the reactor power is zero, as it would be in the early phase of reactor startup. For this set of conditions, the load on the spider with an LEU CD35 core will be compared with that for an HEU core.

The only momentum fluxes are at the top and the bottom surfaces of the control volume. The velocity and the surface area are the same at both locations. The direction of the outward normal of the area is negative at the top surface and positive at the bottom one. Thus, the momentum fluxes at the top and bottom surfaces of the control volume are of equal magnitude, but of opposite sign. Hence, the third term of equation A.1 is zero. Thus, equation A.1 becomes a simple force balance, as follows:

$$F_T - F_B - F_{Spider} - F_{Viscous} + F_{Weight} = 0 \qquad (A.2)$$

This is a scalar equation. The first term, F_T, is the pressure force at the top of the control volume, which is the pressure at the top surface, P_T, times the surface area there, A. Similarly, the second term, F_B, is the pressure force at the bottom of the control volume, which is the pressure at the bottom surface, P_B, times the surface area there. The area is assumed to be the same at both of these surfaces. The third term is the load on the spider. The fourth term is the force due to the shear stress that the reactor vessel walls exerted on the coolant going down the first and the last coolant channels of each element.

The last term is the combined weight of everything inside the control volume, which is listed above as B1 through B4.

The difference of the first two terms in equation A.2 is the product of the pressure drop from top of the control volume to the bottom and A, the area of the top or bottom surface. The required pressure drop can be obtained from the Bernoulli equation with the minor loss terms added to account for frictional and form losses. This equation applied at the elevations of the top and bottom surfaces of the control volume is:

$$P_T + \frac{\rho V_T^2}{2} + \rho g z_T = P_B + \frac{\rho V_B^2}{2} + \rho g z_B + \Delta P_m \tag{A.3}$$

In this equation, ρ is density, V is velocity of the fluid, g is the acceleration due to gravity, and z is elevation, which increases in the upward direction. The subscripts T and B correspond to the top and bottom surfaces of the control volume, respectively, and ΔP_m is the so-called "minor pressure drop" due to frictional and form losses, which can be quite large.

Since V_T and V_B are equal, one can use equation A.3 to obtain as expression for $F_T - F_B$ as:

$$F_T - F_B = (P_T - P_B)A = [\Delta P_m - \rho g(z_T - z_B)]A \tag{A.4}$$

Equations A.2 and A.4 may be combined to obtain:

$$F_{Spider} = \Delta P_m A - \rho g(z_T - z_B)A - F_{Viscous} + F_{Weight} \tag{A.5}$$

ΔP_m is the combined friction and form-loss pressure losses through the entire length of the control volume from top to bottom. The viscous friction pressure drop through the coolant channels produces essentially all of ΔP_m for each core. The very small additional pressure drop through the rest of the control volume will be ignored. Moreover, since this very small additional pressure drop exists for both the HEU and LEU CD35 cores and is essentially the same for both, the effect on the difference of the spider loads for the two cores will be even smaller. This coolant channel friction pressure drop, which is calculated below for each core, is substantial and is what causes the LEU CD35 core to apply a smaller force on the spider than does the HEU core.

$F_{Viscous}$ is small compared to ΔP_m A. A force balance on just the coolant within any coolant channel would show that the friction pressure force difference between the inlet and the outlet must balance the viscous shear forces at the walls of the coolant channel. $F_{Viscous}$ is essentially a result of only the viscous shear stresses on the surfaces of the reactor pressure vessel walls over the 25.5-inch-length of the fuel plate. This is to be compared to the ΔP_m A, which is equal to all the fluid shear stress forces on all of the lateral surfaces of all of the coolant channels in the core, including the two reactor pressure vessel wall surfaces, in addition to the friction pressure drop acting over all of the projected area of the fuel plates edges as viewed from above or below the core. $F_{Viscous}$ reduces the load on the spider, F_{Spider}, and

ignoring it increases the predicted value of F_{Spider}. If it is ignored in both cores, its effect on the comparison of the two cores will be even smaller. Therefore, $F_{Viscous}$ is neglected.

The term, in equation A.5 $\rho g(z_T - z_B)$ A is the product of the total volume of the control volume, the density of water, and g. This is the weight of the control volume if it were filled entirely with water. Since F_{Weight} is the weight of all of the solid and all of the water in the control volume, it is obvious that $F_{Weight} - \rho g(z_T - z_B)$ A is the weight of all of the solid in the control volume reduced by the weight of the water that the solid displaces. Thus, $F_{Weight} - \rho g(z_T - z_B)$ A is just the weight of the solid in water. Hence, from equation A.5 it can be concluded that the load on the spider is the sum of the friction pressure drop force (ΔP_m A), the weight of the core in water, and the weight of the spider in water. Since the weight of the spider in water is very small compared to the weight of the core in water and because the load that the core adds to the spider is of what is of primary interest here, the weight of the spider in water will be neglected. Hence:

$$F_{Spider} = \Delta P_m A + W \tag{A.6}$$

where W is the weight of the core while it is fully submerged in water.

Detailed calculations of the volumes that form each core indicate that each HEU element displaces 2.05 kg of water and each LEU CD35 element displaces 1.82 kg of water. As indicated near the bottom of Table A - 1, from theses weights and the core weight in air, it can be deduced that when fully submerged in water the HEU core weighs 74.1 pounds and the LEU CD35 core weighs 188.3 pounds.

The friction pressure drop through the 25.5-inch length of the fuel plates is estimated by the following relationship:

$$\Delta P = f\frac{L}{D}\ \rho V^2/2 \tag{A.7}$$

where f is the Moody friction factor, L is the length of the fuel plates, D is the hydraulic diameter of the core, ρ is the coolant density, and V is the average velocity through the core coolant channels. The hydraulic diameter is 4 times the core flow area divided by the wetted perimeter of the core.

In concept, a more accurate calculation for ΔP could be obtained by treating the core as a hydraulic network, which would require predicting the flow rate in each individual channel. This approach is used in the PLTEMP/ANL code[A.2]. This code was used to analyze an LEU CD35 core operating at 14.46 MW, 3300 gpm, and an inlet temperature of 145° F. For these conditions the PLTEMP/ANL code analysis predicted a core friction pressure drop of 0.05323 MPa (7.720 psi). These conditions correspond to an average core temperature rise of about 30° F. Thus, the average core temperature in this case is about 145 + 30/2 = 160° F. Therefore, the single equivalent channel model with one equivalent hydraulic diameter and one total core flow area was used to predict the pressure drop for an LEU CD35 core at 3300 gpm and a constant coolant temperature of 160° F. The resultant pressure drop of 0.05286 MPa (7.667 psi) is only 0.7% less than that obtained with the PLTEMP/ANL model, which had 192 individual

coolant channels. Thus, the single equivalent channel model is sufficient for predicting the friction pressure drop in the analysis of the load on the spider and will be used here.

Table A - 1 includes key parameters and results used in the analysis. The core flow area was obtained by summing the calculated flow area obtained for each individual coolant channel. The wetted perimeter for the core was obtained in an analogous manner. This enabled a representative value of the hydraulic diameter to be obtained for the entire core.

The flow rate and flow area together enabled the average velocity to be determined. The relative roughness and the Reynolds number were used in the Colebrook equation to determine the Moody friction factor. The relative roughness is the absolute roughness divided by the hydraulic diameter. The absolute roughness is taken to be $63 \times 10{-}6$ inches. The Reynolds number is $\rho VD/\mu$, where ρ and μ are the coolant density and viscosity, respectively. The ΔP_m in equations A.3, A.4, and A.5, above, is assumed to be equal to ΔP of equation A.7. The product of this pressure drop and the annular flow area between the two reactor pressure vessels, 87.13 in^2, is the force due to the friction pressure drop of the core. As shown in the lower portion of Table A - 1, this force is 1237 pounds for the HEU core and 903.0 pounds for the LEU CD35 core. Near the bottom of the table, the weights of the HEU and LEU CD35 cores fully submerged in water, 74.1 and 188.3 pounds, respectively, are given along with the corresponding HEU and LEU CD35 core spider loads of 1311 and 1091 pounds, respectively. Hence, replacing the HEU core with the CD35 core reduces the load on the spider by 220 (= 1311 − 1091) pounds during operation at the normal core flow of 3750 gpm.

References:

A.1. W. F. Hughes and J. A. Brighton, *Shaum's Outline of Theory and Problems of Fluid Dynamics*, McGraw-Hill Book Company, New York, 1967, p. 29.

A.2. Arne P. Olson and Kalimullah, *A User's Guide to the PLTEMP/ANL Code*, Version 4.1, ANL/RERTR/TM-11-22, Nuclear Engineering Division, Argonne National Laboratory, April 6, 2011.

Table A - 1. Key Spider Load Parameters and Results

Item	HEU Core	LEU CD35 Core
Coolant temperature, F	120	
Coolant Pressure, bar	4.0	
Density kg/m^3	988.66	
Viscosity, Pa-s	5.5693×10^{-4}	
Surface roughness, micro inches	63	
Core flow rate, gpm	3750	
Core length, in	25.5	
O.D. of outer wall of inner pressure vessel, in	5.32	
I.D. of inner wall of outer pressure vessel, in	11.80	
Annular flow area between vessels, in^2	87.13	
Core flow area per element, in^2	6.130	6.686
Core flow area, in^2	49.04	53.49
Core wetted perimeter per element, in	154.9	148.8
Core wetted perimeter, in	1239.2	1190.4
Core hydraulic diameter, in	0.1583	0.1797
Relative roughness	3.980×10^{-4}	3.505×10^{-4}
Core average velocity, ft/s	24.53	22.49
Reynolds number	53373	55561
Moody friction factor	0.02199	0.02167
Core friction pressure drop, ΔP_m, Pa	97910	71453
Core friction pressure drop, ΔP_m, psi	14.20	10.36
$\Delta P_m \times A$, friction pressure drop force, pounds	**1237**	**903**
Weight of element in air, kg	6.25	12.5
Weight of core in air, kg	50	100
Weight of water displaced by one element, kg	2.05	1.82
Weight of water displaced by core, kg	16.4	14.6
Weight of core fully submerged in water, kg	33.6	85.4
Weight of core in air, pounds	110	220
Weight of core fully submerged in water, pounds	**74.1**	**188.3**
Load on spider, pounds	**1311**	**1091**

Nuclear Engineering Division
Argonne National Laboratory
9700 South Cass Avenue, Bldg. 208
Argonne, IL 60439

www.anl.gov

Argonne National Laboratory is a U.S. Department of Energy
laboratory managed by UChicago Argonne, LLC